Interaction of Brain Cancer Stem Cells and the Tumour Microenvironment: A Computational Study

by

Nazgol Shahbandi

A thesis
presented to the University of Waterloo
in fulfillment of the
thesis requirement for the degree of
Master of Mathematics
in
Applied Mathematics

Waterloo, Ontario, Canada, 2012

Author's Declaration

I hereby declare that I am the sole author of this thesis. This is a true copy of the thesis, including any required final revisions, as accepted by my examiners.

I understand that my thesis may be made electronically available to the public.

Abstract

Glioblastoma multiforme (GBM) is one of the most common and aggressive primary brain tumours, with a median patient survival time of 6-12 months in adults. It has been recently suggested that a typically small sub-population of brain tumour cells, in possession of certain defining properties of stem cells, is responsible for initiating and maintaining the tumour. More recent experiments have studied the interactions between this subpopulation of brain cancer cells and tumour microenvironmental factors such as hypoxia and high acidity. In this thesis a computational approach (based on Gillespie's algorithm and cellular automata) is proposed to investigate the tumour heterogeneities that develop when exposed to various microenvironmental conditions of the cancerous tissue. The results suggest that microenvironmental conditions highly affect the characterization of cancer cells, including the self-renewal, differentiation and dedifferentiation properties of cancer cells.

Acknowledgements

I would like to begin by conveying my deep sense of gratitude to my supervisor Prof. Mohammd Kohandel for his guidance, friendly support, supervision and sincere encouragement during years of study. A special thank goes to Prof. Siv Sivaloganathan for his most valuable comments and discussions. Many thanks go to Professor Matt Scott and Professor Giuseppe Tenti for their support during my course of studies. I would also like to thank Dr. Hamid Molavian for his kind generosity to share the results of his studies. I also thank Colin Phipps for his valuable comments on my thesis.

I am very grateful to all the other members of Biomedical Research group; Colin Turner, Turin, Satya, Herbert, Boglarka, Jonathan, Run, Hadi, and specially to Andie, Sattar, Kathleen, Sean Remziyeh, and Alex for sharing the office space and having nice company throughout.

I pay my sincere gratitude to my parents, Mr. Abbas Shahbandi and Mrs. Azam Sadr, for their love, care and sacrifices, which made it possible for me to pursue with higher studies and also to my sister, Naghmeh, and my brother, Nima for their constant support, encouragement and love.

Finally, I would like to thank my dearest, Iman Kamali Sarvestani for his love and constant motivations that encouraged me to start and endlessly continue.

Table of Contents

List of Figures

List of Tables

1. Introduction

In spite of considerable improvements in medical technology, cancer prognosis and treatment remain some of the main challenges of modern medicine. Cancer is a disease characterized by uncontrolled replication of cells as a result of the accumulation of multiple genetic mutations. Despite widespread and significant studies on cancer, conventional treatments remain problematic, survival time is often quiet short and cancer metastasis and reoccurrence are frequently lethal.

Central nervous system cancers (aka brain) cancers are growing neoplasms inside the cranium or in the central spinal canal. The critical role of the central nervous system, the short survival time, deadly invasiveness, and reoccurrence of cancers highlight the critical importance of the appropriate selection of brain cancer treatments.

In-depth studies of cancer cell physiology reveal heterogeneities inside tumours and consequently, the results of studies conducted in the early 60s proposed that the physiological and functional heterogeneities inside the tumour may be explained by considering distinct subpopulations of cancer cells. These considerations lie at the heart of the cancer stem cell hypothesis.

According to the cancer stem cell hypothesis, there is a subpopulation of cancer cells capable of tumour initiation, tumour maintenance, as well as differentiation into other progenitor cells, that play a critical role in invasion and metastasis [Reya et al. 2001, Singh et al. 2004, Dirks 2008]. The annotation of cancer stem

cells is due to their physiological and functional similarities to normal stem cells. Just like normal stem cells, cancer stem cells are capable of colony formation. Furthermore, normal and cancer stem cells may express similar cell surface markers. For instance, brain cancer and normal neural stem cells both express CD 133+ on their membrane [Singh et al. 2004, 2003]. Similar to normal stem cells, cancer stem cells undergo three alternative division pathways: self-renewal, symmetric or asymmetric differentiations. The cells produced through self-renewal inherit all the capabilities of their stem-like parent while differentiated children are more mature cells with a lower potential for proliferation.

Recent studies have reported that the tumour microenvironment closely interacts with cancer cells. Hanahan and Weinberg [Hanahan and Weinberg 2000, Hanahan and Weinberg 2011] characterized all cancer cells by introducing six common features: proliferation inhibitors avoidance, apoptosis escape, self-sufficiency in proliferation, unlimited replication, promotion of angiogenesis, invasion and metastasis. All cancer cells possess most of the aforementioned capabilities. In a most recent paper [Hanahan and Weinberg 2011], they discuss the central role played by the tumour microenvironment in promoting the cancerous properties of these cells. The peculiar properties of the tumour microenvironment (that are partially the result of the tangled and dysfunctional vascular network inside the tumour as well as the metabolic abnormalities of cancer cells) include hypoxia, elevated acidity, and high interstitial fluid pressure.

Hypoxia and acidity, common features of the tumour microenvironment, can play a significant role in the progression of tumour malignancies through the upregulation of proliferation and the promotion of the cancer stem cell phenotype [McLendon and Rich 2011]. Recent studies have reported the observation of CD133+, brain cancer stem cell surface marker expression in cancer stem cell-depleted cultures exposed to hypoxia and acidity [Seidel et al. 2010, Heddleston et al. 2009, Hjelmeland et al. 2011]. Thus, in investigating the dynamics of tumour heterogeneities and tumour progression, it seems that microenvironmental factors play a key role.

The diverse tumour microenvironment and varieties of cancer cells form a complex system of multi-variables. The interaction of cancer cells and the tumour microenvironment complicates the problem further. The study of such a complex system requires powerful tools that can handle multiple variables with ease and can be tuned to satisfy biological considerations. Mathematical and computational models grounded on experimental studies have proved invaluable in studying complicated biological systems of many variables in order to provide a better understanding of the whole system. In addition, they can often capture the complex interaction of the variables, and thus provide the means for an in-depth study of a particular part of the system. Mathematical and computational models are also proving to be increasingly useful in predicting the behaviour of biological systems, in making hypotheses and in designing appropriate biological experiments to test these hypotheses.

In this thesis, we propose a mathematical model and use computational methodologies in order to investigate tumour heterogeneities, with an emphasis on the interaction of tumour microenvironmental factors, hypoxia and acidity, with cancer stem and non-stem cells. The model attempts to capture the dynamics of a heterogeneous population of cancer cells by including the self-renewal, symmetric or asymmetric differentiation of cancer stem cells and the division or dedifferentiation of non-stem cancer cells on exposure to various levels of hypoxia and acidity. Chapter 2 briefly reviews the biological background knowledge of cancers, brain cancers, the tumour microenvironment, cancer cell heterogeneities, and the interactions between cancer cells and the tumour microenvironment. In chapter 2, we also cover the relevant issues and biological prerequisites necessary to set up the mathematical model. The first section of this chapter is devoted to introducing the general concept of cancer, characteristics of cancer cells, and different types of cancer with a focus on brain cancer and the special case of glioblastoma multiforme. In the second section, we provide an overall picture of the tumour microenvironment. Starting with abnormal and sustained tumour angiogenesis, one of the basic reasons for tumour

microenvironment abnormalities, we discuss the phenomenon of hypoxia, mechanisms underlying the cancer cell response to hypoxic conditions and consequences promoted by the hypoxic environment. The low pH levels characteristic of the tumour microenvironment is reviewed, followed by a brief discussion of cancer cell metabolisms and the effects of different metabolic pathways on microenvironmental acidity. Finally, the high interstitial pressure of tumour tissues is considered. The second section of chapter 2 is devoted to a discussion of the cancer stem cell hypothesis. As biological prerequisites of the model construction, the current method of identification of brain cancer stem cells through the expression of CD133+ is discussed along with a discussion of the interaction of cancer stem cell with tumour vascular niches, hypoxia and high acidity. The third chapter starts with a brief review of mathematical cancer growth models. This consists of model categorization and a review of previous work on tumour growth dynamics. The fundamental construction of the model and assumptions is preceded by a discussion of possible division pathways of cancer stem and non-stem cells. In the second section of chapter 3, the preliminary model of cancer cell division pathways is expanded to encompass the suggested phenotypic pattern of cancer cells. After developing the mathematical framework of the model, we construct the master equation governing transition (division) pathways of cancer cells, in section 3. We use a stochastic approach to gain a better understanding of the cellular heterogeneities inside the tumour. Thereafter, we use two steps of filtration of transition rates (out of a brute force process) to provide matching results with biological data, segregated into different microenvironmental conditions (including hypoxic, acidic, acidic-hypoxic and normal conditions). In the first step, realizations are aimed to reproduce the same fraction of cancer stem cells as reported in biological experiments and in the second part, the ability of the system to form neurospheres is taken into account. The initial conditions and constraints for the simulations are tuned to match the initial conditions of the relevant biological experiments. Finally, the results are presented and discussed. We also draw conclusion about

the effects of hypoxia and acidity as well as the simultaneous exposure of acidity and hypoxia on the transition rates of cancer cells and consequently on the tumour heterogeneities. The last chapter demonstrates the result of the implementation of the obtained transition rates under specific tumour microenvironmental conditions in the proposed cellular automata model that can mimic the behaviour of cancer cells in tumour tissue. The cellular automata model is equipped with a pushing mechanism that under specific circumstances enables the central cells to proliferate. The tumour microenvironmental conditions, including oxygen and glucose distribution, metabolic recruitment pattern of the tumour tissue and subsequent pH distribution, are added to the model and interact with the cellular automata. The distribution map of different cell phenotypes are provided along with the corresponding nutrient distribution, in the results section. At the end of the chapter 4, the same results as the third section of chapter 3 are confirmed through the realizations of the cellular automata model. These are discussed in the conclusion section.

2. Biological Background

2.1. Introduction to cancer

Cancer is a large family of diseases, over 100 different types [Hanahan and Weinberg 2000], characterized by uncontrolled division of abnormal cells, which are capable of invading surrounding tissues. Cancer cells may also spread to other organs of the body through blood and lymph vessels (metastasis). One may consider a tumour as an abnormal organ initiated by cancerous cells that through the accumulation of multiple mutations, have gained the ability of unbounded replication.

A large body of ongoing cancer research has been dedicated to identifying the dynamics of genetic changes that lead to cancer [Hanahan and Weinberg 2000]. Although these findings are large steps in recognizing relevant molecular and biochemical pathways, the incompatibility of experimental model cells, such as fibroblasts or cell lines, with actual tumour cells has left us with only a rough approximation of the fate of cells affected by such mutations [Reya et al. 2001].

2.1.1. Features of cancer cells

Cancer cells are cells affected by a series of mutations, which makes them gain cancerous properties. The multi-step, multi-site process of genetic alteration in the genome leads to the transformation of normal cells to cancerous cells [Hanahan and Weinberg 2000, Kinzler and Vogelstein 1996]. Even in "in vitro" experiments on rodent cells in culture, the transformation of cells to tumourigenic cells happens in at least two steps while the transformation of human cells requires more steps than rodents' [Hahn et al. 1999]. In spite of the vast diversity in cancer sites and types, and uncertainty about the trail of mutations leading to tumourigenesis, Hanahan and Weinberg [Hanahan and Weinberg 2000, Hanahan and Weinberg 2011] have proposed six necessary changes in cell physiology to make the cells capable of forming malignancies: self-sufficient signalling for growth, insensitivity to antigrowth signals, apoptosis evasion, potency to unlimited replication, sustained angiogenesis, metastasis and invasion into other tissues. Gaining any of these features is due to the destruction of the corresponding opposing counterpart mechanism in cells. For instance, the transition of normal cells from quiescent to proliferative state is dependent on the existence of mitogenic growth signals. The signal receivers are a group of transmembrane receptors that bind to diffusive growth factors, extracellular matrix component, and cell-cell adhesion/interaction molecules acting as signalling molecules. Cancer cells are strongly independent of exogenous growth

stimulations and are able to generate many of the essential signals for their proliferation. A large body of early-discovered oncogene regulates growth signalling autonomy [Hanahan and Weinberg 2000]. In glioblastoma multiforme, one of the most malignant and common brain tumours, and sarcoma, a cancer initiated by mesodermal cells, the production of platelet-derived growth factor (PDGF) and tumour growth factor-α (TGF-A), respectively, are enablers of the aforementioned growth signalling autonomy [Fedi et al. 1997].

Likewise, the cellular quiescence and tissue homeostasis in normal cells is maintained by several anti-growth signals such as soluble growth inhibitors and immobilized inhibitors in the extracellular matrix and on the surfaces of neighbouring cells. This anti-growth signalling can block the cell proliferation in two ways: first, temporally, where the cells are silent (G0 in cell cycle) till the extracellular matrix signalling allows them to proliferate in the future or second, permanently, where the cells are forced to enter the postmitotic state, that is, they are unable to proliferate anymore [Hanahan and Weinberg 2000]. Cancer cells are rendered insensitive to antigrowth signals by the disruption of retinoblastoma protein (pRb) and its two relatives, the p107 and p130 pathways. In the hypophosphorylated state, pRb seizes and modifies the function of E2F transcription factors that control the expression of vital genes for the transition from the G1 to S phase [Hanahan and Weinberg 2000,Weinberg 1995]. Thus the liberation of E2F transcription factors due to pRb disruption allows the cells to proliferate and makes them insensitive to antigrowth signalling [Hanahan and Weinberg 2000, Hanahan and Weinberg 2011].

The life duration of cells is determined by apoptotic machinery and ruled by controlling the extra/intracellular (ab)normality checks that are the sensory part of the machinery. The effector part of apoptotic machinery consists of cell surface receptors that bind to death or survival factors. For example, P53 tumour suppressor protein is a component of apoptosis circuitry and its inactivation results in the formation of tumours that rarely contain apoptotic cells [Symonds et al. 1994, Hanahan and Weinberg 2000, Hanahan and Weinberg 2011].

Although the three capabilities of growth self-sufficiency, insensitivity to antigrowth signalling and apoptosis evasion seem to be sufficient for a rapidly growing tumour, defunctionalisation of the cell-autonomous program that restricts the amount of cell replication is crucial in the formation of an aggressive tumour. Many studies support the observation that the majority of cancer cells propagated in culture have the ability of unbounded replication, suggesting that the tumour cells acquire this capability during the multi-step process of tumourigenesis and that the immortalization of cells is an essential feature of cancer cells [Hayflick 1997, Hanahan and Weinberg 2000, Hanahan and Weinberg 2011].

During organ formation in normal conditions, the indispensible oxygen and nutrient requirements of cells promotes the well-coordinated growth of vessels (angiogenesis) and parenchyma. While cancer cells do not have the ability to shape the essential angiogenic bed in a normal fashion, they must undergo angiogenesis to be able to grow to a large size [Bouck et al. 1996, Hanahan and Folkman 1996, Folkman 1997]. The normal tissue encourages or blocks the

angiogenesis by counterbalancing positive or negative angiogenic signalling whereas tumour tissue is not capable of balancing positive and negative signals. In order to promote angiogenesis, tumour cells can relatively increase the angiogenesis inducing factors relative to the inhibitors [Hanahan and Folkman 1996]. For instance, cancer cells alter gene expression to amplify the expression of vascular endothelial growth factors (VEGF) and/or fibroblast growth factors (FGF) or they may downregulate the expression of endogenous inhibitors such as thrombospondin-1 or beta-interferon. The upregulation of pro-angiogenic factors and the downregulation of anti-angiogenic ones may occur simultaneously, hence compounding the effect [Singh et al. 1995, Volpert et al. 1997].

There are several proteins responsible for the adhesion of cells to their surroundings. These proteins (that consist of cell-cell adhesion molecules and link the cells to extracellular matrix substrates) are functionally altered in tumour tissue. For example, defunctionalisation or interference in functionality of E-cadherin, a homotypic cell-cell interaction molecule expressed on epithelial cells, leads to the enhancement of invasion and metastasis [Christofori and Semb 1995]. The pathways that normal cells take to obtain the abilities necessary to form malignancies are variable. The acquisition of different features of cancer cells may not occur in the same chronological order from one cancer to another. Independent of the taken steps in genetic alteration taken in order to become cancerous, Hanahan and Weinberg [Hanahan and Weinberg 2000] believe that almost all types of tumour cells share the aforementioned six features, and have coined these as the hallmark capabilities of cancers.

2.1.2. Different types of cancers

Cancers are classified into five major categories: carcinomas, sarcomas, leukemias, lymphomas and central nervous system (CNS) cancers. The intensity of cancers is denoted by four grades which are associated with the level of severity of tumour malignancy where Grade I is a benign, slow-growing tumour while cancers grouped in Grade IV are the most malignant.

2.1.3. Brain cancers, different types and stages

CNS cancers (aka brain cancers) are growing neoplasms inside the cranium or in the central spinal canal. Brain cancers are classified according to the exact site of the tumour, the type of tissue involved, whether they are noncancerous (benign) or cancerous (malignant). But the most important classification for brain cancers is associated with the origin of the preliminary cancerous cells. In the majority of brain cancers, tumour initiating cells are originally parts of the CNS but in some cases the initiating cells originate from a non-adjacent tissue or organ that causes cancer after invasion and metastasis into the brain. Such metastatic cancers are known as secondary cancers as opposed to primary cancers that have the same origin and site for initiating cells and tumour formation. For example, breast cancer is known to be a metastatic disease and often results in secondary cancers in bone, liver, lung and

brain [Lacroix 2006].

The most common types of primary brain tumours are gliomas. Gliomas originate in glial cells, which are non-neuronal cells that provide support and protection for the brain neurons. Different types of glioma are named based on the histological similarities to specific cells, although they may not originate from that type of cell, for example:

- Astrocytomas (cancer cells similar to astrocytes)
- Oligodendroglioma (cancer cells similar to oligodendrocytes)
- Ependymomas (cancer cells similar to ependymal cells)
- Mixed Glioma (contain a combination of cells similar to different types of glial cells)

2.1.4. Particular case of GBM

According to the World health organization (WHO) in 2007, malignant gliomas were classified among the most fatal brain tumours [louis et al. 2007]. Astrocytomas are the most common type of gliomas that develop from, star-shaped glial cells, astrocytes. Grade IV astrocytoma, Glioblastoma Multiforme (GBM), is one of the most frequent, aggressive and chemoresistant primary brain tumours, with a median patient survival time of 6-12 months in adults and a bleak prognosis where tumour recurrence is likely after surgery [Eramo et al. 2006]. Therefore, GBM has attracted significant media attention due to its low long-term survival rate, prevalence, malignancy and resistance to different therapies. This also makes it an important target for current research.

2.2. Abnormal tumour microenvironment

Augmented and unlimited replication of cancer cells in a tissue that is not designed to host them normally promotes the heterogeneity of the tumour microenvironment and causes it to differ from the normal interstitium. In a reciprocal fashion, the tumour microenvironment has a profound effect on cancer cells. Some previous studies point to the close interaction of cell and matrix as well as cell- cell interactions that should be taken into account in determining cancer cell response to internal and external stimuli [Hill et al. 2009]. Such interactions are not restricted to tumorigenic tissues, but play an important and functional role in normal environments as well [Hill et al. 2009].

The tumour microenvironment affects cancer cells through the endocrine, paracrine and autocrine signalling pathways, by means of chemicals, chemicals and physical forces from neighbouring cells and positive feedback signalling loops generated by the cancer cells themselves [Fedi et al. 1997]. Cell responses to such conditions include: alteration in signalling, division, differentiation, apoptosis, adhesion and migration.

Among all the features of the tumour pathophysiologic microenvironment, hypoxia, low pH and nutrient deprivation appear to have the strongest effects on spatial and temporal heterogeneity within the tumour microenvironment [Vaupel and Mayer 2007].

2.2.1. Angiogenesis

As the mass of solid cancer cells grows larger, the density of pre-existing normal vessels inside the tumour decreases. To obtain sufficient oxygen and other nutrients the cells must be at most 100 μm away from a blood vessel [Hanahan and Weinberg 2000]. In normal organogenesis this distance is not exceeded since the vessels grow in a well-organized manner so that the necessary closeness of cells and blood vessels is insured. Normal cells regulate the process of new vessel formation, angiogenesis, inside the organ and maintain the coordinated vessel network. Cancer cells are initially unable to regulate a proper vessel network to keep up with the increasing demand of oxygen and other nutrients inside a tumour [Bouck et al. 1996, Hanahan and Folkman 1996, Folkman 1997]. The inability of cancer cells to generate a thriving mass of cells covered by coordinated vessels is due to the imbalance of pro/anti angiogenic factors. VEGF is the dominant growth factor involved in triggering angiogenesis inside the tumour. VEGF upholds the survival and proliferation of endothelial cells that form the inner lining of vessels. In normal tissues, the effect of VEGF is counterbalanced by anti-angiogenic factors such as thrombospondin so that new normal vessels in processes like wound healing are formed under a fine balance of proangiogenic and antiangiogenic growth factors. When VEGF signalling is upregulated abnormally, as in tumour tissues, the elevated amounts cause the vessels to become more permeable than normal. The aberrant leaky vessels have disfunctionally oversized pores and do not have the regular and efficient coverage for the cells they support [Jain 2008]. These deficiencies increase the interstitial fluid pressure (IFP) in tumour tissues. Hence, the challenges for tumour cells are not only oxygen and nutrient deprivation but also high pressure

inside the tumour due to the vessel leakage and the accumulation of tissue waste products.

On one hand, the lack of sufficient oxygen content in tumours, hypoxia, and on the other hand, the accumulation of wastes products from defective cancer cells, destabilize the microenvironmental homeostasis. The tumour microenvironment is considerably acidic since first, in the absence of oxygen, hypoxia causes the cancer cells to switch to a glycolytic metabolism than the normal aerobic metabolism of respiration; second, the malfunctioning blood vessel network and lymph system are not able to clean the tumour microenvironment; and thirdly, cancer cells abnormally tend to utilize other metabolisms than respiration even in the presence of sufficient oxygen.

The formation of new blood vessels is a result of either the pre-existing vessels sprouting into the tumour, generally known as angiogenesis, or vessel assembly from endothelial precursors, vasculogenesis. Although vasculogenesis was considered to be restricted to embryonic development for a long time, recent studies have demonstrated that some of the endothelial cells inside the tumour are more similar to tumour cells than to pre-existing endothelial cells in terms of somatic mutations [Wang et al. 2010, Ricci-Vitiani et al. 2010]. In GBM, one of the most angiogenic malignancies, a subpopulation of cancer cells strongly promotes angiogenesis through the release of VEGF and stromal-derived factor1. These minor but functionally dominant cancer cells have the same genomic alteration as 20-90% (mean 60.7%) of tumour endothelial cells [Ricci-Vitiani et al. 2010]. This finding suggests that typically more than half of the GBM endothelial cells have their origin in the neoplasm.

Atypical blood and lymph circulation is the golden link in the chain of tumour microenvironment abnormalities. Except for the innate tendency of cancer cells to

switch to other metabolisms than respiration, all other key features of the tumour microenvironment, such as high IFP, hypoxia and acidity are clear results of the tangle of dysfunctional vessels.

In spite of many antiangiogenic methods that cause the destruction of the vasculature inside the tumour, some methods aim to normalize them instead. In these methods the delivery of chemotherapeutic agents is the final goal and is achieved by balancing anti and proangiogenic factors that lost their equilibrium during the growth of the tumour [Jain 2005, Jain 2008].

2.2.2. Hypoxia

The state of low levels of oxygen, hypoxia, is perhaps the most important feature of the tumour microenvironment. The fluctuation of oxygen concentration in the tumour microenvironment is the outcome of irregular blood flow, poor oxygen diffusion across the tumour and the chaotic vascular network within the tumour [Heddleston et al. 2010]. Severe hypoxia may result in upregulation of pro-apoptotic pathways and consequently cell death; genotoxic effects are the outcome of prolonged hypoxia and are caused by the induction of reactive oxygen species (ROS) [Heddleston et al. 2010]. The commonly observed necrotic tumour core is the mass of dead cells that could not survive the hypoxic conditions. Hypoxia may also have other extensive transcriptional effects, for instance the activation of pro-angiogenic pathways.

Persistence of the hypoxic condition inside the tumour tissue leads to the induction of hypoxia inducible factors (HIFs). The activity of HIF proteins boosts the tumour progression through the upregulation of angiogenesis, alteration of cellular

metabolism and invasion [Hill et al. 2009, Heddleston et al. 2010, Keith and Simon 2007, Seidel et al. 2010, Bao et al. 2009, Heddleston et al. 2009, McCord et al. 2009, Li and Rich 2010].

HIF transcription factors are generally categorized into two subunits, α and β, each having three members (HIF-1α, HIF-2α, HIF-3α, and HIF-1β, HIF-2β, HIF-3β). The constantly expressed beta subunits are insensitive to oxygen and act as receptors for their α counterparts [Liao and Johnson 2007]. In normoxic conditions, the activity of HIF-α is decreased by prolyl hydroxylases (PHDs) that bind to Von Hippel Lindau proteins for final degradation of HIF-α via ubiquitin-proteasome pathways [Hill et al. 2009, Berra et al. 2003, Semenza 2004]. In the absence of an adequate level of oxygen, the reduction of oxygen-dependent activity of PHDs increases the unsuppressed expression of HIF-α [Semenza 2004].

Hypoxia inside the tumour varies spatially and temporarily [Heddleston et al. 2010]. Due to the aberrant blood flow and abnormal vascular structure, hypoxic cycles are more considerable in microvasculature regions [Kimura et al. 1996]. The fluctuation of oxygen content causes the alteration of HIF activity. The importance of identifying hypoxic regions is not only limited to the prominent effect of hypoxia in promoting angiogenesis, proliferation and tumour invasion but also extends to the radio-resistance of hypoxic regions [Moeller et al. 2004, Dewhirst et al. 2008].

HIFα is a key regulator that triggers angiogenesis through direct activation of vascular endothelial growth factors [Forsythe et al. 1996, Olsson et al. 2006]. Therefore, HIFα plays a critical role in tumour angiogenesis since the tumour vascular network is known to be strongly dependent on VEGF-recruiting pathways. VEGFs are cell surface bound proteins that promote proliferation, migration and survival of endothelial cells by binding to the specific high affinity transmembrane proteins on endothelial cells [Bao et al. 2006]. In order to form new vasculature

inside the tumour, VEGF promotes the activity of endothelial precursors.

Besides the probable promoted genetic mutations, the upregulation of HIF under low oxygen tension can also affect cell differentiation. In some cancer studies, the origin of the majority of endothelial cells has been shown to be cancer cells. These studies demonstrate that the differentiation of non-endothelial CD133+ cancer cells to endothelial cells is highly positive-correlated with the intensity of hypoxia in a tumour [Wang et al. 2010, Ricci-Vitiani et al. 2010]. Some other studies have demonstrated that hypoxic conditions enhance genetic mutations, which elevate the pluripotency of cancer cells and lead to more malignant tumours [Seidel et al. 2010, Bao et al. 2009, Heddleston et al. 2009, McCord et al. 2009, Li and Rich 2010, McLendon and Rich 2011].

2.2.3. Acidity

The acidity of the tumour microenvironment is a result of abnormalities in the microenvironment and cancer cell characteristics. Hypoxia, as a common feature of the tumour microenvironment, blocks the process of respiration for cells. Although respiration, as the first potential choice of normal cells, is the most efficient cell metabolism to satisfy cell energy requirements (ATP), cancer cells may switch to other metabolisms such as glycolysis and glutaminolysis to survive in hypoxic conditions. Cancer cells may preferentially select a glycolytic metabolism even in the presence of sufficient oxygen for respiration. In this situation, called the Warburg effect or aerobic glycolysis, the produced ATP is one eighteenth of the energy provided by the oxidation of one molecule of glucose in the respiration reaction. Grüning and Ralser [Grüning NM, Ralser M. 2011] have very recently proposed that the reason behind the tendency of cancer cells to glycolysis rather than respiration is to avoid the accumulation of reactive oxygen species that cause oxidative damage.

Hence, the uptake of glucose to generate the energy through glycolysis is more than the amount of glucose uptake in respiration. However, the main problem of having glycolysis rather than respiration in cancer tissues is the accumulation of products of glycolysis reaction such as hydrogen ions. Impairments in the glycolytic pathway result in cancer cells switching to a glutaminolytic metabolism [Helmlinger et al. 2002]. In healthy tissues, neutrality is maintained through the balanced contributions of vascular and lymphatic systems in supplying nutrient and collecting waste and also the involvement of the natural buffering systems. The most prominent buffering reaction is the interconvertion of bicarbonate and carbon dioxide. However, the aberrant structure of the vasculature and lymph inside the tumour tissue, and the excess accumulation of waste products, especially hydrogen ions, makes the tumour microenvironment acidic.

Similar to hypoxia, high acidity of the tumour microenvironment has been observed to affect cancer cell reprogramming and worsen tumour malignancies [Hjelmeland et al. 2011]. The immune system, as the first natural guard against abnormal cancer cells that survive the internal protection paths, is paralyzed in an acidic microenvironment. The situation is even worse, since hypoxia and acidity are both ubiquitous in cancer tumours. Although the spatiotemporal profiles of hypoxia and acidity are not fully correlated [Helmlinger et al. 1997], they are both critical features of the tumour microenvironment and play dominant roles in the progression of tumour malignancies.

The partial pressure of oxygen, which is inversely related to the level of hypoxia, strongly correlates with pH in tumour microenvironment on average. However the heterogeneities between partial pressure of oxygen (pO2) and interstitial pH profiles and incompatible relation between local pO2 and pH profile have been reported in some “in vivo” experiments [Helmlinger et al. 1997].

In spite of the aforementioned relationship between of pH and hypoxia, these two

prominent microenvironmental factors seem to act independently to promote vascular endothelial growth factors [Fukumura et al. 2001]. In vivo experiments done by Fukumura et al. support the autonomous role of acidity and hypoxia in VEGF up-regulation [Fukumura et al. 2001]. Their study, focused on brain cancers, proposing that although the effect of acidity and hypoxia are not correlated on VEGF promotion, there is no additive effect of both in regions exposed to hypoxia and acidity simultaneously. An explanation for this non-additive effect may be the fatal consequences of the coincidence of hypoxia and acidity that causes apoptosis [Fukumura et al. 2001]. Casciari et al. in their 1992 experiments have confirmed the results of Fukumura et al. [Casciari et al. 1992]. Their experiment investigated cell growth rates and metabolism under different oxygen and glucose concentrations and extracellular pH. They state that cell growth rates in regions exposed to hypoxia and acidity simultaneously is less than that when exposed to only one of hypoxia or high acidity.

2.2.4. High interstitial fluid pressure

Mainly due to abnormal angiogenesis, IFP is highly elevated in solid tumours. Other factors involved in elevation of IFP are lymph vessel abnormalities, interstitial fibrosis and the contraction of the interstitial matrix mediated by stromal fibroblasts [Heldin et al. 2004]. The elevated level of IFP in tumours opposes the transcapillary oxygen and nutrient transport and waste collection that makes the situation bleak for cancer cells. However, a major concern about high IFP is the resulting decreased efficiency in therapeutic agent uptake. Some methods have been introduced in order to improve therapeutic agent uptake, for instance, Heldin et al. proposed the usage of signal-transduction antagonists to lower IFP [Heldin et al. 2004]. However,

considering the chaotic and dysfunctional vasculature inside the tumour, it is hard to maintain the IFP at normal levels.

2.3. Brain cancer stem cell hypothesis

2.3.1. Stem cells and cancer stem cells hypothesis

There are many different types of standard treatments designed to stop tumour growth, but the overwhelmingly frequent failures of these conventional procedures have revealed that the current knowledge (about tumour growth dynamics, the interaction of cancer cells with the tumour microenvironment and the disruptive mechanism of therapeutic agents) is not comprehensive enough. One source of the complexity of tumour development and growth is tumour heterogeneity. These heterogeneities are the result of on-going mutagenesis and/or the differentiation of cancer cells [Reya et al. 2001]. The expression of some differentiation markers by tumour tissues supports the cancer cell differentiation argument [Reya et al. 2001]. The diverse clusters of cancer cells inside the heterogeneous tumour do not only differ in phenotype and differentiation state, but also in proliferative potential and ability to increase tumour progression. For the first time, some evidence in leukaemia and more recently in solid tumours, such as breast cancers, supports the distinct functionality of different subpopulations of cancer cells [Singh et al. 2004]. This evidence suggests that there may be a small subpopulation of cancer cells capable of tumour initiation, tumour maintenance, and differentiation to some other progenies [Reya et al. 2001, Singh et al. 2003, Singh et al. 2004, Dirks 2008]. The existence of such a subpopulation of cancer cells is proposed in the “cancer stem cell hypothesis”. According to the cancer stem cell hypothesis, although this subpopulation is a small fraction of tumour cells, it is the dominant factor in the

progression of a tumour malignancy and is known to be both necessary and sufficient to maintain tumours. Due to the four basic similarities they share with normal stem cells [Fuchs and Segre 2000, Weissman 2000, Reya et al. 2001], they are known as “cancer stem cells”. In analogy with normal stem cells, cancer stem cells (CSC) are able to differentiate to other cell types, they can self renew through symmetric division, they are capable of forming colonies, and they express the same surface markers as normal stem cells. They are also comparable with normal stem cells in the size of the population, as many studies have reported that the population of cancer stem cells is 5-15% of the bulk of tumour cells [Dirks 2008, Chaffer et al. 2011].

2.3.2. CD133

Beside the functional similarities between normal and cancer stem cells, they also have some physiological resemblances; for instance, some of the well-known biomarkers to target normal neural stem cells are also expressed by neural cancer stem cells. Nestin, a cytoplasmic intermediate filament protein, is expressed by normal and cancerous stem cells [Hockfield and McKay 1985, Lendahl et al. 1990, Gates et al. 1995]. But nestin is not a perfect marker for normal or cancer stem cells since the neural progenitors do express nestin as well. Therefore, in spite of the similar identity of normal and cancer stem cells biomarkers, the absence of reliable biomarkers for normal neural stem cells clouds the issue of identification of neural cancer stem cells.

Lately, direct isolation of normal neural stem cells from human foetal brain suggested that the cell surface marker CD133 (AC 133, prominin1) could be a good candidate to target normal and cancerous neural stem cells [Singh et al. 2004, Singh et al. 2003]. Singh et al. (2003) reported that after fractionation and purification of brain cancer cells which CD133+ expression, they found that like normal stem cells, this minor subtype of neural cancer cells are capable of proliferation, differentiation

and self renewal. Despite these analogous functional characteristics, normal and cancer neural stem cells express nestin and CD133+, while none of them express the neural differentiation markers [Singh et al. 2003, Singh et al. 2004].

2.4. Cancer stem cells and tumour microenvironment

The condition of the tumour microenvironment that is determined by the level of hypoxia, acidity, IFP, nutrient concentration, and generally extracellular matrix composition, accompanied by the distribution of different cell types in the heterogeneous tumour strongly affect the stem cell fate to self-renew or to differentiate [Moore and Lemishka 2006]. The dependence of cancer stem cells' fate (self renewal or differentiation) to tumour microenvironmental factors is even higher than normal stem cells since the intrinsic and extrinsic cellular mechanisms are all exaggerated inside the aberrant structure of tumours. Therefore, based on the specific constellation of microenvironmental factors, the tumour region is partitioned into sub-regions which each upregulates specific features of cancer cells; one may promote the self- renewal of cancer cells while others may suppress it [Calabrese et al. 2007, Gilbertson and Rich 2007, Jandial et al. 2008].

2.4.1. Cancer stem cells and vascular niches

Normal stem cells quiescence, self-renewal and differentiation are controlled by microenvironmental factors. Protective niches that normal stem cells lie in, suppress the excessive proliferation and differentiation of stem cells and keep them quiescent [Calabrese et al. 2007, Moore and Lemishka 2006]. Nonetheless, inside tumour tissues, the critically abnormal microenvironment and mature types of neighbouring

cells are not able to suppress the cancer stem cells' self-renewal. The perivascular niches are known to be one of the self-renewal promoting niches for BCSCs [Calabrese et al. 2007]. The endothelial cells are well recognized to dominantly affect BCSCs and secrete factors that promote self-renewal rather than quiescence or differentiation. Endothelial cells that closely interact with cancer stem cells encourage self-renewal through the secretion of supporting factors [Calabrese et al. 2007]. On the other hand, cancer stem cells upregulate the process of angiogenesis through the secretion and recruitment of pro-angiogenic factors such as VEGF, VEGFR2, angiopoietin 2, and stromal derived factor 1 [Bao et al. 2006, Calabrese et al. 2007, Gilbertson and Rich 2007, Folkins et al. 2009, Lathia et al. 2010]. This reciprocal interaction of cancer stem cells and the tumour microenvironment results in the formation of perivascular niches to host cancer stem cells that seem to mimic normal stem cell niches in healthy tissues [Calabrese et al. 2007, Gilbertson and Rich 2007, Jandial et al. 2008].

The effectiveness of anti-angiogenic therapies for GBM patients suggests that angiogenesis and a vascular bed are indispensible features to maintain GBM [Aghajanian et al. 2011,Batchelor et al. 2007]. The interesting fact is the use of anti-angiogenic therapies does not affect the proliferation and survival of nonstem cancer cells and the improvements are due to blocking the growth of the tumour via depleting the vasculature from the cancer stem cells niches [Gilbertson and Rich 2007].

In spite of the ability of GBM cancer stem cells to upregulate angiogenesis, recent studies have revealed the contribution of vasculogenesis in GBM tumours [Wang et al. 2010,Ricci-Vitiani et al. 2010]. According to Vitiani et al. and Wang et al. (2010), phenotypic similarities between cancer stem cells and almost half of tumour endothelial cells suggest the cancerous origin of endothelial cells. They have

suggested that together with vasculature formation by sprouting of pre-existing vessels through angiogenesis, the differentiation of cancer stem cells to endothelial cells produces a large proportion of the GBM vascular network [Wang et al. 2010, Ricci-Vitiani et al. 2010]. The ratio of endothelial cells that have the same genomic alteration as the GBM cancer stem cells is reported to vary from 20% to 90% (Mean 60%) of total endothelial cells inside the tumour [Ricci-Vitiani et al. 2010].

The vital importance of cancer stem cells existence in tumour maintenance, the reciprocal impact of vasculature network on cancer stem cells and the partial effectiveness of anti-angiogenic therapies in malignancies such as GBM highlights the necessity of more research in this field.

2.4.2. Cancer stem cells and hypoxia

The spatiotemporal fluctuation of oxygen inside the tumour causes transcriptional activity of hypoxia inducible factors that respond to hypoxia through pro-angiogenic or pro-glycolytic pathways [Heddleston et al. 2010]. Hypoxia increases the number of cells expressing CD133, known as a marker for BCSC, in gliomas [Platet et al. 2007].

In contrast with HIF-1α that is a hypoxia inducible factor expressed by stem and non-stem cancer cells, HIF- 2α is only expressed by cancer stem cells [Bao et al. 2009]. The poor survival of GBM patients is negatively correlated with the expression of HIF-2α inside the tumour. The mechanism that HIF-2α uses to provoke angiogenesis, the same as HIF-1α, is through the increase of the expression of VEGF [Bao et al. 2009, Bao et al. 2006]. However, the increase in VEGF expression has been shown to occur in a cell-specific manner so that the VEGF expression induced by hypoxia in BCSCs is higher than the level of VEGF expressed in non-stem cancer cells exposed to the same level of hypoxia [Bao et al. 2009].

In a related study, Heddleston et al. (2009) proposed that hypoxia promotes the self-renewing capacity of cancer stem cells and upregulates the reprogramming of non-stem cancer cells toward a stem-like phenotype [Heddleston et al. 2009]. The promotion of stem-like phenotypes by hypoxia functionally leads to increased neurosphere formation and biologically results in the upregulation of stem cell factors such as OCT4, NANOG and c-MYC [Heddleston et al. 2009].

Seidel and colleagues reported the same results with a focus on the role of HIF-2α [Seidel et al. 2010]. First, they hypothesized that HIF-2α plays a significant role in inducing the stem-like phenotype in the hypoxic region of GBM tumours. To test this hypothesis, they knocked down HIF-2α and observed the reduced inducement of the stem-like phenotype due to hypoxia [Seidel et al. 2010].

Another difference between HIF-1α and HIF-2α is their sensitivity to hypoxia. HIF-1α, which is associated to both stem and non-stem cancer cells, is only activated in severe hypoxic condition (when the oxygen level is less than 1%); whereas HIF-2α associated with stem cells, is expressed in less severe levels of hypoxia (when the oxygen concentration is 2% to 5%) [Bao et al. 2009]. The relevance of such an affiliation of hypoxia inducible factors has been confirmed by some other studies [Seidel et al. 2010].

Suggesting the necessity of the presence of at least one cancer stem cell for active metastatic growth, Hill et al. (2009) have provided a more detailed view of the effect of hypoxia on metastasis [Hill et al. 2009]. Under hypoxic conditions, cancer stem cells start to respond to the oxygen shortage through the transcriptional factors, HIF-1α and HIF-2α which each has a different role in tumour progression. HIF-1α promotes the undifferentiated state of cancer stem cells through the upregulation of Notch signalling. HIF-1α is also known to upregulate motility, invasion and metastasis through the elevation of CXCR4 (specific receptor for stromal derived factor-1), MMPs (matrix metalloproteinases), uPAR (urokinase receptor), and VEGF. Equally important, HIF-2α controls the cancer stem cell maintenance through the induction of Oct-4 (octamer-binding transcription factor 4) and also increases cancer stem cell proliferation by activating c-MYC [Hill et al. 2009].

Hence, hypoxia generally influences cancer stem cells in proliferation, self-renewal, differentiation, motility, invasion and metastasis and affects the tumour microenvironment by the promotion of angiogenesis and vasculogenesis.

2.4.3. Cancer stem cells and acidity

The tumour microenvironment acidity is due to abnormalities in the microenvironment and the characteristics of cancer cells. Hypoxia, as a common feature of the tumour microenvironment, inhibits the process of respiration for cells and also upregulates the glycolytic pathways. Accompanied by the abnormal tendency of cancer cells to switch to glycolysis rather than respiration (Warburg effect), the inefficiency of the natural buffering system in responding to the accumulated amount of hydrogen ions due to the aberrant vascular and lymphatic systems, results in an acidic microenvironment inside solid tumours.

Despite the prominent effect of high acidity on cancer cells, cancer stem cells are also reciprocally influenced by the high acidity of the tumour microenvironment. In their recent study, Hjelmeland et al. (2011) have proposed that the exposure to low pH of glioma cells leads to the enhancement of stem-like biological and functional properties of the cancer cells. Independent of hypoxia, acidity promotes the expression of pluripotency markers that are normally expressed by neural stem cells such as Olig2, Oct4 and Nanog. The increase in expression of these markers in the low pH range is from six to eight fold higher than under normal pH conditions. On the other hand, the expression of differentiation markers under acidic conditions is noticeably decreased. In addition to the biological effect, low pH promotes neurosphere formation and tumorigenic capacity of glioma stem cells. Neurospheres are non-adherent and free floating spherical structures generated by neural stem cells.

Moreover, high acidity upregulates angiogenesis through the increased induction of

VEGF. The expression of HIF-2α, as a hypoxia-inducible factor associated with cancer stem cells, is increased noticeably, while there is no significant change in the expression levels of HIF-1α under the exposure of low pH [Hjelmeland et al. 2011].

2.5. Summary

Cancer stem cells are believed to be the predominant factors driving tumour progression and strongly correlate with tumour malignancies. Therefore, the dependence of cancer stem cell behaviour on the microenvironment highlights the importance of developing both a comprehensive spatiotemporal map of the tumour microenvironmental factors (nutrients concentration, pH and IFP) and a deeper understanding of the dynamics of cancer stem cell behaviour.

3. Modeling Cancer Stem Cell

GBM is the most common brain tumour found in adults. GBM is also the most aggressive type of primary brain tumour with a very poor prognosis and low long-term survival rates. Regardless of their age, most patients with GBM die in less than one year. The dominant role of GBM cancer stem cells to boost neurosphere formation, cancer invasion and metastasis, beside their prominence as a potential source of vasculogenesis along with angiogenesis in tumour tangled vascularisation highlights the importance of in-depth studies about BCSC dynamics.

Tumour microenvironmental factors such as hypoxia, acidity, and the abnormal vascular network highly influence the fate of stem and non-stem cancer cells to become quiescent, proliferating, differentiating or reprogramming toward a stem-like phenotype. In addition, the efficiency of the therapy is highly dependent on the tumour microenvironmental conditions and the state of BCSC.

The interaction of cancer cells and tumour microenvironmental factors is highly complex and not well investigated. On the other hand, animal or in vitro studies are not accurate enough and suffer from lack of correlation with human data. Along with

aforementioned issues, the low survival rates and the excessive cost of using ineffective therapies necessitate the development of mathematical models and computer simulations to model tumour growth.

The advantages of in silico modeling of cancer growth is that one can control variables such as different types of cancer cells and the various microenvironmental factors simultaneously to simplify the complex interaction map between the involved variables. Also, the order of importance among the affecting factors can be revealed through systematic approaches utilizing the mathematical and computational models. This is analogous to biological experiments with various genetically modified mice. Moreover, the merit of mathematical and statistical tools to analyze biological data and make testable hypotheses must not be underestimated [Kam et al. 2012].

3.1. General models for cancer growth

The proposed models for tumour growth, invasion and metastasis can be divided into three broad categories: continuum, discrete and hybrid models. In continuum models, a cancer tumour is considered to be a continuous porous solid comprised of cancer cells where the pores are filled with interstitial fluid. In contrast, discrete models are focused on the individual cancer cell and its contributions towards` tumour survival and progression. These agent-based (cell-based) models are conventionally classified with respect to the incorporation of cell structure details in the model; the model may consider the cells as nuclei-centered species or deformable structures [Preziosi 2003, Araujo and McElwain 2004, Anderson et al. 2007, Byrne and Drasdo 2009, Lowengrub et al. 2010, , Rejniak and McCawley 2010, Rejniak et al 2010, Rejniak and Anderson 2011].

The complex interactions between cancer cells and the tumour microenvironment

over different time and space scales necessitate the combination of continuum and discrete models. Hybrid models, mixtures of continuum and discrete models, can provide insights which can not be obtained using either method alone. Hybrid models benefit from the agent-based setup of discrete models to model the cell-cell, cell-ECM interactions and take advantage of continuous methods to model the integrated tumour tissue [Rejniak and Anderson 2010].

3.1.1. Previous work

Tumour proliferative growth and invasion have been widely studied through theoretical and computational modeling [Perumpanani and Sherratt 1996, Sherratt and Nowak 1992, Tracqui 1995]. Duchting and Vogelsaenger were among of the pioneers of computational-mathematical modeling of tumour proliferation. They proposed a three-dimensional cellular automaton on a cubic lattice to model the growth of small tumours. The model considered the cells' requirements for nutrition but not cell-cell interaction or other microenvironmental factors [Duchting and Vogelsaenger 1985].

Afterwards, Qi and colleagues (1993) reproduced Gompertzian results for tumour proliferation. They used a two-dimensional cellular automaton where only those cells with empty neighbours were able to divide. The inability of cancer cells to push aside neighbouring cells in order to make space for their division weakened the ability of their model to satisfy biological constraints and restricted the simulated tumour size to very small size. They also considered the dissolution of dead cells as a result the models could not generate the necrotic cores of tumours. The transition switches from quiescent to proliferative states were chosen stochastically however, as considered in Duchting and Vogelsaenger's model, the role of nutrition to turn on and off the division cycles is not negligible [Duchting and Vogelsaenger 1985, Qi et al. 1993].

The concepts of cancer cell migration and macroscopic behaviour patterns of cancer cells affected by growth factors have been introduced more recently by Smolle and Stettner [Smolle and Stettner 1993]. Duchting and Vogelsaenger, they considered a cubic lattice. Although the cubic or square lattices simplify the study of automata organization, the resultant asymmetric and other artificial lattice effects are not desired [Duchting and Vogelsaenger 1985].

For example, modeling of macroscopic tumour growth can be found in the work of Wasserman and colleagues (1996). They applied the finite element technique to model the macroscopic behaviour of cancer tumour. Chaplain and Sleeman also used an analogous methodology to construct a model governed by a strain-energy function according to nonlinear elasticity theory [Chaplain and Sleeman 1993].

Gompertz models have also been used extensively in tumour growth modeling. These models describe the evolution of tumour volume over time. The tumour growth rate is considered to be exponential at first and gets saturated at large times [Steel 1997]. These models have been criticized for the fact that tumours may contain a number of clones with different growth rates and different nutritional needs, but the Gompertz model cannot incorporate these diversities [Duchting and Vogelsaenger 1985].

To add the competitive effect of multi-clonal tumours, Cruywagen and colleagues proposed the Jansson-Revesz equation. This equation assumes logistic growth (Lotka-Volterra equation) of tumours equipped with the possibility of conversion of one species to another. They also added a diffusive term to each Jansson-Revesz equation to compensate for the biological passive cellular motion [Cruywagen et al. 1995]. In spite of the ability of these models to describe the general size of the tumour, the lack of cellular motility and inability to expand the modeling to multiple populations beyond two, is a severe limitation [Marusic et al. 1994].

To model the growth of the tumour necrotic core, the continuum mechanics approach has been widely used. In such models, spatiotemporal differential equations are used to describe the necrosis growth. For instance, Adam (1986) used an ordinary differential equation and a reaction-diffusion equation to reflect the mass

conservation of tumour cells and nutrient diffusion respectively [Adam 1986]. A comparable approach was used by Ward and King (1997). They formed a system of nonlinear partial differential equations to describe the growth of an avascular tumour and nutrients diffusion within the tumour [Ward and King 1997]. More recently, Byrne and Chaplain (1998) improved Ward and King's model by adding the explicit effects of apoptosis and necrosis [Byrne and Chaplain 1998].

The selection of the type and intensity of therapy to treat the cancer has a major effect on the growth trends of tumours. There are some notable models that consider the impact of therapy on tumour growth, among these, work done by Tracqui and colleagues (1995) and Woodward and colleagues (1996) are noteworthy [Tracqui et al. 1995, Woodward et al. 1996].

3.1.2. Stem cell growth models

Cancer stem cells, like their normal counterparts, are able to divide symmetrically or asymmetrically. Through the symmetrical process, cancer stem cells divide into two progenitors (full-differentiation) or two cancer stem cells (full-self-renewal). The asymmetric process ends in the birth of one cancerous progenitor and one cancer stem cell. These can be summarized as below:

$$S \rightarrow S + S$$
$$S \rightarrow S + P$$
$$S \rightarrow P + P$$

Where S denotes a cancer stem cell and P is a progenitor. Progenitors are more mature cells with the potential for a restricted number of divisions as opposed to the limitless capability of cancer stem cells for symmetric and asymmetric divisions.

The recent mathematical model of Boman and colleagues supports the hypothesis that the self-renewal of cancer stem cells is largely responsible for the formation of

the overpopulated cancerous clones found in colorectal cancer [Boman et al. 1997]. Wichmann and Loeffler have proposed a cancer stem cells hierarchical model for the hematopoietic system [Wichmann and Loeffler 1985]. Michor and colleagues have added treatment analysis to the hierarchical model of cancer stem cells as have Johnson et al. for chronic myeloid leukemia and colorectal cancer respectively [Michor et al. 2005, Johnston et al. 2007]. In the case of gliomas, the proposed continuous models by Swanson and colleagues [Swanson et al. 2008] and Stein et al. [Stein et al. 2007] are remarkable examples. Swanson et al. do not consider the cancer stem cell hypothesis but base their model on a microenvironmental heterogeneous bed for a homogenous population of brain cancer cells. Stein and colleagues, distinguished two subpopulations of brain cancer cells, are in the tumour core and the often more invasive cancer cells in tumour margins. Improving the Wichmann and Loeffler's model, Ganguly and Puri [Ganguly and Puri 2006, 2007] pioneered the application of the cancer stem cell hypothesis to model gliomas.

To illustrate the mechanisms behind brain tumour growth, our group has recently proposed a stochastic discrete model [Turner et al. 2009]. The assumed stochasticity not only matches the observed biological phenomena, but also makes the model applicable when working with small numbers of cells [Turner et al. 2009, Clayton et al. 2007]. This model aims to characterize brain tumours and predict the effectiveness of potential therapies. According to our previous model, the classification of cancer cells into stem and non-stem cancer cells is of major importance since the presence of cancer stem cells is the dominant factor in tumour growth and progression. Moreover, the incidence of self-renewal division rather than full-differentiation of cancer stem cells make the tumours more resistant to therapies and increase the survival rates of tumour [Turner et al. 2009].

Recent studies of tumour microenvironmental factors and their interactions with cancer cells in tumour progression have revealed that non-stem cancer cells can dedifferentiate into stem-like cancer cells [Wang et al. 2010, Ricci-Vitiani et al. 2010, Seidel et al. 2010, Bao et al. 2009, Heddleston et al. 2009, Hjelmeland et al. 2011, Chaffer et al. 2011, Denysenko et al. 2010]. The new cells produced through

cell reprograming are able to form neurospheres and also express the biomarkers of normal stem cells. The functional and biological features of these stem-like cancer cells assert their abilities to form neurospheres as well as the expression of stem cell surface markers. This data proves compelling evidence that the tumour microenvironment can promote the stem cell even in the initial absence of cancer stem cells depleted culture.

3.2. Model Foundation and assumptions

The current model is based on the model proposed by Turner et al. [Turner et al. 2009]. In the previous model, two basic subpopulations of cancer cells were assumed: cancer stem cells and progenitors. Hence the symmetric and asymmetric division of cancer stem cells and progenitors can be summarized as below:

$$S \rightarrow S + S$$
$$S \rightarrow S + P$$
$$S \rightarrow P + P$$

$$P \rightarrow P + P$$
$$P \rightarrow S$$

the first three division pathways are cancer stem cells pathways and the last two are for progenitors. The first pathway denotes the symmetric division of cancer stem cells, self-renewal, and the third represents the symmetric full-differentiation. The second, asymmetric pathway of cancer stem cell division is known to have a slightly more of an effect on tumour malignancies compared with the first. The fourth pathway shows the division of a progenitor. As opposed to stem cells, progenitor replications are limited hence their division process will terminate at some point. While the last pathway denoting the progenitor dedifferentiation confers immortality to the bulk of cancer progenitor cells. The existence of the last pathway has been

reported by Chaffer et al. [Chaffer et al. 2011]. In their recent work, Weinberg and colleagues [Chaffer et al. 2011] have challenged the conventional hierarchical model of the cancer stem cells. Their experimental results go against the traditional view of unidirectional differentiation of cancer cells. Instead they have proposed a bidirectional interconversion between cancer stem cells and non-stem cancer cells. Focusing on the human mammary epithelial cells in breast cancer, they have also reported the spontaneous reprograming of more differentiated cell types, progenitors, to stem-like cancer cells. Hence, as mentioned in the last division pathway, progenitors may transform to stem cells or at least to a progenitor from a different phenotype explicitly rather than through division [Chaffer et al. 2011]. According to the reported gradual increase in fraction and saturation of cancer stem cells and progenitors in their model, we have assumed 8 different phenotypes of cancer cells from a stem cell phenotype as the first, and fully mature cancer cells that are enabled to replicate. Considering this assumption, division pathways for the first phenotype, a cancer stem cell, can be rewritten as below:

$$S \rightarrow S + S$$
$$S \rightarrow S + P_1$$
$$S \rightarrow P_1 + P_1$$

Herein, P_1 is a progenitor with the most similarities with cancer stem cells while the next generation of progenitors, P_2, differs more from a cancer stem cell than a P_1 phenotype. The P_1 division and dedifferentiation pathways are:

$$P_1 \rightarrow P_2 + P_2$$
$$P_1 \rightarrow S$$

Following the same procedure for other phenotypes of progenitors (we assumed we have seven different types of these) we form the following division and dedifferentiation pathways:

$$P_2 \rightarrow P_3 + P_3$$

$$P_2 \rightarrow P_1$$

$$P_3 \rightarrow P_4 + P_4$$

$$P_3 \rightarrow P_2$$

$$P_4 \rightarrow P_5 + P_5$$

$$P_4 \rightarrow P_3$$

$$P_5 \rightarrow P_6 + P_6$$

$$P_5 \rightarrow P_4$$

$$P_6 \rightarrow M + M$$

$$P_6 \rightarrow P_5$$

$$M \rightarrow \varnothing$$

where M denotes the most mature cell type inside the tumour. M cells are not able to replicate through division, but they may die in response to the tough and fatal conditions in the tumour microenvironment.

The division format for progenitors, dictates their limited ability to replicate; each P_i divides into two progenitors P_{i+1}. Thus, through the introduced pathways we assume the replication ability of progenitors to be restricted to at most 6 times, of course except for the dedifferentiation detours of progenitors.

Beside the assumption of sudden switching of progenitors to less differentiated phenotypes and gradual differentiation and dedifferentiation of cancer stem cells and progenitors respectively, we made another assumption on the rate of division and dedifferentiation pathways. Here after, we suppose that the division rates for all types of progenitors are the same. We assumed the same argument for the differentiation rate of progenitors so that the division rate of all P_i (i=1:6) is identical (will be denoted by ρ_P afterwards) and so the dedifferentiation rate (will be represented by γ).

Following Turner et al. (2009), we also assumed that the death rate of an M cell is

zero. This is a valid assumption in short time scales (see the experimental data presented in the next section). However the possibility of each cancer stem cell division incidence as a determining factor of tumour survival is distinct from others. Hence the division rates are as follows:

$$S \xrightarrow{r_1 * \rho_S} S + S$$

$$S \xrightarrow{r_2 * \rho_S} S + P_1$$

$$S \xrightarrow{r_3 * \rho_S} P_1 + P_1$$

for i=1 to 6

$$P_i \xrightarrow{\rho_P} P_{i+1} + P_{i+1}$$

$$P_i \xrightarrow{\gamma} P_{i-1}$$

where P_7 is M and

$$M \xrightarrow{\Gamma \approx 0} \varnothing$$

Our last assumption in constructing the model is that the cell divisions are stochastic. We considered that the selection of the self-renewal, division, differentiation and dedifferentiation of cancer cells has a random component. The existence of the random compartment is supported by the work of Till and McCulloch for hematopoietic stem cells [Till et al. 1964]. Till and colleagues [Till et al. 1964] and Clayton et al. [Clayton et al. 2007] have also assumed that the process of cancer cell division is a Markovian process. The Markovian property of a process states that the probability of being at state x_n at time t_n, given that the system is in x_{n-1} at time t_{n-1}, is independent of the state of the process at earlier time steps. This indicates that the Markovian process is a memoryless process. We assumed Markovian property for the stochastic process of cancer cell division in our model that lets us look at the state of cancer stem cells and non-stem cancer cells in a step-wise manner so that only knowing the current state of the system lets us predict the next state.

In agreement with the recent work of Laslo and colleagues [Laslo et al. 2006], Till and McCulloch proposed that control mechanisms change the fate of hematopoietic cells through biasing the probability of each stochastic division incidence. Finally, we assumed that tumour microenvironmental factors are biasing and modifying the transition probabilities of the stochastic process of cancer cell divisions.

3.2.1. Markov process

For N(t), a time dependent discrete random variable, a Markov process is a stochastic process that satisfies:

$$p(n_k, t_k | n_{k-1}, ..., n_1; t_{k-1}, ..., t_1) = p(n_k, t_k | n_{k-1}, t_{k-1}) \quad (1)$$

where p(n) denotes the probability mass function and $p(A|B)$ is the conditional probability of the event A occurring given that the event B occurred.

According to our last assumption, the process of cell divisions is a stochastic process that in each time step the state of the system is determined based on the system state at most recent time step that is equivalent to have a (memory-less) independent system from far past or future states. Such a description completely matches a Markov process where N(t)=n(t) is a vector representing the number of different types of cancer cells at time t.

We assumed that the Markov process of cancer cell division is a time homogeneous process so that the transition probabilities are time-independent. However, we assumed that the transition probabilities depend tumour microenvironment factors.

3.2.2. Chapman-Kolmogorov equation

According to the chain rule of probability for any arbitrary stochastic process N(t) the following argument is universally true:

$$p(n_1, n_2, n_3; t_1, t_2, t_3) = p(n_3; t_3 \mid n_2, n_1; t_2, t_1)\, p(n_2; t_2 \mid n_1; t_1)\, p(n_1; t_1) \quad (2)$$

where $p(n_1,n_2,n_3;t_1,t_2,t_3)$ is the joint probability of N(t) to have

$$(N_1(t_1), N_2(t_2), N_3(t_3)) = (n_1, n_2, n_3) \ .$$

Hence having $p(n_1; t_1)$ and transition probabilities, one can form a master equation to describe the joint probability, $p(n_1,.n_2, n_3; t_1,.t_2, t_3)$.

Combining the chain rule of probability, equation (2), and the Markovian property of stochastic process N(t), equation (1), and assuming the time ordering $t_1 \le t_2 \le t_3$ we have:

$$p(n_1,...,n_k;t_1,...,t_k) = p(n_k,t_k \mid n_{k-1},t_{k-1})...p(n_2,t_2 \mid n_1,t_1)\, p(n_1;t_1) \quad (3)$$

Hence having $p(n_1; t_1)$ and transition probabilities, one can form a master equation to describe the joint probability, $p(n_1,...,n_k; t_1,...,t_k)$.

Seeking for the transition probabilities we return to equation (2) and sum it over all values of n_2 (as the middle stage of transition):

$$p(n_1, n_3; t_1, t_3) = p(n_1; t_1) \sum_{n_2=-\infty}^{\infty} p(n_3, t_3 \mid n_2, t_2)\, p(n_2, t_2 \mid n_1, t_1) \quad (4)$$

Although equation (4), the Chapman-Kolmogorov Equation, clarifies the relations between transition probabilities, it's still hard to handle to find the general form of $p(n_k; t_k)$.

Taking $\tau' = t_3 - t_2$ in equation (4) and approaching τ' to 0 we seek for $p(n_3; t_3)$. Now, we define $q(n,t;\tau)$ as the probability of a transition occurs between t and $t+\tau$ for a system that is in state n at time t. Assume that $q(n,t;\tau)$ is equal to $a(n,t)\tau$ when τ approaches 0. For more than one transition between t and $t+\tau$ for infinitesimal small τ, the probability is $o(\tau)$ so that as $o(\tau)/\tau$ approaches 0.

We also define $\omega(n^*|n,t)$ as the probability of transition from state n to n* at time t, in accordance with Gillespie's procedure [Gillespie 1991]. Hence the probability that a system in state n at time t transits to state n* at time t* between t and $t+\tau$ is equal to $a(n,t)\tau\omega(n^*,n|\ t^*)$. Considering the fact that the probability of no transition between t and $t+\tau$ is $1-a(n,t)\tau$ so the probability of having the process at state n* at $t+\tau$ can be written as a Kronecker delta function:

$$\delta_{i,j} = \begin{cases} 1 & if \quad i = j \\ 0 & if \quad i \neq j \end{cases}$$

so it is equal to 1 when n=n* and it's 0 when n≠n*. Therefore the transition probability from state n at t to n* can be written as

$$p(n^*, t^{**} \mid n,t) = [1 - a(n,t)\tau]\delta_{n^*,n} + a(n,t)\tau\omega(n^* \mid n,t^*) + o(\tau) \quad (5)$$

where t* is between t and t** and $\tau = t^{**} - t^*$.

Assuming that $\omega(n^*|n,t^*)$ as a smooth function, we can substitute t* with t (that is infinitesimally close to t*) in equation(5). Hence we have:

$$p(n^*, t^{**} \mid n,t) = [1 - a(n,t)\tau]\delta_{n^*,n} + a(n,t)\tau\omega(n^* \mid n,t) + o(\tau) \quad (6)$$

Note that summing over all possible values for n* we have:

$$\sum_{n^*=-\infty}^{\infty} \omega(n^* \mid n,t) = 1 \quad (7)$$

In line with the notation used by Van Kampen [Van Kampen 2007], we define W as below:

$$W(n^* \mid n,t) = a(n,t)\omega(n^* \mid n,t) \quad (8)$$

Combining equations (7) and (8), we have

$$\omega(n^* \mid n,t) = \frac{W(n^* \mid n,t)}{\sum_{n^*=-\infty}^{\infty} W(n^* \mid n,t)} \quad (9)$$

now we use the definition of W, equation (8), to rearrange equation (6):

$$p(n^*, t^{**} \mid n,t) = [1 - \sum_{n^*=-\infty}^{\infty} W(n^* \mid n,t)\tau]\delta_{n^*,n} + \tau W(n^* \mid n,t) + o(\tau) \quad (10)$$

Following Van Kampen [Van Kampen 2007], we suppose this stochastic process to be a time homogenous Markov process. For a time homogenous Markov process the transition probability from one state to another is only based on states rather than time i.e. p(n*,t**|n,t)=p(n*|n). Thus, a(n,t)=a(n) and ω(n*|n,t*)= ω(n*|n). Also we define:

$$a_0(n) = \sum_{n^*=-\infty}^{\infty} W(n^* \mid n) \quad (11)$$

Hence, substituting in Equation (10) we have:

$$p(n^*, t^{**} \mid n,t) = (1 - a_0(n)\tau)\delta_{n^*,n} + W(n^* \mid n)\tau + o(\tau) \quad (12)$$

Thus, for temporary homogenous Markov processes, the probability of the process to be in state n* at t** given that it is in state n at t only depends to the time difference between t and t**, τ. For more consistency to the notation used by Van Kampen, we designate this probability as T_τ= p(n*,t**|n,t).

Now we return to the Chapman Kolmogorov Equation (4). Using T_τ instead of

p(n*,t**|n,t) in Equation (12 and taking) and taking $\tau=t_2-t_1$ and $\tau'=t_3-t_2$ Van Kampen [Van Kampen 2007] proceeded as below to find the rate of change of p(n|t):

$$
\begin{aligned}
T_{\tau+\tau'}(n_3\mid n_1) &= \sum_{n_2=-\infty}^{\infty} T_{\tau'}(n_3\mid n_2)T_{\tau}(n_2\mid n_1)\\
T_{\tau+\tau'}(n_3\mid n_1) &= \sum_{n_2=-\infty}^{\infty} [(1-a_0(n_2)\tau')\delta_{n_3,n_2}+W(n_3\mid n_2)\tau'+o(\tau')]T_{\tau}(n_2\mid n_1)\\
T_{\tau+\tau'}(n_3\mid n_1) &= \sum_{n_2=-\infty}^{\infty} [(1-a_0(n_2)\tau')\delta_{n_3,n_2}T_{\tau}(n_2\mid n_1)]+\tau'\sum_{n_2=-\infty}^{\infty} W(n_3\mid n_2)T_{\tau}(n_2\mid n_1)+o(\tau')\sum_{n_2=-\infty}^{\infty} T_{\tau}(n_2\mid n_1)\\
T_{\tau+\tau'}(n_3\mid n_1) &= (1-a_0(n_3)\tau')T_{\tau}(n_3\mid n_1)+\tau'\sum_{n_2=-\infty}^{\infty} W(n_3\mid n_2)T_{\tau}(n_2\mid n_1)+o(\tau')\sum_{n_2=-\infty}^{\infty} T_{\tau}(n_2\mid n_1)
\end{aligned}
$$

(13)

Remembering the definition of a_0 :

$$
\begin{aligned}
\frac{T_{\tau+\tau'}(n_3\mid n_1)-T_{\tau}(n_2\mid n_1)}{\tau'} &= -a_0(n_3)T_{\tau}(n_2\mid n_1)+\sum_{n_2=-\infty}^{\infty} W(n_3\mid n_2)T_{\tau}(n_2\mid n_1)+\frac{o(\tau')}{\tau'}\sum_{n_2=-\infty}^{\infty} T_{\tau}(n_2\mid n_1)\\
\frac{T_{\tau+\tau'}(n_3\mid n_1)-T_{\tau}(n_2\mid n_1)}{\tau'} &= -\sum_{n_2=-\infty}^{\infty} W(n_2\mid n_3)T_{\tau}(n_3\mid n_1)+\sum_{n_2=-\infty}^{\infty} W(n_3\mid n_2)T_{\tau}(n_2\mid n_1)+\frac{o(\tau')}{\tau'}\sum_{n_2=-\infty}^{\infty} T_{\tau}(n_2\mid n_1)\\
\frac{T_{\tau+\tau'}(n_3\mid n_1)-T_{\tau}(n_2\mid n_1)}{\tau'} &= \sum_{n_2=-\infty}^{\infty} [-W(n_2\mid n_3)T_{\tau}(n_3\mid n_1)+W(n_3\mid n_2)T_{\tau}(n_2\mid n_1)]+\frac{o(\tau')}{\tau'}\sum_{n_2=-\infty}^{\infty} T_{\tau}(n_2\mid n_1)
\end{aligned}
$$

(14)

and considering the fact that $o(\tau)/\tau$ approaches to 0 for infinitesimal small values of τ, we have:

$$
\frac{d}{d\tau}p(n_3,t_3\mid n_2,t_2)=\frac{d}{d\tau}T_{\tau}(n_3\mid n_1)=\sum_{n_2=-\infty}^{\infty}[W(n_3\mid n_2)T_{\tau}(n_2\mid n_1)-W(n_2\mid n_3)T_{\tau}(n_3\mid n_1)]
$$

(15)

the above discussion to derive Equation (15) can be found in Turner's work [Turner 2009] in detail. To form a master equation governing the heterogeneous population of cancer cells, we use Equation (15).

3.3. Forming the master equation

Herein, incorporating the self-renewal, division, differentiation and dedifferentiation pathways of cancer cells we form the master equation governing the stochastic process of cancer stem cells dynamics, i.e. the population of each phenotype of cancer cells at time t, given that the system starts at:

$$(N_S(0),N_{P1}(0),N_{P2}(0),N_{P3}(0),N_{P4}(0),N_{P5}(0),N_{P6}(0),N_M(0))=$$
$$(n_S^0,n_{P1}^0,n_{P2}^0,n_{P3}^0,n_{P4}^0,n_{P5}^0,n_{P6}^0,n_M^0)$$

where $N_x(t)$ represents the number of cancer cells of phenotype x at time t. To use Equation (15) we first need to justify the assumptions we made to form Equation (15) for the stochastic process of division.

3.3.1. Justification of assumptions

First assumption: the stochastic process of cell division and reprograming is a Markov process. Till and colleagues [Till et al. 1964] and more recently Clayton and colleagues [Clayton et al. 2007] have used the Markovian property for stem cell divisions and were able to successfully reproduce the experimental results. On the other hand, mentioned division and reprograming pathways relate the population of each P_i to the population of P_{i-1} or P_{i+1} that is just one step forward or backward. We assume that the process of cell division is a memory-less process that only depends on the state of the system in short distances (one step forward or backward). That is equivalent to Markovian property of a stochastic process.

Second assumption: the Markov process of cell division and reprograming is a time homogenous process. We use the identical set of rates for self-renewal, cancer stem cell asymmetric division, cancer stem cell symmetric differentiation, progenitor division, progenitor reprograming (dedifferentiation) and the death of totally mature cells (M phenotype) regardless to time. As mentioned in section 3.2, these fixed rates are denoted by ρ_S*r_1, ρ_S*r_2, ρ_S*r_3, ρ_P, γ, and Γ respectively. Hence the assumption of temporally homogeneity of the process is logical.

One may criticise this time-homogeneity assumption stating that the division and reprograming rates are dominantly influenced by the tumour microenvironment so that for example, the dedifferentiation rate of progenitors in hypoxia or high acidity is higher than the rate in normal condition. We took into account this issue by considering different sets of transition rates for regions with diverse microenvironmental features. We will comprehensively explain the above-mentioned categorization later in this chapter.

3.3.2. Master equation

We are interested to find the joint probability of $N_S(t)=S$, $N_{P1}(t)=P_1$, …, $N_M(t)=M$ given that:

$(N_S(0),N_{P1}(0),N_{P2}(0),N_{P3}(0),N_{P4}(0),N_{P5}(0),N_{P6}(0),N_M(0))$

$=(n_S^0,n_{P1}^0,n_{P2}^0,n_{P3}^0,n_{P4}^0,n_{P5}^0,n_{P6}^0,n_M^0)$

to make it easier to read, we used the notation p(A) as follows:

$$p(S,P_1,P_2,P_3,P_4,P_5P_6,M;t\mid n_S^0,\ldots,n_M^0;0)=p(A)$$

Note that all probabilities are conditioned to initial state although we skip writing for simplification. Using Equation (15) and all possible transitions mentioned in section 3.2 we have:

$$\frac{d}{dt}p(A) = \rho_S r_1[(S-1)p(S-1,P_1,...,M) - Sp(S,P_1,...,M)]$$

$$+\rho_S r_2[Sp(S,P_1-1,...,M) - Sp(S,P_1,...,M)]$$

$$+\rho_S r_3[(S+1)p(S+1,P_1-2,...,M) - Sp(S,P_1,...,M)]$$

$$+\rho_P[(P_1+1)p(S,P_1+1,P_2-2,...,M) - P_1 p(S,P_1,...,M)]$$

$$+\gamma[(P_1+1)p(S-1,P_1+1,P_2,...,M) - P_1 p(S,P_1,...,M)]$$

$$+\rho_P[(P_2+1)p(S,P_1,P_2+1,P_3-2,...,M) - P_2 p(S,P_1,...,M)]$$

$$+\gamma[(P_2+1)p(S,P_1-1,P_2+1,...,M) - P_2 p(S,P_1,...,M)]$$

$$+\rho_P[(P_3+1)p(S,P_1,P_2,P_3+1,P_4-2,...,M) - P_3 p(S,P_1,...,M)]$$

$$+\gamma[(P_3+1)p(S,P_1,P_2-1,P_3+1,...,M) - P_3 p(S,P_1,...,M)]$$

$$+\rho_P[(P_4+1)p(S,P_1,P_2,P_3,P_4+1,P_5-2,...,M) - P_4 p(S,P_1,...,M)]$$

$$+\gamma[(P_4+1)p(S,P_1,P_2,P_3-1,P_4+1,...,M) - P_4 p(S,P_1,...,M)]$$

$$+\rho_P[(P_5+1)p(S,P_1,P_2,P_3,P_4,P_5+1,P_6-2,M) - P_5 p(S,P_1,...,M)]$$

$$+\gamma[(P_5+1)p(S,P_1,P_2,P_3,P_4-1,P_5+1,P_6,M) - P_5 p(S,P_1,...,M)]$$

$$+\rho_P[(P_6+1)p(S,P_1,P_2,P_3,P_4,P_5,P_6+1,M-2) - P_6 p(S,P_1,...,M)]$$

$$+\gamma[(P_6+1)p(S,P_1,P_2,P_3,P_4,P_5-1,P_6+1,M) - P_6 p(S,P_1,...,M)]$$

$$+\Gamma[(M+1)p(S,P_1,P_2,P_3,P_4,P_5,P_6,M+1) - Mp(S,P_1,...,M)]$$

(16)

Equation (16) considers all possible transitions to be at state (S, P1, P2, …, M) at time t.

3.3.3. Averaging the master equation

We simplified the interpretation of Equation (16) to the expected values of subpopulations. Recall that the definition of expected value for a discrete random variable X is:

$$E[X] = \sum_{i=1}^{\infty} x_i p(X = x_i)$$

To find the expected value of each population we multiplied Equation (16) by components of random variable. For instance, we multiplied Equation (16) by S as the first step to find the average of the cancer stem cell population. Next, summing over all possible states of the system, {A}, and taking the derivative out of the summation we have:

$$\sum_{\{A\}} S \frac{d}{dt} p(A) = \frac{d}{dt} \sum_{\{A\}} S p(A) = \frac{d}{dt} \langle S \rangle = \frac{d}{dt} E[S] \quad (18)$$

where E[S] represent the expected value of cancer stem cells. In the following we explain the procedure in detail to find the average values of each subpopulation in detail.

3.3.4. Average of cancer stem cell population

Multiplying by S and summing over all possible values for states of the system we have:

$$
\begin{aligned}
\frac{d}{dt}\sum_{\{A\}} Sp(A) \;=\; & \rho_S r_1 \sum_{\{A\}}\Big[S(S-1)\,p(S-1,P_1,\ldots,M) - S^2 p(S,P_1,\ldots,M)\Big] \\
& +\rho_S r_2 \sum_{\{A\}}\Big[S^2 p(S,P-1,\ldots,M) - S^2 p(S,P_1,\ldots,M)\Big] \\
& +\rho_S r_3 \sum_{\{A\}}\Big[S(S+1)\,p(S+1,P_1-2,\ldots,M) - S^2 p(S,P_1,\ldots,M)\Big] \\
& +\rho_P \sum_{\{A\}}\Big[S(P_1+1)\,p(P_1+1,P_2-2,\ldots,M) - SP_1 p(S,P_1,\ldots,M)\Big] \\
& +\gamma \sum_{\{A\}}\Big[S(P_1+1)\,p(S-1,P_1+1,P_2,\ldots,M) - SP_1 p(S,P_1,\ldots,M)\Big] \\
& +\rho_P \sum_{\{A\}}\Big[S(P_2+1)\,p(S,P_1,P_2+1,P_3-2,\ldots,M) - SP_2 p(S,P_1,\ldots,M)\Big] \\
& +\gamma \sum_{\{A\}}\Big[S(P_2+1)\,p(S,P_1-1,P_2+1,\ldots,M) - SP_2 p(S,P_1,\ldots,M)\Big] \\
& +\rho_P \sum_{\{A\}}\Big[S(P_3+1)\,p(S,P_1,P_2,P_3+1,P_4-2,\ldots,M) - SP_3 p(S,P_1,\ldots,M)\Big] \\
& +\gamma \sum_{\{A\}}\Big[S(P_3+1)\,p(S,P_1,P_2-1,P_3+1,\ldots,M) - SP_3 p(S,P_1,\ldots,M)\Big] \\
& +\rho_P \sum_{\{A\}}\Big[S(P_4+1)\,p(S,P_1,P_2,P_3,P_4+1,P_5-2,\ldots,M) - SP_4 p(S,P_1,\ldots,M)\Big] \\
& +\gamma \sum_{\{A\}}\Big[S(P_4+1)\,p(S,P_1,P_2,P_3-1,P_4+1,\ldots,M) - SP_4 p(S,P_1,\ldots,M)\Big] \\
& +\rho_P \sum_{\{A\}}\Big[S(P_5+1)\,p(S,P_1,P_2,P_3,P_4,P_5+1,P_6-2,M) - SP_5 p(S,P_1,\ldots,M)\Big] \\
& +\gamma \sum_{\{A\}}\Big[S(P_5+1)\,p(S,P_1,P_2,P_3,P_4-1,P_5+1,P_6,M) - SP_5 p(S,P_1,\ldots,M)\Big] \\
& +\rho_P \sum_{\{A\}}\Big[S(P_6+1)\,p(S,P_1,P_2,P_3,P_4,P_5,P_6+1,M-2) - SP_6 p(S,P_1,\ldots,M)\Big] \\
& +\gamma \sum_{\{A\}}\Big[S(P_6+1)\,p(S,P_1,P_2,P_3,P_4,P_5-1,P_6+1,M) - SP_6 p(S,P_1,\ldots,M)\Big] \\
& +\Gamma \sum_{\{A\}}\Big[S(M+1)\,p(S,P_1,P_2,P_3,P_4,P_5,P_6,M+1) - SMp(S,P_1,\ldots,M)\Big]
\end{aligned}
$$

Now we change the labelling of state so that all conditional probabilities change to the probability of the system to be at the state (S, P1, P_2, …, M).

$$\frac{d}{dt}\sum_{\{A\}} Sp(A) = \rho_S r_1 \sum_{\{A\}} [S(S+1)p(S,P_1,...,M) - S^2 p(S,P_1,...,M)]$$

$$+\rho_S r_2 \sum_{\{A\}} [S^2 p(S,P_1,...,M) - S^2 p(S,P_1,...,M)]$$

$$+\rho_S r_3 \sum_{\{A\}} [S(S-1)p(S,P_1,...,M) - S^2 p(S,P_1,...,M)]$$

$$+\rho_P \sum_{\{A\}} [S(P_1)p(S,P_1,P_2,...,M) - SP_1 p(S,P_1,...,M)]$$

$$+\gamma \sum_{\{A\}} [(S+1)(P_1)p(S,P_1,P_2,...,M) - SP_1 p(S,P_1,...,M)]$$

$$+\rho_P \sum_{\{A\}} [SP_2 p(S,P_1,P_2,P_3,...,M) - SP_2 p(S,P_1,...,M)]$$

$$+\gamma \sum_{\{A\}} [SP_2 p(S,P_1,P_2,...,M) - SP_2 p(S,P_1,...,M)]$$

$$+\rho_P \sum_{\{A\}} [SP_3 + p(S,P_1,P_2,P_3,P_4,...,M) - SP_3 p(S,P_1,...,M)]$$

$$+\gamma \sum_{\{A\}} [SP_3 p(S,P_1,P_2,P_3,...,M) - SP_3 p(S,P_1,...,M)]$$

$$+\rho_P \sum_{\{A\}} [SP_4 p(S,P_1,P_2,P_3,P_4,P_5,...,M) - SP_4 p(S,P_1,...,M)]$$

$$+\gamma \sum_{\{A\}} [SP_4 p(S,P_1,P_2,P_3,P_4,...,M) - SP_4 p(S,P_1,...,M)]$$

$$+\rho_P \sum_{\{A\}} [SP_5 p(S,P_1,P_2,P_3,P_4,P_5,P_6,M) - SP_5 p(S,P_1,...,M)]$$

$$+\gamma \sum_{\{A\}} [SP_5 p(S,P_1,P_2,P_3,P_4,P_5,P_6,M) - SP_5 p(S,P_1,...,M)]$$

$$+\rho_P \sum_{\{A\}} [SP_6 p(S,P_1,P_2,P_3,P_4,P_5,P_6,M) - SP_6 p(S,P_1,...,M)]$$

$$+\gamma \sum_{\{A\}} [SP_6 p(S,P_1,P_2,P_3,P_4,P_5,P_6,M) - SP_6 p(S,P_1,...,M)]$$

$$+\Gamma \sum_{\{A\}} [SMp(S,P_1,P_2,P_3,P_4,P_5,P_6,M) - SMp(S,P_1,...,M)]$$

After simplification and considering Equation (18) we form the derivative of the average population of cancer stem cell as follows:

$$\frac{d}{dt}\langle S\rangle = \rho_S r_1 \langle S\rangle - \rho_S r_3 \langle S\rangle + \gamma\langle P_1\rangle \quad (19)$$

It is clear that changes in the population of cancer stem cells depend on the initial population and also on the population of P_1 while the reprograming of P_1 cells increases the S cells population.

In addition r_1, r_2, and r_3 are not independent. When a cancer stem cell encounters the proper conditions to go to the division cycle, it inevitably chooses one of self-renewal, asymmetric division or symmetric differentiation. Hence $r_1+r_2+ r_3 =1$.

Now we define $r := r_1 - r_3$. Knowing r, we can find r_2 and for other cases, always r_1-r_3 appears. Thus the expected value of the cancer stem cell population can be rewrite as:

$$\frac{d}{dt}\langle S\rangle = \rho_S r \langle S\rangle + \gamma\langle P_1\rangle \quad (20)$$

3.3.5. Average of the progenitors populations

Following the same procedure as discussed in the pervious section, we form the equations to find the expected value for the population of first type of progenitors, P_1. Note that, herein we have multiplied the original master Equation (16) by P_1 and then summated over all possibilities for A. revising the labelling as we have done before, the master equation in this case reads as follows:

$$
\begin{aligned}
\frac{d}{dt}\sum_{\{A\}} P_1 p(A) \;=\; & \rho_S r_1 \sum_{\{A\}} \Big[P_1 S p(S, P_1, \ldots, M) - P_1 S p(S, P_1, \ldots, M) \Big] \\
& + \rho_S r_2 \sum_{\{A\}} \Big(\big[P_1 - 1 \big) S p(S, P_1, \ldots, M) - P_1 S p(S, P_1, \ldots, M) \Big] \\
& + \rho_S r_3 \sum_{\{A\}} \Big[(P_1 + 2) S p(S, P_1, \ldots, M) - P_1 S p(S, P_1, \ldots, M) \Big] \\
& + \rho_P \sum_{\{A\}} \Big[P_1 (P_1 - 1)\, p(P_1, P_2, \ldots, M) - P_1^2 p(S, P_1, \ldots, M) \Big] \\
& + \gamma \sum_{\{A\}} \Big[P_1 (P_1 - 1)\, p(S, P_1, P_2, \ldots, M) - P_1^2 p(S, P_1, \ldots, M) \Big] \\
& + \rho_P \sum_{\{A\}} \Big[P_1 P_2 p(S, P_1, P_2, P_3, \ldots, M) - P_1 P_2 p(S, P_1, \ldots, M) \Big] \\
& + \gamma \sum_{\{A\}} \Big[(P_1 + 1) P_2 p(S, P_1, P_2, \ldots, M) - P_1 P_2 p(S, P_1, \ldots, M) \Big] \\
& + \rho_P \sum_{\{A\}} \Big[P_1 P_3 p(S, P_1, P_2, P_3, P_4, \ldots, M) - P_1 P_3 p(S, P_1, \ldots, M) \Big] \\
& + \gamma \sum_{\{A\}} \Big[P_1 P_3 p(S, P_1, P_2, P_3, \ldots, M) - P_1 P_3 p(S, P_1, \ldots, M) \Big] \\
& + \rho_P \sum_{\{A\}} \Big[P_1 P_4 p(S, P_1, P_2, P_3, P_4, P_5, \ldots, M) - P_1 P_4 p(S, P_1, \ldots, M) \Big] \\
& + \gamma \sum_{\{A\}} \Big[P_1 P_4 p(S, P_1, P_2, P_3, P_4, \ldots, M) - P_1 P_4 p(S, P_1, \ldots, M) \Big] \\
& + \rho_P \sum_{\{A\}} \Big[P_1 P_5 p(S, P_1, P_2, P_3, P_4, P_5, P_6, M) - P_1 P_5 p(S, P_1, \ldots, M) \Big] \\
& + \gamma \sum_{\{A\}} \Big[P_1 P_5 p(S, P_1, P_2, P_3, P_4, P_5, P_6, M) - P_1 P_5 p(S, P_1, \ldots, M) \Big] \\
& + \rho_P \sum_{\{A\}} \Big[P_1 P_6 p(S, P_1, P_2, P_3, P_4, P_5, P_6, M) - P_1 P_6 p(S, P_1, \ldots, M) \Big] \\
& + \gamma \sum_{\{A\}} \Big[P_1 P_6 p(S, P_1, P_2, P_3, P_4, P_5, P_6, M) - P_1 P_6 p(S, P_1, \ldots, M) \Big] \\
& + \Gamma \sum_{\{A\}} \Big[P_1 M p(S, P_1, P_2, P_3, P_4, P_5, P_6, M) - P_1 M p(S, P_1, \ldots, M) \Big]
\end{aligned}
$$

(21)

Hence the average value of P_1 cells is:

$$\frac{d}{dt}\langle P_1\rangle = \rho_S r_2 \langle S\rangle + 2\rho_S r_3 \langle S\rangle - \rho_P \langle P_1\rangle - \gamma(\langle P_1\rangle - \langle P_2\rangle) \quad (22)$$

Revising in terms of r, Equation (22) changes to:

$$\frac{d}{dt}\langle P_1\rangle = (1-r)\rho_S \langle S\rangle - \rho_P \langle P_1\rangle - \gamma(\langle P_1\rangle - \langle P_2\rangle) \quad (23)$$

Similar to the procedure used to derive the expected value for P_1, the averages of other progenitors are as listed below. For convenience, the expected values of cancer stem cell population and P_1 cells are also shown here:

$$\frac{d}{dt}\langle S\rangle = \rho_S r \langle S\rangle + \gamma \langle P_1\rangle \quad (24)$$

$$\frac{d}{dt}\langle P_1\rangle = (1-r)\rho_S \langle S\rangle - \rho_P \langle P_1\rangle - \gamma(\langle P_1\rangle - \langle P_2\rangle) \quad (25)$$

$$\frac{d}{dt}\langle P_2\rangle = \rho_P(2\langle P_1\rangle - \langle P_2\rangle) - \gamma(\langle P_2\rangle - \langle P_3\rangle) \quad (26)$$

$$\frac{d}{dt}\langle P_3\rangle = \rho_P(2\langle P_2\rangle - \langle P_3\rangle) - \gamma(\langle P_3\rangle - \langle P_4\rangle) \quad (27)$$

$$\frac{d}{dt}\langle P_4\rangle = \rho_P(2\langle P_3\rangle - \langle P_4\rangle) - \gamma(\langle P_4\rangle - \langle P_5\rangle) \quad (28)$$

$$\frac{d}{dt}\langle P_5\rangle = \rho_P(2\langle P_4\rangle - \langle P_5\rangle) - \gamma(\langle P_5\rangle - \langle P_6\rangle) \quad (29)$$

$$\frac{d}{dt}\langle P_6\rangle = \rho_P(2\langle P_5\rangle - \langle P_6\rangle) - \gamma\langle P_6\rangle \quad (30)$$

$$\frac{d}{dt}\langle M\rangle = 2\rho_P \langle P_6\rangle - \Gamma\langle M\rangle \quad (31)$$

Solving the above system of differential equations at the steady state, results in the answers in terms of one of the phenotypes, ρ_S, ρ_P, γ, and Γ. Although the results may seem to be useful, their dependence on the transition rates leaves them inapplicable. Hence, tuning the transition rates is the preliminary stage to solve the system. Recalling the dominant effect of the tumour microenvironment on tumour growth, cancer progression and specifically, cancer stem cell maintenance we classified the transition rates based on the affecting microenvironmental factors.

Current work is focused on the effect of hypoxia and high acidity on transition rates and consequently tumour survival and growth.

3.4. Tuning the transition rates

To tune the transition rates, we used a deterministic filtration and next applied a stochastic procedure. Using an exhaustive key search on ρ_S, ρ_P, r, and γ, we first found the proper combinations of transition rates, which satisfy a deterministic test on capability of a system to produce a predetermined fraction of stem cells at steady state in accordance with biological data. Second, we used a stochastic approach to filter the results of the first part once more comparing the ability of the subsequent system to form neurospheres. Again, the results have been selected in accordance with the neurosphere essay experiments.

As mentioned before, the low accuracy of available neural stem cell biomarkers and the contradictory results of experiments done on non-stem cancer cells to show the properties of cancer stem cells convinced us to consider the first four phenotypes of the system as cancer stem cells and others as non-stem cancer cells. Thus we assumed that S, P_1, P_2, and P3 cells express CD133+ while P_4, P_5, P_6, and M cells are CD133- cells.

3.4.1. Microenvironmental features categorization

The oxygen concentration is known to have a profound effect on the cancer cells survival and progression. In addition to mediating survival and proliferation, oxygen levels in the brain affect the cell metabolism, cell signalling and gene expression [Heddleston et al. 2010, Keith and Simon 2007, Seidel et al. 2010, Heddleston et al. 2009, Fukumura et al. 2001, Hjelmeland et al. 2011, Pouyssegur et al. 2006, Gordan and Simon 2007]. Many studies have reported that the reduction in oxygen concentration (from 20% t0 3-5%) promotes the stem-like properties of cancer cells [Ivanovic et al. 2004, Kovacevic-Filipovic et al. 2007, Studer et al. 2000, Zhang et al. 2006]. Although, Tofilon and colleagues claim that 20% of oxygen concentration considered in in vitro studies (atmospheric condition) is fairly high for culturing GBM cells, they demonstrated same argument that hypoxia upregulates the cancer stem cell phenotype [McCord et al. 2009]. Mentioning that oxygen level is 14% in alveolar [Guyton and Hall 2006], 5-10% in normal brain tissue [Evans et al. 2004, Dings et al. 1998], 0.1-10% in a GBM tumour tissue [Evans et al. 2004a, b, Dings et al. 1998], and 6-7% for majority of GBM cells [Evans et al. 2004] and comparing their experiments results under 7% of oxygen with other studies under normal culture condition of 20% of oxygen, Tofilon and colleagues demonstrated the promotion of self-renewal, differentiation potentials, and enhanced stem-like genomic and protein-expression of GBM tumour stem cell cultures under the hypoxic condition [McCord et al. 2009]. With an emphasis on recruitment of HIF2α in GBM cancer stem cell culture. Heddleston et al. [Heddleston et al. 2009] and Acker and colleagues [Seidel et al. 2010] have also reported the promoting effect of hypoxia on the cancer stem cell phenotype.

Likewise the hypoxia, high acidity of the tumour microenvironment dominantly affects the maintenance of cancer stem cells. Recently, Rich and colleagues have reported the results of their experiment investigating the influence of high acidic stress in the tumour microenvironment on cancer cells [Hjelmeland et al. 2011].

They state that initiating with cancer stem cell-depleted cultures, fraction of cancer cells expressing the CD133+ and colony formation ability increased under the acidic condition (pH=6.5), while the elevation of extracellular pH, from 6.5 to 7.5 reduces the expression of cancer stem cell marker, CD133, and neurosphere formation potentials [Hjelmeland et al. 2011]. Although the pH level inside the GBM tumour has been reported to be as low as 5.9, the differences of outcomes under normal (7.1-7.5)[vaupel et al. 1989]) and acidic conditions differs considerably. Even before the popularity of the cancer stem cells hypothesis, Casciari and colleagues reported that the growth rate of tumour cells increases under acidic condition [Casciari et al. 1992]. Moreover, they compared the correlation of growth rate with oxygen concentration as well as glucose content. Additionally, they investigated the simultaneous effect of acidity and hypoxia on tumour growth. Their results showed that under hypoxic conditions the growth rate of a tumour decreases as the pH level decreases. This may appear to contradict the effect of hypoxia and acidity in promoting tumour progression, but the coincidence of both hypoxia and acidity may lethally modify the tumour microenvironment so that not only normal cells but also cancer cells can not survive. Jain's group has reported results that do not support the additive effect of simultaneous hypoxia and acidity on tumour tissue [Fukumura et al. 2001]. In their study on upregulation of VEGF by hypoxia and acidity in brain tumours [Fukumura et al. 2001], they claim that, although the effect of hypoxia and acidity independently upregulate VEGF, the recruitment of VEGF under simultaneous hypoxia and acidity is less than the summation of the effect of each in separate experiments. Their justification to explain the sub-linear effect of hypoxia and acidity is the same as the reasoning of Casciari et al. (1992).

Thus, focusing on hypoxia and acidity as dominant features of the GBM tumour microenvironment, we have divided the microenvironmental space into four different regions of, normal, hypoxic, acidic and hypoxic-acidic sub-regions (Table 1).

Table 1: Microenvironmental heterogeneity inside cancer tumours. Oxygen concentration and acidity of tumour microenvironment as the dominant determiners of tumour progression divide the tumour microenvironment to four sub-region of hypoxic acidic, hypoxic non-acidic, normoxic acidic, and normal.

	Acidic	Non-acidic
Hypoxic	pH<6.5 and pO2<2%	pH≈7.5 and pO2<2%
Normoxic (non-hypoxic)	pH<6.5 and pO2≈21%	pH≈7.5 and pO2≈21%

In the following sections, we demonstrate the deterministic and stochastic filtration of transition rates, in which we obtain separate sets of results for each sub-region mentioned above. Hence at the end of the filtration, four sets of transition rates for hypoxic, acidic, hypoxic-acidic, and normal regions are provided.

3.4.2. Deterministic filtration

The saturation of the fraction of stem cells [Turner 2009], including S cells, P_1, P_2, and P_3 cells in current model, suggested to us that we should carry out the filtration based on the reported fraction of CD133+ cells in experiments. Table 2 explains the biological experiments done by different research groups on fraction of GBM cancer stem cells. In silico model assumptions are designed to match the conditions of the discussed biological experiments.

In their experiment, Rich and colleagues [Heddleston et al. 2009] have cultured glioma non-stem cancer cells from a human patient specimen in 24 well plates at a density of 10 cells per well. Then they immediately subject the cultures to hypoxic condition (2% O2) or normoxic condition (21% O2) for 9 days ($p<0.05$) [Heddleston et al. 2009]. Experiments 1 and 2 in Table 2 represent a summary of their experiments. Acker's group has reported comparable results from their experiment [Seidel et al. 2010]. To investigate the effect of an acidic

microenvironment on cancer stem cell fraction, Hjelmeland et al. [Hjelmeland et al. 2011] have culture a glioma stem cell- depleted bulk of 5 cancer cells under pH level of 6.5 for 10 days. Their conditions and results are summarized in Table 2.

To simulate the experimental conditions, we considered a random combination of non-stem cancer initiating cells so that ten initiating cells are randomly chosen from among P_4, P_5, P_6, and M cells. Using a brute force method we have selected those combinations of transition rates that gave a proper fraction of cancer stem cells as reported in biological data. Brute force method (aka proof of exhaustion or proof by cases) checks the validity of the statement of the question for finite number of cases and selects those ones which the proposition in the question holds for.

Note that fraction of cancer stem cells is the fraction of the summation of S, P_1, P_2, and P_3 cells to the total number of cancer cells in the culture. Table 3 explains the simulation conditions used to match the biological data provided in Table 1.

Table 2: the biological experiments show that hypoxia and acidity affect cancer stem fractions in in vitro studies. The condition of experiments and results are summarized as below.

Experiment	Region	Initiating cells per well	Type of initiating cells	Duration of experiment	Oxygen content of cell culture	pH level of cell culture	CD133+ fraction	Comments	Reference
1	Normal	10	Non-stem cancer cells	9 days	21%	7.5 (Normal)	10-15%	The fraction of cancer stem cells is thirds of hypoxic condition	Seidel et al. 2010 , Heddleston et al. 2009
2	Hypoxic non-acidic	10	Non-stem cancer cells	9 days	1-2%	7.5 (Normal)	45%	The fraction of cancer stem cells is twice of normoxic condition	Seidel et al. 2010, Heddleston et al. 2009
3	Acidic non-hypoxic	5	GSC depleted	10	21%	6.5	30%	The fraction of cancer stem cells is twice of non acidic condition	Hjelmeland et al. 2011
4	Normal condition compared with acidic region in [Hjelmeland et al. 2011]	5	GSC depleted	10	21%	7.5	15%	The fraction of cancer stem cells is thirds of hypoxic condition	Hjelmeland et al. 2011

Table 3:Numerical procedures' initial conditions and constrains. The results of these simulations are combinations of transitions rates that satisfy the initial condition of experiments in Table 1 and obtain matching fraction of cancer stem cells as reported in Table 1.

Numerical procedure	Region	Initiating cells per well	Experiment duration	Initiating cells per well	Oxygen content	PH	CD133+ fraction	Comments	Consistent with experiment:
1	Normal	Non stem cells	9 days	10 cells randomly chosen among P4, P5, P6& M	21%	7.5 Normal	15%(±1%)	The fraction of cancer stem cells is thirds of hypoxic condition	Experiment 1 & 4
2	Hypoxic	Non stem cells	9 days	10 cells randomly chosen among P4, P5, P6& M	2%	7.5 Normal	45%(±1%)	The fraction of cancer stem cells is twice of normoxic condition	Experiment 2
3	Acidic	GSC depleted	9 days	10 cells randomly chosen among P4, P5, P6& M	21%	6.5 Acidic	30%(±1%)	The fraction of cancer stem cells is twice of non acidic condition	Experiment 3

The only region that is not covered in biological experiments in Table 2 and simulations in Table 3 is the hypoxic- acidic region. To the knowledge of the author, no one has tried to see the explicit effect of the coincidence of hypoxia and acidity on cancer stem cells. However, valuable studies of Jain and colleagues [Fukumura et al. 2001] and also Casciari's group [Casciari et al. 1992] of the upregulation of VEGF and tumour growth rate respectively have shed light on the simultaneous effect of hypoxia and acidity. We predict that considering the lethal condition of an acidic and hypoxic extracellular condition, the fraction of cancer stem cells is not the summation of fractions of hypoxic and acidic regions, although the effect of hypoxia and acidity on VEGF is known to be independent in brain tumours [Fukumura et al. 2001]. Hence, we formed a simulation as shown in Table 4, to find the matching combination of transition rates for the hypoxic and acidic region.

3.4.3. Results of deterministic filtration

Solving the system of differential equations (Equation 24 to 31), we picked those combinations of transition rates, which were able to generate the same fraction of cancer stem cells as reported in biological experiments (Table 2). Among different feasible combinations of transition rates we have filtered at most 630 combinations out of 50000 initial combinations. These results fed the second round of simulations and have been filtered again based on a stochastic criterion of the ability to form the neurospheres and colonies.

Table 4: fraction rate of cancer stem cells imposed to hypoxia and acidity simultaneously. The fraction is the average values of hypoxic and acidic cases independently.

Numerical procedure	Region	Cell type	Experiment duration	Initiating cells per well	Oxygen content	PH	CD133 fraction	Comments
4	Hypoxic & Acidic	GSC depleted	9 days	10 cells randomly chosen among P4, P5, P6& M	2%	6.5 Acidic	37.5%(±0.01)	The fraction of cancer stem cells is equal to the average of fractions in hypoxic and acidic regions.

3.4.4. Gillespie's algorithm and neurosphere essays

In spite of a saturation state for the fraction of cancer stem cells, the number of cancer cells will not be saturated essentially. Thus, to solve the system of differential equations (Equation 24 to 31) the solution at steady state cannot be accepted.

Gillespie's algorithm is one of the alternatives to gain a suitable trajectory of the system and solution(s). Popularized by Dan Gillespie, Gillespie's algorithm has been formed to simulate the time evolving behaviour of chemical or biological systems, which have small number of reactants [Gillespie 1977]. The method produces a good prediction of stochastic process based on the initial condition of reactants, reactions, and transition rate of each reaction. The first step to use the Gillespie's algorithm is to form the matrix of reactions and vector of transition rates of reactions.

Herein, we form the stoichiometry matrix (SM), the reaction matrix, for the proposed model. Recalling the transition pathways of cancer cells, we assign each transition pathway to be as a row in stoichiometry matrix. Considering each cell type as a reactant and assigning each to a column in stoichiometry matrix we form a 16*8 matrix containing the information about the transition pathways and cell types so that SM (i, j) is equal to the number of cell type j increasing (+) or decreasing (-) through the transition i. Hence, for the proposed model the stoichiometry matrix is as follows in the next page.

The transition rates for each state form the propensity vector. The size of the vector is equal to the number of reaction (transition pathways) and each element stores the transition rate for the corresponding transition so that the i-th element is the transition rate for i-th transition. Considering A= (S, P_1, …, M) as the current sate of the system, the propensity vector (VP) for the current model is as follows:

$$VP=\left[\begin{array}{cccccccccccccccc} \rho_S r_1 & \rho_S r_2 & \rho_S r_3 & \rho_P & \gamma & \rho_P & \gamma & \rho_P & \gamma & \rho_P & \gamma & \rho_P & \gamma & \rho_P & \gamma & \Gamma \end{array}\right]\times A'$$

$$SM = \begin{bmatrix} 1 & 0 & 0 & 0 & 0 & 0 & 0 & 0 \\ 0 & 1 & 0 & 0 & 0 & 0 & 0 & 0 \\ -1 & 2 & 0 & 0 & 0 & 0 & 0 & 0 \\ 0 & -1 & 2 & 0 & 0 & 0 & 0 & 0 \\ 1 & -1 & 0 & 0 & 0 & 0 & 0 & 0 \\ 0 & 0 & -1 & 2 & 0 & 0 & 0 & 0 \\ 0 & 1 & -1 & 0 & 0 & 0 & 0 & 0 \\ 0 & 0 & 0 & -1 & 2 & 0 & 0 & 0 \\ 0 & 0 & 1 & -1 & 0 & 0 & 0 & 0 \\ 0 & 0 & 0 & 0 & -1 & 2 & 0 & 0 \\ 0 & 0 & 0 & 1 & -1 & 0 & 0 & 0 \\ 0 & 0 & 0 & 0 & 0 & -1 & 2 & 0 \\ 0 & 0 & 0 & 0 & 1 & -1 & 0 & 0 \\ 0 & 0 & 0 & 0 & 0 & 0 & -1 & 2 \\ 0 & 0 & 0 & 0 & 0 & 1 & -1 & 0 \\ 0 & 0 & 0 & 0 & 0 & 0 & 0 & -1 \end{bmatrix}$$

Briefly, Gillespie's algorithm randomly choses one of the rows of the stoichiometry matrix based on the assigned weight in the propensity matrix. Thus, although the selection of a transition pathway is random, rows corresponding to higher transition rates are more likely to be selected. The next step after selecting a reaction or transition is the revision of all reactants or cell types based on the selected reaction. This procedure will continue and move forward with random time steps till the maximum time is met.

Neurosphere essay and colony formation is a functional property of cancer stem cell. Hence, beside the expression of CD133+ as a physiological property, the capability of cell cultures in forming neurospheres is a sign of the presence of cancer stem cells. Using Gillespie's algorithm, we have formed a set of simulations to re-filter the transition rates resulted from deterministic filtration. Each simulation has been run for 1000 times and experimental conditions such as the combination of initiating cells and extracellular hypoxia or acidity were fixed according to corresponding biological data. The biological experiments and simulations are summarized in Table (5) and Table (6).

Table 5: Experiments on neurosphere formation and cancer stem cell fraction, conditions and results.

Experiment	Region	Initiating cells per well	Cell type	Experiment duration	Oxygen content	PH	CD133 fraction	Neurosphere formation fraction	Comments	Reference
1	Normal	10	Non stem cells	9 days	21%	7.5 Normal	15%	8.3%	The neurosphere formation potentials of normal regions is half of the hypoxic regions	Seidel et al. 2010, Heddleston et al. 2009
2	Hypoxic nonacidic	10	Non stem cells	9 days	1-2%	7.5 Normal	45%	21%	The neurosphere formation potentials of hypoxic regions is twice of the hypoxic regions	Seidel et al. 2010, Heddleston et al. 2009
3	Acidic non-hypoxic	5	GSC depleted	10 day	21%	6.5	30%	0.6%	The neurosphere formation potentials of acidic regions is three folds of the normal regions	Hjelmeland et al. 2011
4	Normal compared with acidic region	5	GSC depleted	10 day	21%	7.5	15%	0.2%	The neurosphere formation potentials of normal regions is thirds of the acidic regions	Hjelmeland et al. 2011
Our prediction	Acidic hypoxic	10	GSC depleted	10 day	2%	6.5	37.5%	15%	The neurosphere formation potentials of acidic-hypoxic regions is equal to the average of acidic and hypoxic regions	Fukumura et al., Casciari et al.

Table 6: Simulation, initial conditions and assumption according to biological experiments. Four different sets of simulations have been run to regenerate the biological experiments results. Simulations 1, 2, and 3 are corresponding to experiments 1 to 4. The last simulation, 4, reproduces the predicted data as discussed for the last numerical solution of deterministic filtering.

Simulation	Region	Experiment duration	Initiating cells per well	Oxygen content	PH	Neurosphere formation fraction	Comments	Consistent with experiment:
1	Normal	9 days	10 cells randomly chosen among P4, P5, P6& M	21%	7.5 Normal	8.3% (±0.03%)	The neurosphere formation potentials of normal regions is half of the hypoxic regions	Experiment 1 & 4
2	Hypoxic	9 days	10 cells randomly chosen among P4, P5, P6& M	2%	7.5 Normal	21%(±0.03%)	The neurosphere formation potentials of hypoxic regions is twice of the hypoxic regions	Experiment 2
3	Acidic	9 days (in accordance with experiment 1 & 2)	10 cells randomly chosen among P4, P5, P6& M	21%	6.5 Acidic	20%(±0.03%)	The neurosphere formation potentials of acidic regions is three folds of the normal regions	Experiment 3
4	Hypoxic & Acidic	9 days	10 cells randomly chosen among P4, P5, P6& M	2%	6.5 Acidic	15%(±0.03%)	The neurosphere formation potentials of acidic-hypoxic regions is equal to the average of acidic and hypoxic regions	Based on our prediction

3.5. Results

Double filtration of transition rates by deterministic criterion of the formed fraction of cancer stem cells and the stochastic norm of neurosphere formation potentials left us with a few combinations of rates that can be easily clustered and analysed.

At the first step the transition rate value assignment by a brute force method resulted in 50000 sets of transition rates as input where ρ_S, ρ_P, γ, and r were changing.

As mentioned before, Γ is assumed to be an infinitesimally small number ($\Gamma \approx 0$) in all simulations. Moreover r_1, r_2, and r_3 are dependent values summing to 1. We considered r in the first set of deterministic simulations and then in the second round of stochastic ones, we expand it over different possibilities of r_1, r_2, and r_3. Hence, the effect of different combinations of r_1, r_2, and r_3 (for a fixed value of r) is also considered. Table 7-10 contain the final results for transition rates. The diversity of results ranges between 2 to 41 different sets of transition rates. The hypoxic region with 41 sets of results has the largest data size while hypoxic-acidic region, normal and acidic region data sizes are decreasing with 17, 9 and 2 sets of transition rates as results.

Considering the diversity of results provokes the question of whether the results of each region are clustered into different groups. We first tried to figure out the clustering of results by a visual inspection of the graphs. Figures 1 to 4 illustrate the positions of results in each region. Note that values of ρ_S, and ρ_P are equal and the values of r_1, r_2, and r_3 are dependent. These make it possible for us to investigate the correlation of different results in one region by considering the relationship between γ, r_2, and r_3.

Figures 1 to 3 suggest that there may be different clusters of the results in each region, the position of results over all microenvironmental regions imply that the inter-region clustering can be neglected. Figure 4 simultaneously shows the results loci for all regions.

Table 7: Normal region, resulted transition rates (9 sets) for normal regions. These results produce 15%(±1%) cancer stem cells in culture and form neurospheres in 8.3% (±0.03%) of wells. The experimental conditions and simulations assumption can be found in Table 2-6.

Set	ρ_S	ρ_P	r	r_1	r_2	r_3	γ
1	0.6931	0.6931	-0.90	0.05	0.00	0.95	0.47
2	0.6931	0.6931	-0.80	0.00	0.20	0.80	0.47
3	0.6931	0.6931	-0.70	0.15	0.00	0.85	0.45
4	0.6931	0.6931	-0.50	0.00	0.50	0.50	0.44
5	0.6931	0.6931	-0.50	0.05	0.40	0.55	0.46
6	0.6931	0.6931	-0.40	0.05	0.50	0.45	0.45
7	0.6931	0.6931	-0.30	0.35	0.00	0.65	0.43
8	0.6931	0.6931	-0.30	0.05	0.60	0.35	0.44
9	0.6931	0.6931	-0.30	0.00	0.70	0.30	0.44

Table 8: Acidic region, resulted transition rates (2 sets) for acidic region. These results produce 30%(±1%) cancer stem cells in culture and form neurospheres in 20% (±0.03%) of wells. The experimental conditions and simulations assumption can be found in Table 2-6.

Set	ρ_S	ρ_P	r	r_1	r_2	r_3	γ
1	0.6931	0.6931	-0.50	0.00	0.50	0.50	0.68
2	0.6931	0.6931	-0.30	0.00	0.70	0.30	0.66

Table 9: Hypoxic region, resulted transition rates (17 sets) for hypoxic region. These results produce 45%(±1%) cancer stem cells in culture and form neurospheres in 21% (±0.03%) of wells. The experimental conditions and simulations assumption can be found in Table 2-6.

Set	ρ_S	ρ_P	r	r_1	r_2	r_3	γ
1	0.6931	0.6931	-0.90	0.00	0.10	0.90	0.93
2	0.6931	0.6931	-0.80	0.05	0.10	0.85	0.91
3	0.6931	0.6931	-0.70	0.00	0.30	0.70	0.90
4	0.6931	0.6931	-0.70	0.10	0.10	0.80	0.92
5	0.6931	0.6931	-0.70	0.05	0.20	0.75	0.92
6	0.6931	0.6931	-0.60	0.20	0.00	0.80	0.89
7	0.6931	0.6931	-0.60	0.15	0.10	0.75	0.89
8	0.6931	0.6931	-0.60	0.10	0.20	0.70	0.89
9	0.6931	0.6931	-0.50	0.25	0.00	0.75	0.89
10	0.6931	0.6931	-0.50	0.20	0.10	0.70	0.89
11	0.6931	0.6931	-0.50	0.10	0.30	0.60	0.89
12	0.6931	0.6931	-0.50	0.05	0.40	0.55	0.89
13	0.6931	0.6931	-0.50	0.20	0.10	0.70	0.90
14	0.6931	0.6931	-0.50	0.15	0.20	0.65	0.90
15	0.6931	0.6931	-0.50	0.05	0.40	0.55	0.91
16	0.6931	0.6931	-0.40	0.10	0.40	0.50	0.87
17	0.6931	0.6931	-0.40	0.05	0.50	0.45	0.87
18	0.6931	0.6931	-0.40	0.25	0.10	0.65	0.88
19	0.6931	0.6931	-0.40	0.15	0.30	0.55	0.88
20	0.6931	0.6931	-0.40	0.00	0.60	0.40	0.88
21	0.6931	0.6931	-0.30	0.30	0.10	0.60	0.86
22	0.6931	0.6931	-0.30	0.20	0.30	0.50	0.86
23	0.6931	0.6931	-0.30	0.00	0.70	0.30	0.86
24	0.6931	0.6931	-0.30	0.35	0.00	0.65	0.87
25	0.6931	0.6931	-0.30	0.15	0.40	0.45	0.87
26	0.6931	0.6931	-0.30	0.10	0.50	0.40	0.87
27	0.6931	0.6931	-0.30	0.05	0.60	0.35	0.87
28	0.6931	0.6931	-0.30	0.00	0.70	0.30	0.87
29	0.6931	0.6931	-0.30	0.25	0.20	0.55	0.88
30	0.6931	0.6931	-0.30	0.20	0.30	0.50	0.88
31	0.6931	0.6931	-0.30	0.15	0.40	0.45	0.88
32	0.6931	0.6931	-0.20	0.05	0.70	0.25	0.84
33	0.6931	0.6931	-0.20	0.00	0.80	0.20	0.85
34	0.6931	0.6931	-0.20	0.25	0.30	0.45	0.87
35	0.6931	0.6931	-0.20	0.10	0.60	0.30	0.87
36	0.6931	0.6931	-0.20	0.05	0.70	0.25	0.87
37	0.6931	0.6931	-0.10	0.25	0.40	0.35	0.83
38	0.6931	0.6931	-0.10	0.05	0.80	0.15	0.83
39	0.6931	0.6931	-0.10	0.00	0.90	0.10	0.83
40	0.6931	0.6931	0.00	0.05	0.90	0.05	0.83
41	0.6931	0.6931	0.00	0.00	1.00	0.00	0.83

Table 10: Acidic-hypoxic region, resulted transition rates (17 sets) for acidic-hypoxic region. These results produce 37.5%(±1%) cancer stem cells in culture and form neurospheres in 15% (±0.03%) of wells. The experimental conditions and simulations assumption can be found in Table 2-6.

Set	ρ_S	ρ_P	r	r_1	r_2	r_3	γ
1	0.6931	0.6931	-0.10	0.25	0.40	0.35	0.72
2	0.6931	0.6931	0.00	0.40	0.20	0.40	0.70
3	0.6931	0.6931	0.00	0.30	0.40	0.30	0.70
4	0.6931	0.6931	0.00	0.25	0.50	0.25	0.70
5	0.6931	0.6931	0.00	0.40	0.20	0.40	0.71
6	0.6931	0.6931	0.00	0.50	0.00	0.50	0.72
7	0.6931	0.6931	0.00	0.45	0.10	0.45	0.72
8	0.6931	0.6931	0.10	0.40	0.30	0.30	0.67
9	0.6931	0.6931	0.10	0.50	0.10	0.40	0.68
10	0.6931	0.6931	0.10	0.40	0.30	0.30	0.68
11	0.6931	0.6931	0.10	0.30	0.50	0.20	0.68
12	0.6931	0.6931	0.10	0.20	0.70	0.10	0.68
13	0.6931	0.6931	0.10	0.15	0.80	0.05	0.68
14	0.6931	0.6931	0.10	0.35	0.40	0.25	0.69
15	0.6931	0.6931	0.10	0.30	0.50	0.20	0.69
16	0.6931	0.6931	0.20	0.30	0.60	0.10	0.66
17	0.6931	0.6931	0.20	0.25	0.70	0.05	0.66

Figure 1: Transition rates for normal region. Each point represents one combination of resulted transition. Since ρ_S, and ρ_P are equal and fixed over all regions, the answer space can be defined by γ, r_2, and r_3.

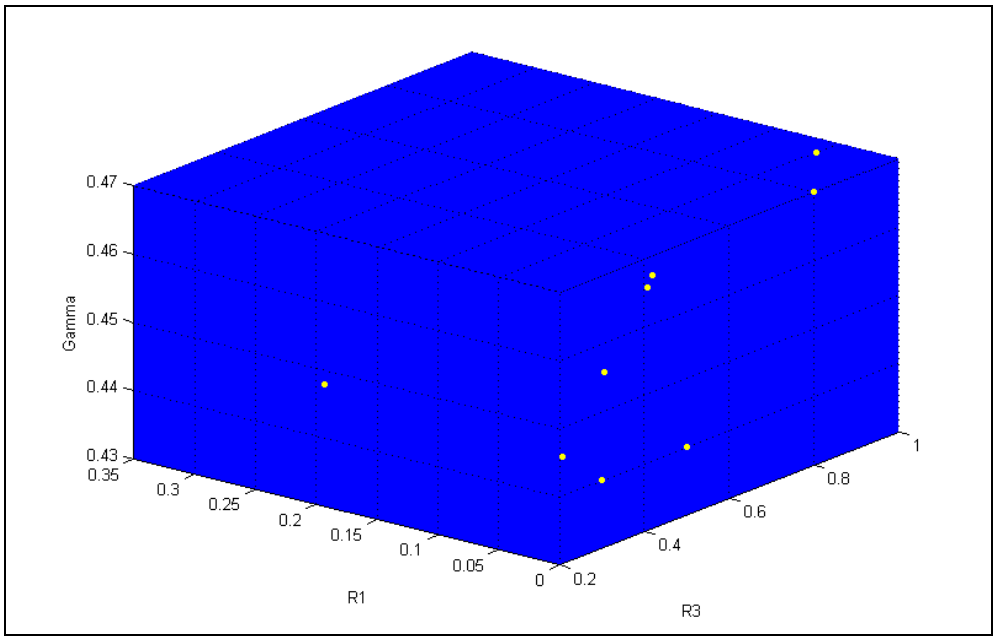

Figure 2: Transition rates for hypoxic region. Each point represents one combination of resulted transition. Since ρ_S, and ρ_P are equal and fixed over all regions, the answer space can be defined by γ, r_2, and r_3.

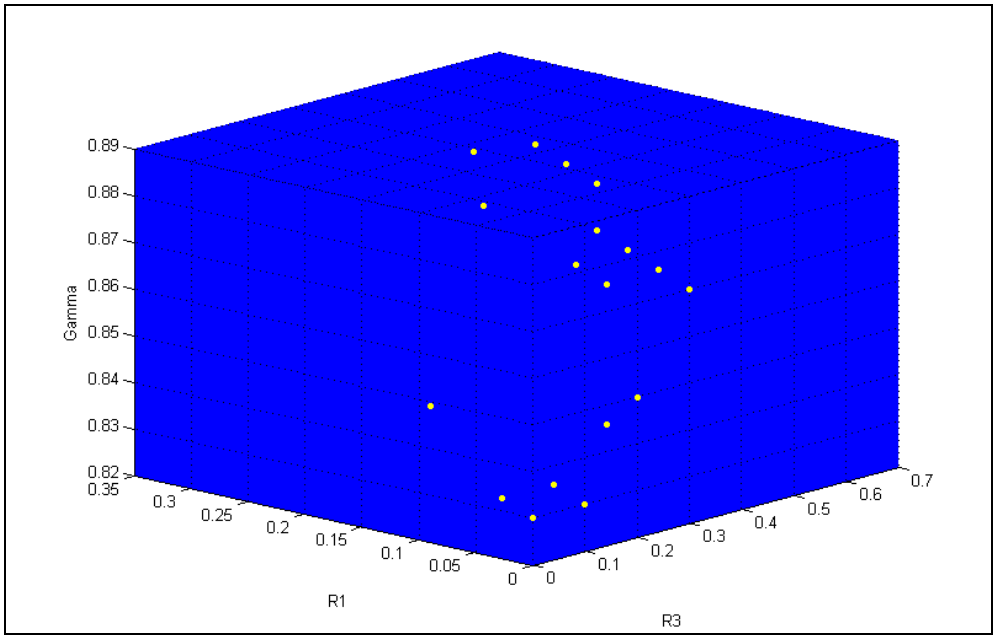

Figure 3: Transition rates for acidic-hypoxic region. Each point represents one combination of resulted transition. Since ρ_S, and ρ_P are equal and fixed over all regions, the answer space can be defined by γ, r_2, and r_3.

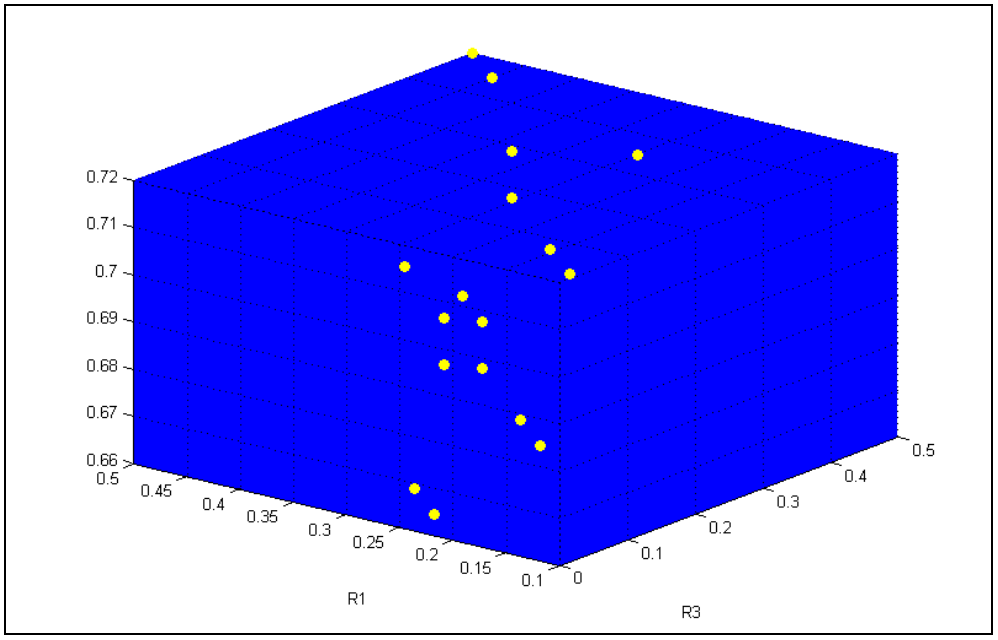

Figure 4: Comparison of transition rates for different regions. Blue, green, red, and yellow represent the transition rates for normal, acidic, hypoxic, and acidic-hypoxic regions respectively. Although the rates for each region seem to be clustered in different groups, the distance among transition rates for different regions are large enough to make the intera-region differences negligible. Second graph shows the same information from another point of view.

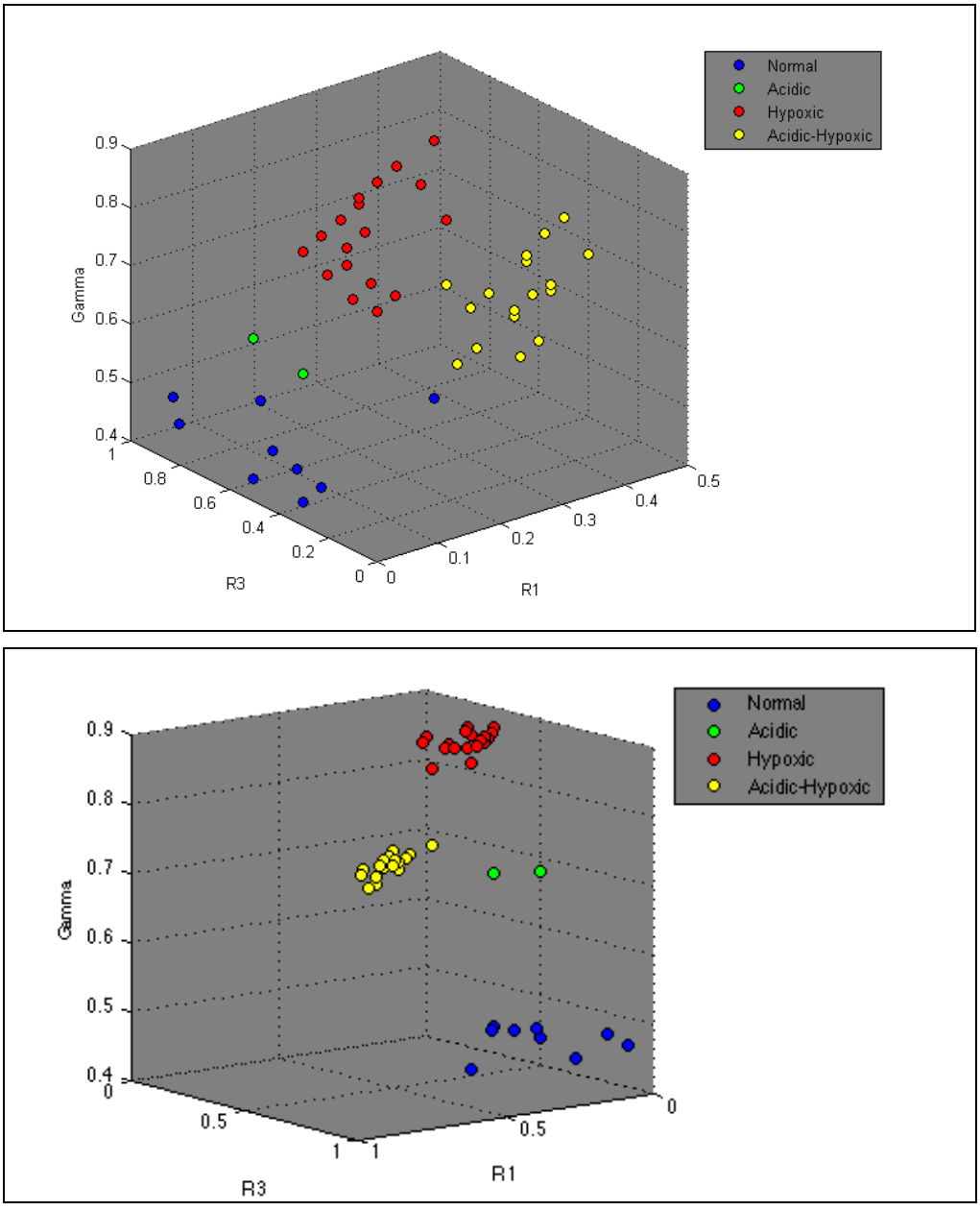

3.6. Discussion

As illustrated in Figures 1 to 3, our results for each region may belong to two or three different clusters. However, the overall comparison of all regions (Figure 4) suggests that the average of each set of results can properly represent and characterize the entire set. In addition to summarizing data for one combination of transition rates for each region, we also compare and interpret the microenvironmental effects on division, differentiation, and self-renewal of cancer stem cells as well as the modifications of non-stem cancer cells division and dedifferentiation.

3.6.1. Hypoxia, dedifferentiation and symmetric differentiation

Figure 5 shows the prominent promotion of dedifferentiation in the hypoxic region. Non-stem cancer cells located in the normal region have the lowest rate of reprograming. Although acidic and hypoxic-acidic regions clearly up regulate the dedifferentiation, the hypoxic region shows the largest proportion of non-stem cancer cell reprograming (0.8 to 0.9).

We hypothesize that hypoxia up regulates the cancer stem cell phenotype through the promotion of dedifferentiation of non-stem cancer cells. On one hand, this hypothesis is supported by all biological experiments used in constructing the model, and on the other hand, it can be expanded to justify experimental results obtained by other research groups. For instance, Philips and colleagues [Chen et al. 2010] have proposed a hierarchy of cancer cells that are able to initiate and maintain Gliomas. According to their experiments (done in 3% oxygen), a subgroup of non-stem cancer cells are at the top of hierarchy and are able to generate cancer stem cells as well as non-stem cancer cells. They have proposed that the capability of this subgroup of non-stem cancer cells to promote tumour progression is even higher that

those cancer stem cells marked by the neural stem cells marker, CD133+. Our model and resulting transition rates can explain their results. Since hypoxia prominently promotes dedifferentiation of non-stem cancer cells, tumour progression and cancer stem cells maintenance are dominantly affected by reprograming of non-stem cancer cells rather than the self-renewal of cancer stem cells. Thus in hypoxic regions, the population of less-mature non-stem cancer cells may be larger than other regions.

Another identified characteristic of the transition rates in hypoxic region is the augmented transition rate for symmetric differentiation of cancer stem cells (r_3). The variance is clearly apparent when compared to its counter part in normal regions.

Figure 5: Distribution of results for four regions, normal(blue), Acidic (green), Hypoxic (red), and Acidic-hypoxci (yellow). The points are clearly devided based on the dedifferentiation and symmetric differentaition rates for each region (Except the acidic and acidic-hypoxic regions that seem to have similar dedifferentaition rates).

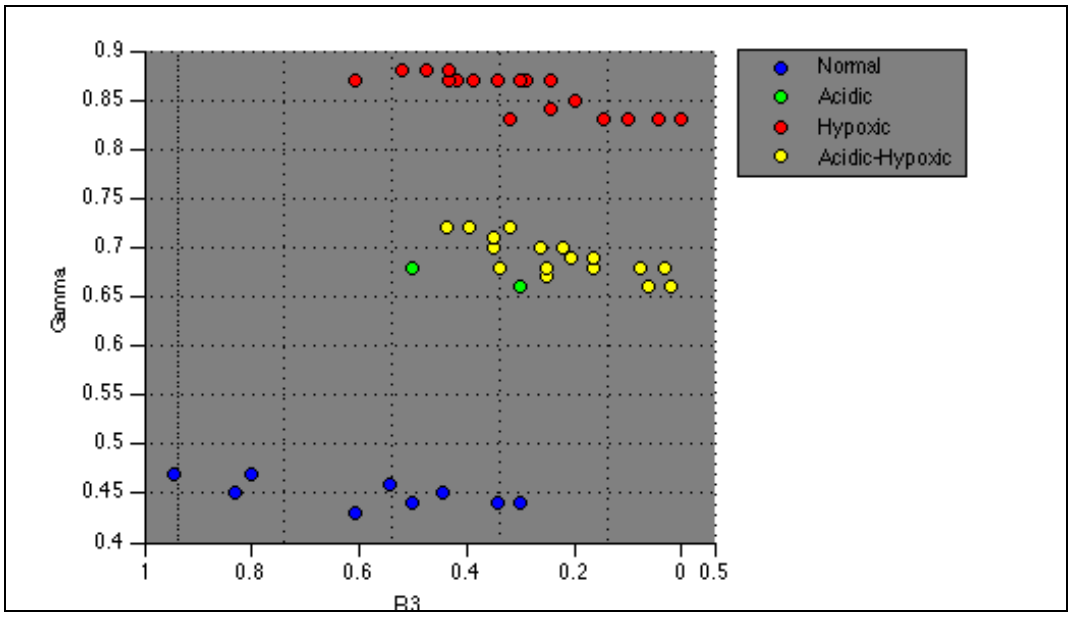

3.6.2. Acidity and dedifferentiation

Figure 6 demonstrates the loci of each region results in γ, r_1 plane. Although in Figure 5 the locus of acidic region results and acidic-hypoxic region seem to be merged, Figure 6 illustrates the clear differences between r_1 values for the two results sets for acidic and acidic-hypoxic regions. Our simulation results also show a sharp decrease of r_1 values in acidic region though the dedifferentiation of non-stem cancer cells has significantly increased compared to normal regions.

Figure 6: Distribution of results for four regions, normal(blue), Acidic (green), Hypoxic (red), and Acidic-hypoxci (yellow). The points are clearly devided based on the dedifferentiation and self-renewal rates for each region). Although acidic and acidic-hypoxic regions equally affect the dedifferentiation, they differ considarably in promotion of self-renewal in cancer stem cells.

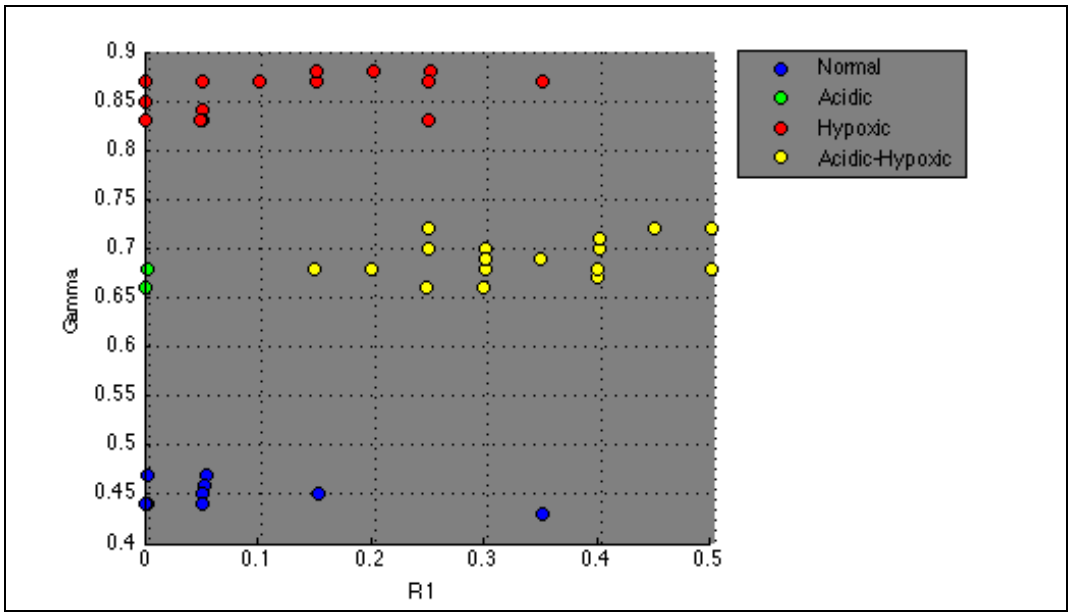

3.6.3. Acidic-hypoxic regions and self-renewal

According to our simulation results the coincidence of hypoxia and acidity mostly promotes the self-renewal of cancer stem cells (Figure 7). The distribution of results for different regions in the r_1, r_3 plane illustrates that the self-renewal rate for cancer stem cells residing in acidic-hypoxic region is much higher than for those in regions under normal microenvironmental conditions. The transition rate for symmetric differentiation of cancer stem cells in acidic-hypoxic areas is also considerably less than for those in normal, acidic and hypoxic regions. In addition, the dedifferentiation of non-stem cancer cells in acidic hypoxic regions is almost the same as for those in acidic regions.

Based on our simulation results we hypothesize that acidic-hypoxic regions promote tumour progression and cancer stem cell maintenance through the up regulation of cancer stem cell self-renewal. This hypothesis also justifies the experimental results reported by Fukumura et al. [Fukumura et al. 2001] about the non-additive effect of simultaneous hypoxia and acidity on tumour progression. Although the dedifferentiation rate in hypoxic areas is much higher than in acidic regions, the rate in acidic-hypoxic regions is equal to that in areas with high acidity. In addition, self-renewal promotion in both hypoxic and acidic regions is considerably less than that in acidic-hypoxic regions. Thus, rather than having an average effect of independent exposure to hypoxia and acidity, we noticed an independent effect of simultaneous acidity and hypoxia that dominantly influences the self-renewal of cancer stem cells.

Figure 7: Distribution of results for four regions, normal(blue), Acidic (green), Hypoxic (red), and Acidic-hypoxci (yellow). The points are clearly devided based on the symmetric differentiation and self-renewal rates for each region. Acidic-hypoxic region shows the most domimnant effect on self-renewal, while the symmetric differentiation rate of this region is the lowest among all other areas.

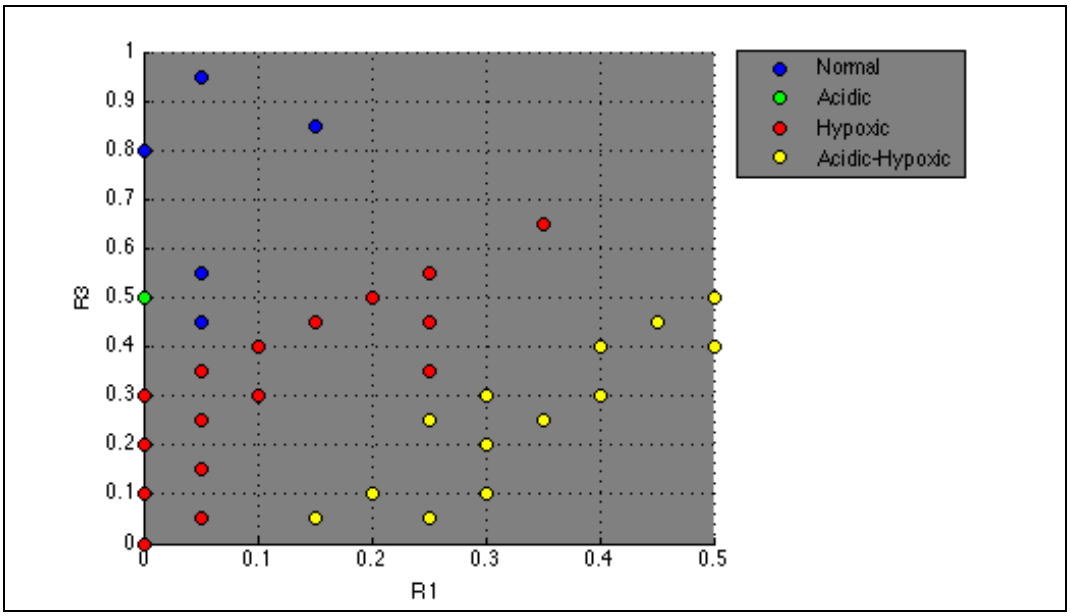

3.6.4. Implications for cancer therapy

As modern cancer therapies are improving to target specific cell types, the need for identifying which cell type(s) to target is becoming increasingly important. The aforementioned results can provide a hint as to which subpopulation(s) of cancer cells may be the critical group to target, based on the instantaneous state of the tumour.

The self-renewal down-regulation of cancer stem cells and simultaneous dedifferentiation promotion in acidic regions necessitates the selection of a therapy that focuses on cancer progenitors. Likewise, since the dedifferentiation rate of cancer progenitors is highly augmented in hypoxic regions, selecting a therapy that primarily targets progenitors is more appropriate. However, the self-renewal of cancer stem cells is higher than normal regions. Thus, the therapy secondary target must be cancer stem cells. In an acidic-hypoxic region, the promotion of cancer stem cells is higher than in hypoxic and acidic regions; therefore a suitable therapy must focus on cancer stem cells while not neglecting cancer progenitors because of the high dedifferentiation rates observed in this region.

4. Simulated tumour growth

In this chapter we use a cellular automaton model to investigate the growth dynamic of cancer cells under tumour microenvironment condition. We developed our model by considering the effect of the extracellular matrix inside the tumour tissue, cellular heterogeneity, division and dedifferentiation, and cell pushing.

4.1. Cellular automata model

Implication of cellular automata in cancer modeling has been pioneered by Düchting and Vogelsaenger to model the effect of radiotherapy on cancer tumours [Duchting and Vogelsaenger 1984] and has rapidly become popular [Deutsch and Dormann 2005]. Among more recent models, the model proposed by Ferreira et al. of tumour morphology [Ferreira et al. 2002], the model proposed by Patel et al. of cell metabolism and invasion with a focus on the glycolytic phenotype [Patel et al. 2001], and Anderson's model of tumour invasion [Anderson 2005], are current cellular automaton models of cancer growth. Ferreira's model considered the

concentration of nutrients in the tumour microenvironment and formed a probabilistic model that generates matching nutrient consumption heterogeneities to available biological experiments [Ferreira et al. 2002]. Patel et al. emphasized the metabolic differences and heterogeneities affected by vessel density inside the tumour [Patel et al. 2001]. However, like Ferreira and colleagues' work [Ferreira et al. 2002], they only considered one phenotype of cancer cells residing in a continuous field of chemicals in their hybrid cellular automaton model. As an improvement, Anderson has added different phenotypes of cancer cells to his proposed model [Anderson 2005]. Although Anderson has considered the heterogeneity of cancer cells, the random assignment of cell phenotypes to new cancer cells disconnects the cellular automata from the tumour microenvironment. Kansal et al. [Kansal et al. 2000a, b] formed a three-dimensional cellular automaton model to investigate the growth of GBM. They have used a Voronoi representation rather than cubic representation. In the Voronoi representation, the grid sizes vary and consequently the formed tumour is geometrically more similar to biological observations. Following this, Mansury et al. [Mansury et al. 2006] have upgraded Kansal' model by adding two different subpopulations of proliferative or migrating cancer cells and using game theory to investigate the system 'pay-off' for each subpopulation. The interaction of cancer cells and the tumour microenvironment was previously studied by the same group in and agent-based model of brain cancer growth [Mansury et al. 2002]. Gatenby and Vincent [Gatenby and Vincent 2003] have used game theory and continuous population dynamic approaches to identify essential conditions for tumour invasion. They have proposed that the failure of ordinary cytotoxic treatment is due to the adaptation of cancer cells to their new microenvironment.

Herein, we introduce a two- dimensional cellular automaton model composed of 8 different phenotypes of cancer cells all are residing in a 20μm-square lattice and each behaving distinctly from the others in response to microenvironmental conditions and its neighbouring cells. Cell phenotypes that are different agents in the model can affect the fate of other cells through nutrient consumption, blocking of proliferating cells, or pushing other cells to make space for their division.

4.1.1. Cell division

The same division pathways used in the previous chapter are implemented in a square lattice of cellular automata to model the proliferation of cancer cells. Each cell can have three different states of proliferation, quiescence and death. We will extensively describe conditions that bring a cell to a proliferative, quiescent or dead cell in future section of this chapter. Regardless of the reasons that lead to each of above-mentioned states, the model runs a different algorithm for each. So that a dead cell is considered as a blocking obstacle for neighbouring cells' proliferation and movement until the debris are all collected. A quiescent cell remains in a non-proliferative state unless the conditions that caused quiescence change. Finally, a proliferative cell goes through division pathways unless it is an M cell that cannot proliferate anymore. We designed our cellular automata to be traceable so that for each present cell in the square lattice, the type of the cell and previous proliferation state are known and help to determine the current proliferation state and the type of daughter cell after division or dedifferentiation. The preliminary layout of the initiating cells is arbitrary, though in the presented simulations they are approximately located in the centre. The types of initiating cells are selected to match the conditions of neurosphere assay experiments. The placement of new cells after division are decided according to vacancy of four possible neighbouring positions of parent cells (up, down, left, and right), considering one of the daughter cells take the place of the parent cell. If there is more than one vacancy, a position is randomly picked. However, the occupancy of all positions does not necessarily lead the parent cell to a quiescent state; in this case cancer cells may try to push neighbouring cells to make some space for new daughters. The mechanisms to run the cell pushing is a complex combination of cell signalling and physical forces.

4.1.2. Pushing

Each cell agent may be able to proliferate even if all its four neighbouring positions are occupied. We consider a fixed pushing radius for all cell types (equal to 5 cell) in our cellular automata model. A proliferating cell surrounded by other cells can push its neighbours to the closest vacant position at most 5 cells away. Hence, even a cell blocked at the center of 11 by 11 square lattice of cells may divide if other necessary conditions are satisfied.

The pushing mechanism implemented in our model is as follows: a counter finds the vertically or horizontally closest vacant position in lattice. The counter cancels the process if it reaches an obstacle. The obstacle may be a dead cell or a vacant position with improper extracellular matrix condition where neither the required level of adhesion nor the acceptable ranges of pressure are satisfied. As the next step, the counter will be checked for the maximum radius of pushing allowed in the model (herein, we fixed it for 5). If it passes this step, the whole chain of cells from the parent cell to the vacant position will be moved to make empty the neighbouring position of proliferating cells. If the counter points to a position out of the allowed range, the proliferative cell is doomed to quiescence. Figure 9 shows the flowchart of the simulation and the certain step of Pushing process implementation.

4.1.3. Implementation of extracellular matrix

Cells viability and activities are closely dependent on an adequate level of adhesion to and proper range of pressure from the surrounding matrix. We simplified the effect of cell adhesion and surrounding pressure to a randomly assigned matrix. This matrix, which we call the ECM matrix hereafter, plays the role of the extracellular

matrix as well as the probable presence of normal cells inside the tumour tissue. As an improvement to the current model, the ECM matrix can be modified to better match the biological features of Extracellular matrix inside the tumour tissue.

4.2. Cell metabolisms

The tendency of cancer cells to switch to a glycolytic metabolism, even in the presence of adequate content of oxygen, known as Warburg effect, sheds light on the importance of both cell metabolisms in tumour progression and microenvironmental modifications. Hence, in tumour tissue (not only in hypoxic regions but also in normoxic regions) cancer cells may switch to glycolysis rather than respiration.

$$\mathrm{Respiration}: C_6H_{12}O_6 + 6O_2 \rightarrow 6CO_2 + 6H_2O + 36ATP$$

$$Glycolysis: C_6H_{12}O_6 \rightarrow 2C_3H_5O_3^- + 2H^+ + 2ATP$$

Comparing the respiration and glycolysis reaction equations, the production of energy (ATP) for one molecule of glucose in respiration is 18 folds the amount produced by glycolysis. On the other hand, the presence of hydrogen ions among glycolysis metabolism products introduces the glycolysis acidic effect. Despite of the existence of a natural prominent buffering system in soft tissues, that is the interconversion of bicarbonate (HCO_3^-) and carbon dioxide (CO_2), increase of concentration of hydrogen ions (H^+) causes an indispensible effect on interstitial pH. The interstitial buffering system is as follows:

$$CO_2 + H_2O \leftrightarrow HCO_3^- + H^+$$

In addition to the enrolment of the glycolytic metabolism, the impairment of cancer cells may lead to recruitment of glutaminolysis [Helmlinger et al. 2002], as follows:

Glutaminolysis: $C_5H_{10}N_2O_3 + 2H_2O + O_2 \rightarrow C_3H_5O_3^- + 2NH_4^- + 2CO_2 + H^+$

Therefore, similar to nutrient diffusion, cellular metabolism dominantly affects the tumour microenvironment as the concentration and consumption of oxygen and the interstitial pH levels inside the tumour depend on the prevalent metabolism.

To model the distribution of nutrient, oxygen and acidity in tumour microenvironment, we adopted the model proposed by Molavian et al. [Molavian et al. 2009]. In their model, Molavian et al. used a mathematical approach to find the pH level as a function of distance from a blood vessel. They reproduced the biological results of Helmlinger et al. [Helmlinger et al. 1997], and modeled the metabolic toggling of cancer cells between respiration and glycolysis. Their explanation of the metabolic spatial gradient can justify the observed plateau in pH graph (Figure 8). Their scenario is as follows: in the normoxic perivascular regions, respiration is the dominant employed metabolism while the recruitment of glycolysis increases as the distance from the vessel and the level of hypoxia increase. Thus at intermediate distances from blood vessels the cell metabolism is a combination of respiration and glycolysis and cells entirely switch to a glycolytic metabolism in anoxia (Figure 8) [Molavian et al. 2009].

According to Michaelis-Menten kinetics, the consumption of oxygen and glucose satisfy the equations below:

$$P_O = rP_G \frac{C_O}{C_O + k_O} f_1(C_O)$$

$$P_G = rP_G \frac{C_G}{C_G + k_G} f_2(C_O)$$

Where P_O and P_G are the consumption of oxygen and glucose, r is the ratio of glucose consumption to oxygen consumption, k_O and k_G are the Michaelis-Menten constants, C_O is the concentration of oxygen, and f_1 and f_2 are adjustment functions that control metabolism switching between respiration and glycolysis [Molavian et al. 2009].

Figure 8: Experimental and simulated plots for pH and pO2. The pH level decreases as the distance from the blood vessel increases. Similar to pH, the concentration of oxygen decreases as the distance from the vessel increases so that in 300 μm from the blood vessel the level of oxygen is almost zero. Inset graph shows the ratio of oxygen consumption to glucose consumption. The figure is adapted from Molavian et al 2009.

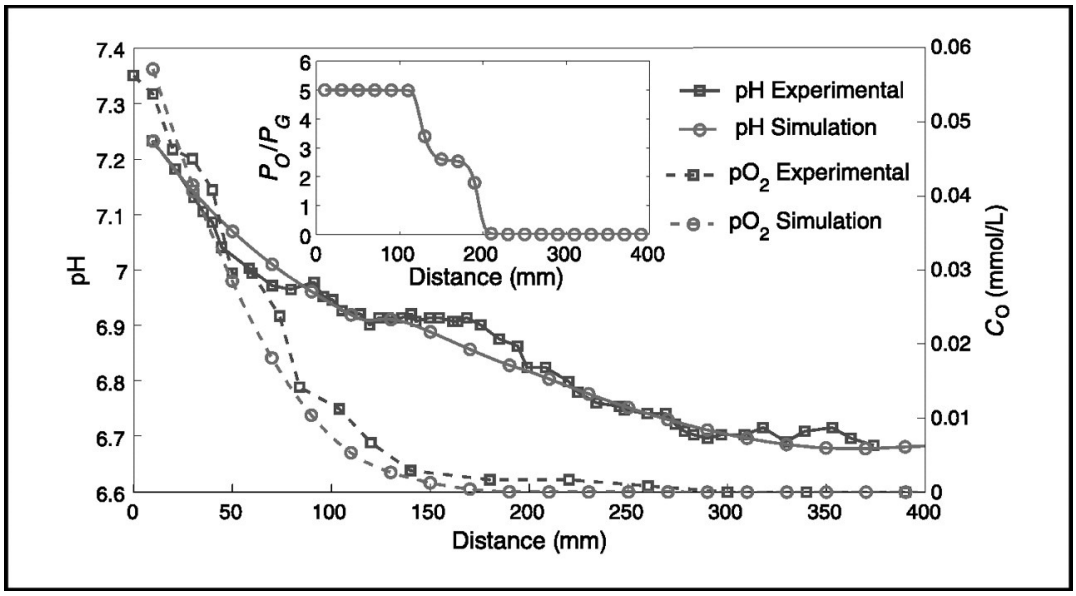

The steady state solution of the partial differential equation determines the concentration of chemicals in interstitial space. The partial diffusion equation is as follows:

$$\frac{\partial C_i}{\partial t} - D_i \nabla^2 C_i = P_i \quad (32)$$

and the steady state of Equation (32) reads for:

$$P_i + D_i \nabla^2 C_i = 0 \quad (33)$$

where C_i is the concentration of chemical i, D_i is the diffusion constant of chemical i, and P_i is the production or consumption of chemical i.

We have expanded this model to match the layout of the current lattice of tumour cells so that there is a frame of vessels surrounding cancer cells (as boundary conditions in Equation 33) and chemicals diffuse into the tissue according to the discretized format of Equation (32). Hence at each time step of simulation the

discretized diffusion equation for each chemical reads for:

$$P_{i,j} + D\left(\frac{C_{i,j+1} - 2C_{i,j} + C_{i,j-1}}{\Delta x} + \frac{C_{i+1,j} - 2C_{i,j} + C_{i-1,j}}{\Delta y}\right) = 0 \qquad (34)$$

where $C_{i,j}$ and $P_{i,j}$ respectively shoes the concentration and production (consumption) of species in position (i,j) of the lattice. The spatial layout of our square lattice model requires the equality of Δx and Δy. The diffusion constants of each species into the tissue and permeability constants of each species through the blood vessel are listed in Table (11).

Table 11: Diffusion and permeability constants and intravenous concentration of chemicals. Regenerated from Molavian et al. [Molavian et al. 2009].

Compound	D (cm2/s)	μ (cm/s)	Intravenous Concentration (mM)
O2	1.46 e−5 [Nicholas MG and Foster 1994]	3.0 e−5 [Crone and Levitt 1963]	6.5 e−2 [Molavian et al. 2009]
Glucose	1.10 e−6 [Casciari et al. 1988]	3.0 e−5 [Crone and Levitt 1963]	7.5 e−1 [Molavian et al. 2009]
CO2	8.9 e−7 [Molavian et al. 2009]	3.0 e−5 [Crone and Levitt 1963]	1.7 [Molavian et al. 2009]
Glutamine	1.1e−6 [casciari et al. 1992]	3.0 e−5 [Crone and Levitt 1963]	3.98 e−5 [Molavian et al. 2009]
Bicarbonate −	2.2 e−7 [Molavian et al. 2009]	1.7 e−5 [Chan et al. 1983]	15 [Molavian et al. 2009]
Lactate −	1.9 e−6 [casciari et al. 1992]	1.2 e−4 [Crone and Levitt 1963]	2 [Bell et al. 1968]
H +	1.9 e−6 [Fatt et al. 1998]	1.2 e−4 [Crone and Levitt 1963]	3.98 e−5 [Bell et al. 1968]
Cl −	2.26 e−7 [casciari et al. 1992]	1.2 e−4 [Crone and Levitt 1963]	1.05 e+2 [Bell et al. 1968]
Na+	3.14 e−7 [casciari et al. 1992]	1.2 e−4 [Crone and Levitt 1963]	1.22 e+2 [Bell et al. 1968]

4.3. Implementation of cell division, pushing algorithm and cellular metabolisms in cellular automata model

Following flowchart demonstrates the implementation of cell division, and Pushing algorithm as described before. The type of the cells, distribution of the nutrients and pH, and previous state of the cell step in during different parts of the algorithm and strongly affect the fate of the cell (Figure 9).

4.3.1. The effect of ECM on tumour growth of single-type cells

The following figure (Figure 10), illustrates the effect of ECM absence on our simulated tumour. In order to clarify the Impact of the ECM, the distribution of nutrients and pH as well as the pushing mechanism are neglected. The tumour is assumed to contain a single type of cells in following results. Therefore, cancer cells are dividing according to their initial states and availability of vacancies in neighbouring positions. The layout of the generated tumour completely matches the prediction. Since the initiating cells are located in the centre of the lattice and the division algorithm selects the vacancies either horizontally or vertically the tumour is almost a diamond concentric with the lattice.

Figure 9: The flow chart of simulation algorithm.

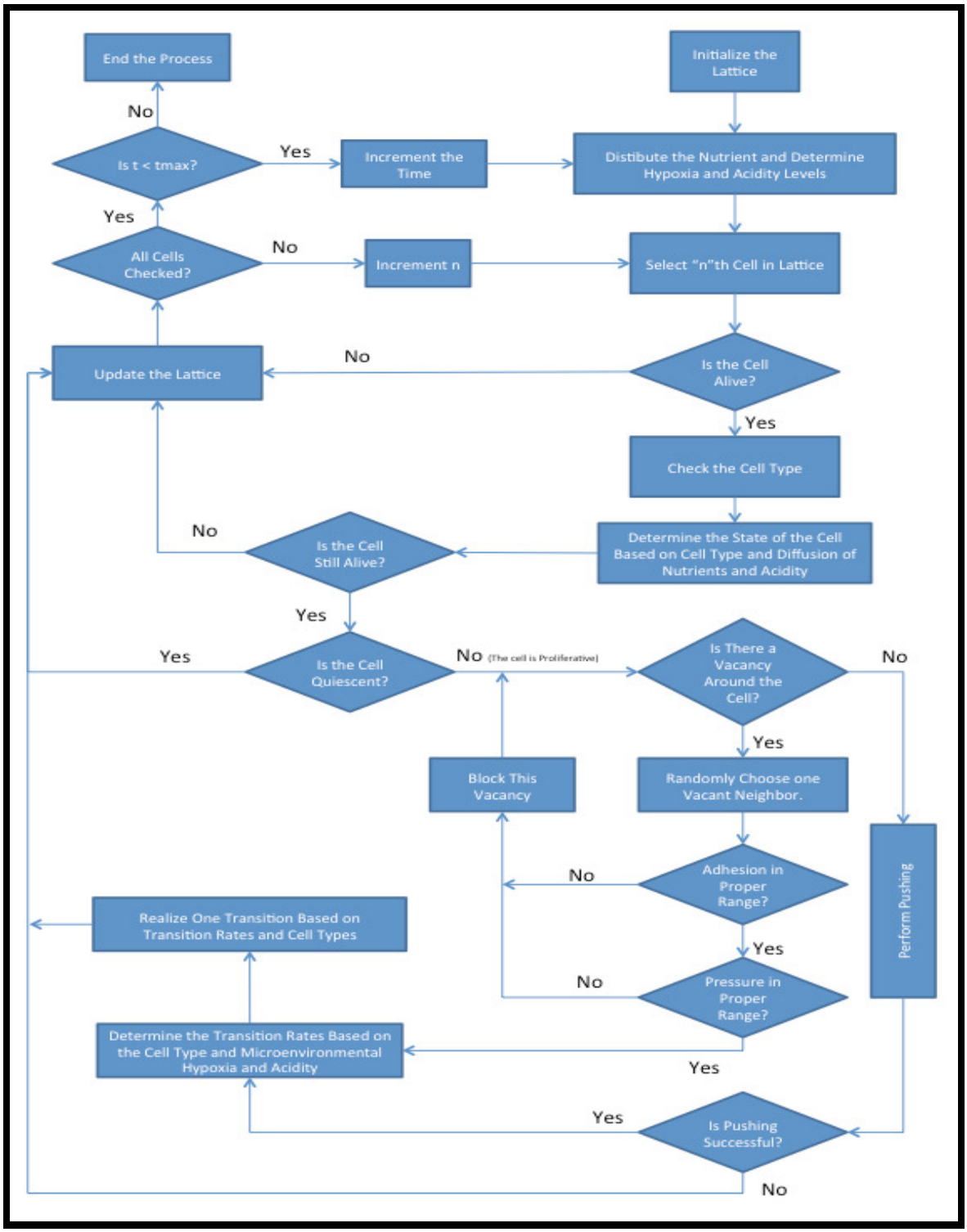

Figure 10: Tumour growth without considering the effect of ECM, nutrients and pH distribution, and Pushing algorithm. The vacancies selection in a horizontal or vertical manner caused the diamond-like shape of the generated tumour.

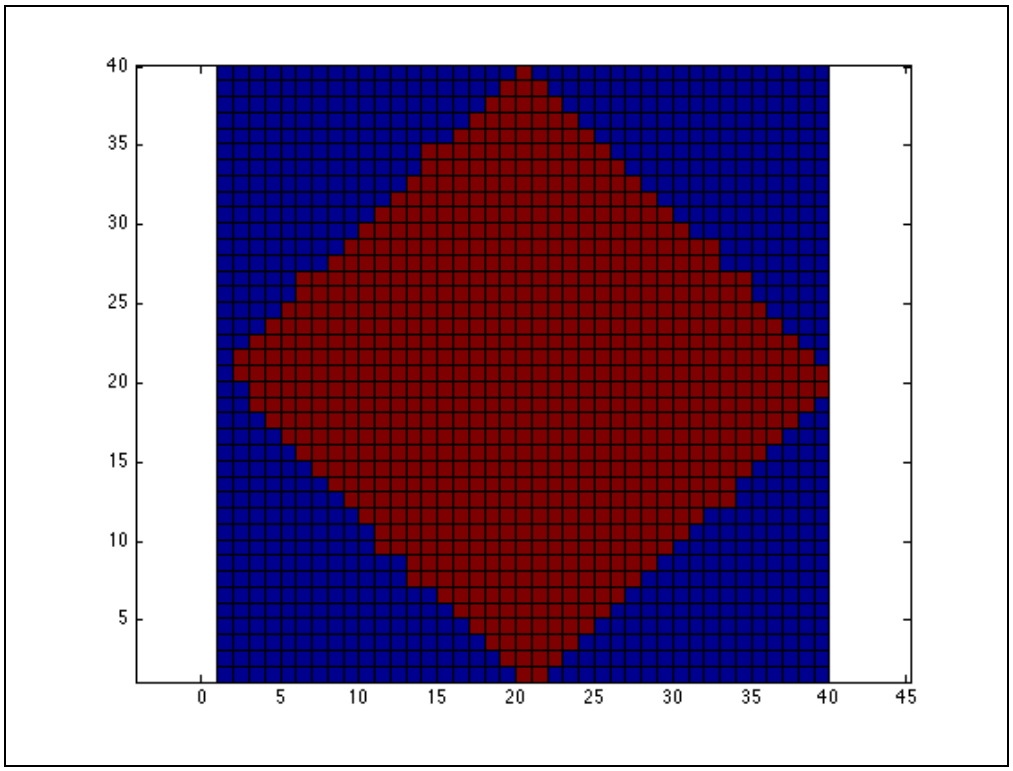

The presence of ECM modifies the tumour 2-D layout to a more circular shape. Moreover, the restrictions on the pressure and adhesion levels lead to the appearance of empty spots inside the tumour where the ECM is not in a proper range, hence the cells can not locate in those positions due to the high levels of pressure or inadequate adhesion. Following figure (Figure 11) shows the simulated tumour of single type of cancer cells in a lattice with randomly assigned ECM. The asymmetric layout is due to the stochastisity of the simulation. To illustrate the effect of the ECM, the pushing algorithm is inactivated and nutrients and pH distributions are neglected.

Figure 11: Tumour growth affected by ECM. Pushing algorithm is inactivated as well as the effect of nutrient and pH distribution.

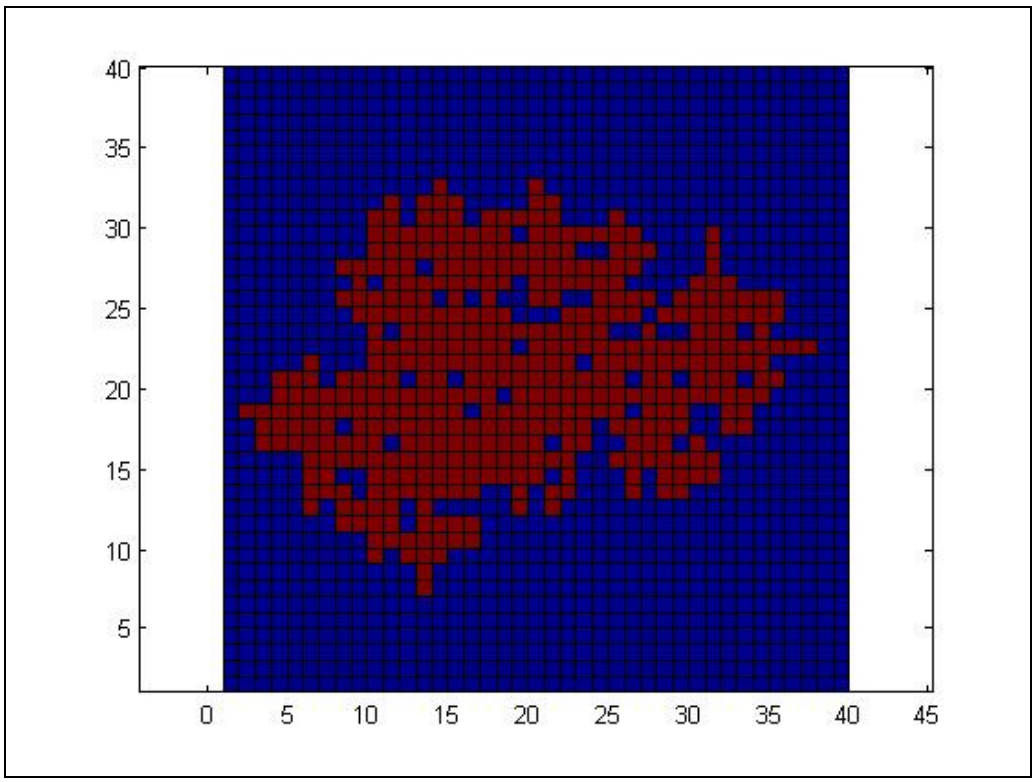

4.3.2. The effect of pushing on single-type cell tumour growth

The pushing algorithm enables the surrounded cell to proliferate. Hence in a simulation with activated pushing algorithm more proliferating cells are dividing simultaneously. Thus the apparent prediction is that the colony size of a pushing-activated tumour is larger than an inactivated-pushing tumour during the same time scale. Comparison of Figure (12) with Figure (11) supports this prediction. In this figure the simulation is run for a pushing-activated tumour. The effect of ECM, and nutrient, and pH distribution are neglected. The empty spots will be filled if we run the simulation for a longer period.

Figure 12: Tumour growth affected by pushing algorithm. ECM is inactivated as well as the effect of nutrient and pH distribution. Comparison of this result with figure 11 illustrates the promoting effect of pushing algorithm on colony size of the tumour.

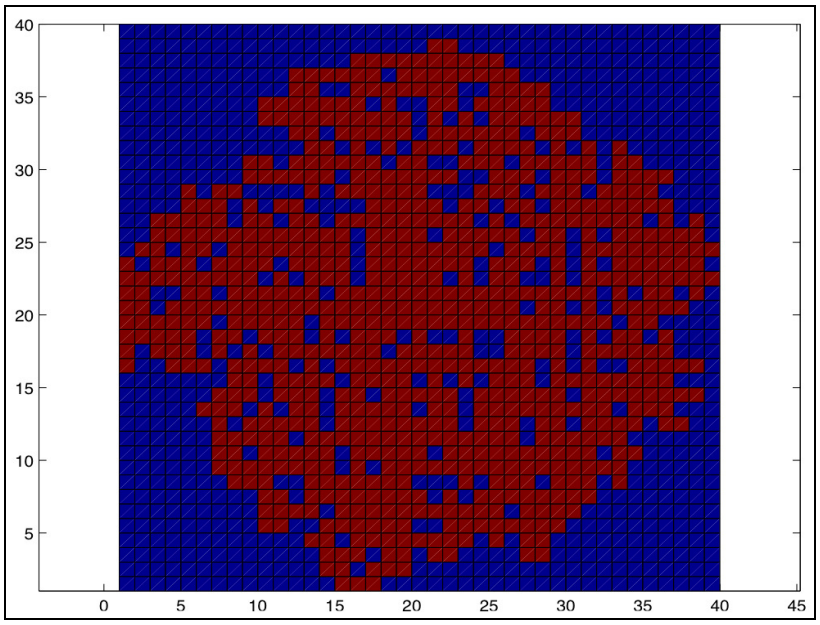

4.3.3. The effect of nutrients and pH distribution on single-type cell tumour growth

The distribution of nutrients and pH affects the cancer cell division, differentiation, death, and metabolism. Considering the type of residing cell, the concentration of oxygen and acidity at each grid of lattice determines the probabilities of possible transitions. However, in the early stages the viability, quiescence or proliferation of a cell is determined by hypoxia and acidity intensity of the tumour microenvironment. The following figures (Figure 13) show growth of tumours under conditions of symmetric and asymmetric distribution of nutrients. Apparently, under the asymmetric distribution of nutrients the tumour is skewed to the vessel that is rich in nutrients whereas the low concentration of nutrients in other parts results in the quiescence of residing cells.

4.3.4. Implementation of different phenotypes of cancer cells into the cellular automata model

In the presented 2D cellular automata model, we implemented tumour heterogeneities by introducing two basic groups of cancer cells: cancer stem cells that express CD 133+ in biological experiments and non-stem cancer cells that are recognized as CD133- cancer cells in biological experiments. According to the aforementioned transition pathways, the first four phenotype of cancer cells, S, P_1, P_2, and P_3, are assigned to cancer stem cells whereas P_4, P_5, P_6, and M cells are signed to presents the non-stem cancer cells. To bring the double species-cellular automata model close enough to the aforementioned 8 species model of cancer cells, we add another characterization of age to the cancer cells so that a cancer cells with age of 1 represent a P_1 cell and a cancer cell with age of 7 represents a M cell. Age 0 is assigned to S cells. Figure 14 shows the results of implementing two types of

cancer cells in cellular automata model.

Figure 13: Tumour growth under symmetric (first) and asymmetric (second) distribution of nutrients. The tumour growth is skewed from the vessels with nutrients concentration less than minimum requirements of proliferating cells. Both tumours are generated from single-type of cancer cells located at the centre of the lattice. The concentration of oxygen and glucose are $6.5*10^{-2}$ mM and $7.5*10^{-1}$ mM in vascular frame for the first image. The concentration of oxygen is different in four vessels of the second image and is $8.5*10^{-2}$ mM, $5.5*10^{-2}$ mM, $5.5*10^{-2}$ mM, $5.5*10^{-2}$ mM for upper, lower, left and right vessels respectively. The concentration of Glucose is equal in all vessels and it is $7.5*10^{-1}$ mM.

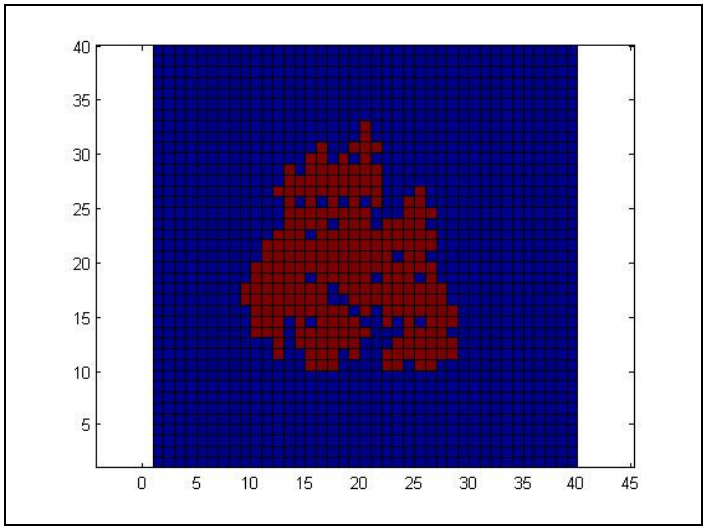

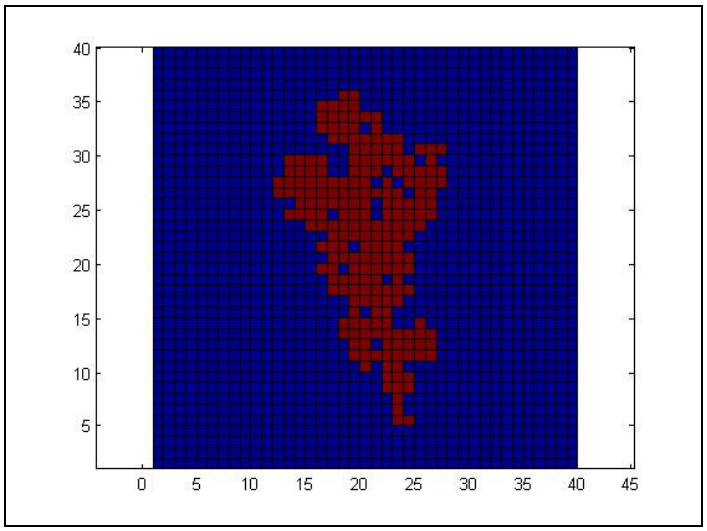

Figure 14: Implementation of different phenotypes of cancer cells in 2D cellular automata model. Red, blue and green squares are representing non-stem cancer cells, Cancer stem cells and empty spots respectively. The transition rates for this specific realization are 0.05, 0.15, 0.1, 0.4, 0.5, 0.1for ρ_S, ρ_P, r_1, r_2, r_3, and γ respectively.

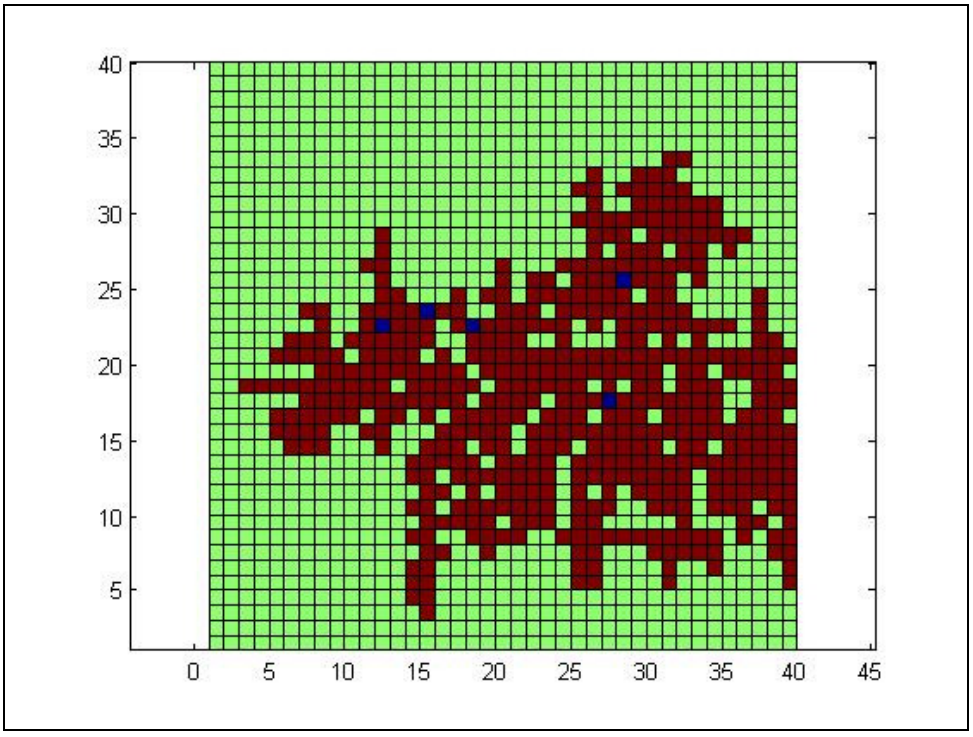

4.4. Results and Discussion

Recalling the results for transition pathways for each microenvironmental region, herein, the implementation procedure and the obtained realization are presented in a forward model and discussed.

4.4.1. Summarizing the transition rates for each microenvironmental region

Table (12) summarizes result sets of transition rates in different microenvironmental regions. Presented values are the average of transition rates presented in Tables (7-10) over each region. Considerable distance among loci of results for different regions (Figures 4-7) suggests that even the average of each set can characterize the whole set distinctly. We have implemented the following values as the transition rates in the 2D cellular automata model.

Table 12: The transition rate for different microenvironmental regions.

Average	Hypoxic Region	Acidic Region	Hypoxic-acidic Region	Normal Region
ρ_S	0.693147	0.693147	0.693147	0.693147
ρ_P	0.693147	0.693147	0.693147	0.693147
r	-0.382927	-0.400000	0.064706	-0.522222
r_1	0.115854	0.000000	0.335294	0.077778
r_2	0.385366	0.600000	0.394118	0.322222
r_3	0.498780	0.400000	0.270588	0.600000
γ	0.876098	0.670000	0.690588	0.450000

4.4.2. Results

We implemented the above-mentioned transition rates into the cellular automata model. The cellular automata also consider a randomly assigned extracellular matrix. The function of this matrix in the model is as discussed before; each grid in the cellular lattice is able to reside a cell if the relevant value of ECM matrix for this grid is in appropriate ranges to provide necessary adhesion while keeping the pressure low enough. The values of ECM grids are checked during cell division and

pushing mechanisms.

In addition to the ECM and cellular heterogeneities, the distribution of nutrient and pH affect the tumour growth. A cancer cell is forced to quiescent state or death if the concentration of nutrients is not enough for proliferation or survival. Therefore, asymmetric distribution of nutrients forms the morphological alterations in tumour growth. As demonstrated in the previous section, inadequate level of oxygen concentration in one side of the lattice frame, for example, causes the tumour to skew to the direction that can provide sufficient level of nutrient for cell survival and growth. Herein, the realizations of the tumour growth exposed to simulated tumour microenvironment are presented. The results confirm the prediction of previous chapter.

Figure (15) shows the distribution of pH and oxygen and the consumption of glucose and oxygen by tumour cells. In this realization the concentrations of nutrients in vascular frame are asymmetric so that the tumour lattice is exposed to normal, acidic and hypoxic-acidic conditions in the same lattice. The distribution of pH (up left), oxygen (up Right) and the consumption of glucose (down left) and oxygen (down right) are resented in Figure (15). Due to the Impact of cellular metabolism on pH distribution, the tumour is visible in the lattice representing the pH distribution (up left).

Figure (16) and (17) show the produced tumour exposed to the microenvironmental conditions illustrated in Figure (15).

The color code for the lattice presented in Figure (16) is aimed to highlight the tumour heterogeneities regards to the seven introduced phenotypes of cancer progenitor cells, P_1, P_2, P_3, P_4, P_5, P_6, and M cells. As demonstrated by colors in figure (16), maturity of cancer cells is more likely in normal regions than hypoxic-acidic or acidic parts. On the other hand, the acidic region promotes the stem-like phenotype of less mature progenitors, P_1, P_2, P_3, through differentiation of cancer stem cells, while acidic-hypoxic region up regulates the self-renewal of S cell. Table (12), summarized results of previous chapter, supports the produced results.

Figure 15: The distribution of pH (up left), oxygen (up Right) and the consumption of glucose (down left) and oxygen (down right). In this realization the lattice includes are three microenvironmental regions of hypoxic-acidic (right quarter of lattice), acidic (upper quarter), and normal (almost left and lower quarter). Due to the Impact of cellular metabolism on pH distribution, the tumour is visible in the lattice representing the pH distribution (up left).

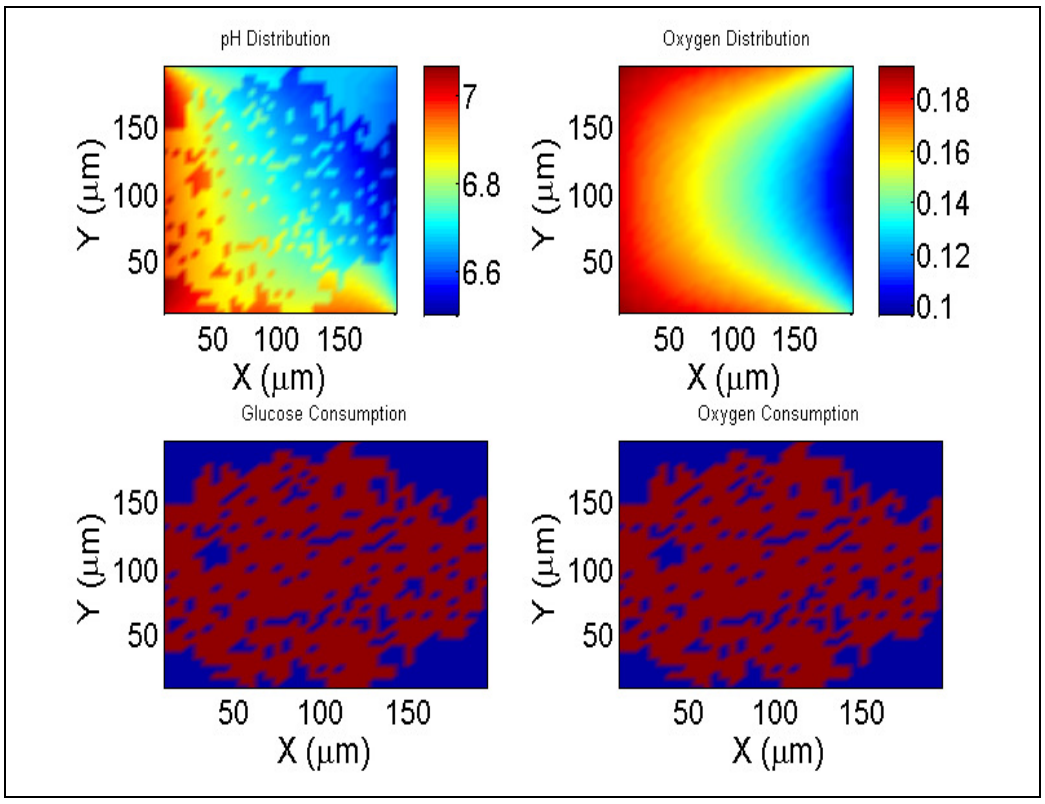

Figure 16: Tumour heterogeneities due to the microenvironmental conditions. Presented lattice is the tumour grown under the microenvironmental conditions shown in Figure (15). Lower and left quarters of the tumour are exposed to the normal conditions while right and upper quarters are exposed to acidic-hypoxic and acidic microenvironmental conditions respectively. Values of grids that interpreted as colors show the residing cell phenotype so that value 1 associates with P_1 cells and 7 represent an M cell. As demonstrated by colors, the maturity of cancer cells is more likely in normal regions. Furthermore, The acidic region promotes the stem-like phenotype of less mature progenitors, P_1, P_2, P_3, through dedifferentiation of cancer cells, while acidic-hypoxic region up regulates the self-renewal of S cell.

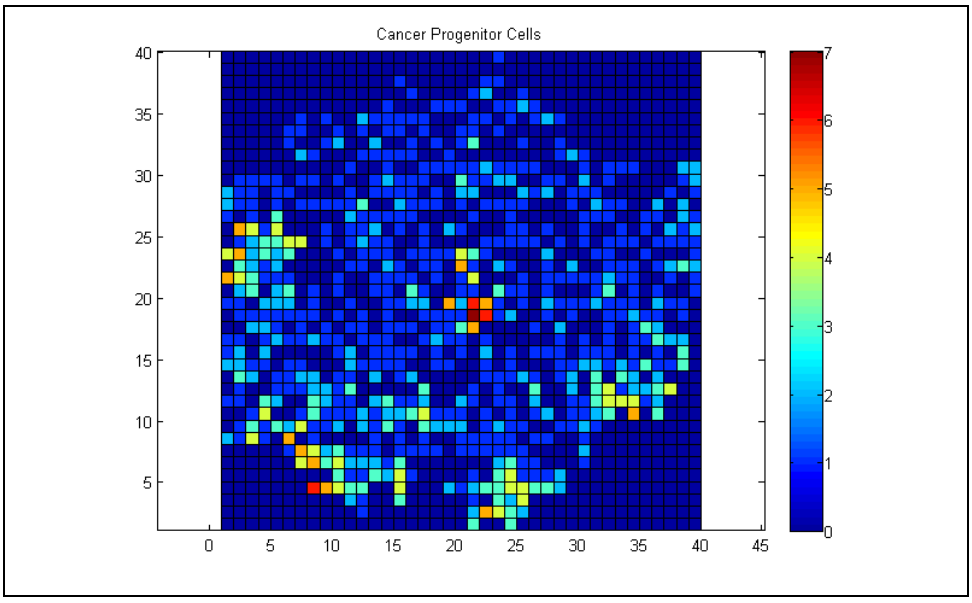

Figure (17) focuses on the S cells in cancer cell population. S cells as the only phenotype that is able to self-renew, symmetrically and asymmetrically differentiate is different from other stem-like phenotypes presented in the model. Normal regions host smaller population of S cells than acidic or acidic-hypoxic regions. This figure supports the argument concluded from recent experimental observations that acidic conditions of tumour microenvironment promotes the stem-like phenotype in cancer cells.

Figure 17: The heterogeneity in tumour exposed to microenvironmental conditions presented in Figure (15). S phenotype of cancer cells (denoted in red) is promoted in acidic and acidic-hypoxic regions.

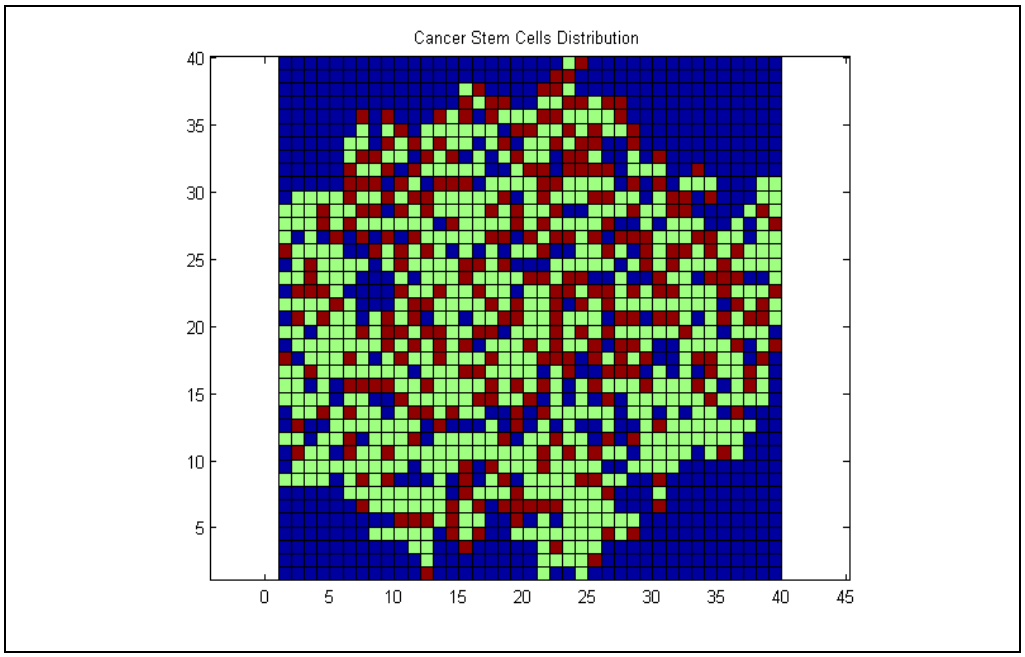

Figures (18-20) sow the results for another realization with the same constrains on nutrient and pH concentration. In this realization, we studied the tumour growth for a longer period. As demonstrated in Figures (18-20), the results of this realization confirm the conclusions of the aforementioned realization. However, longer period of time highlighted the tumour heterogeneities in different microenvironmental conditions.

Figure 18: The distribution of pH (up left), oxygen (up Right) and the consumption of glucose (down left) and oxygen (down right). In this realization the lattice includes are three microenvironmental regions of hypoxic-acidic (right quarter of lattice), acidic (upper quarter), and normal (almost left and lower quarter). Due to the Impact of cellular metabolism on pH distribution, the tumour is visible in the lattice representing the pH distribution (up left). Longer period of realization time, allowed the tumour to grow all over the lattice.

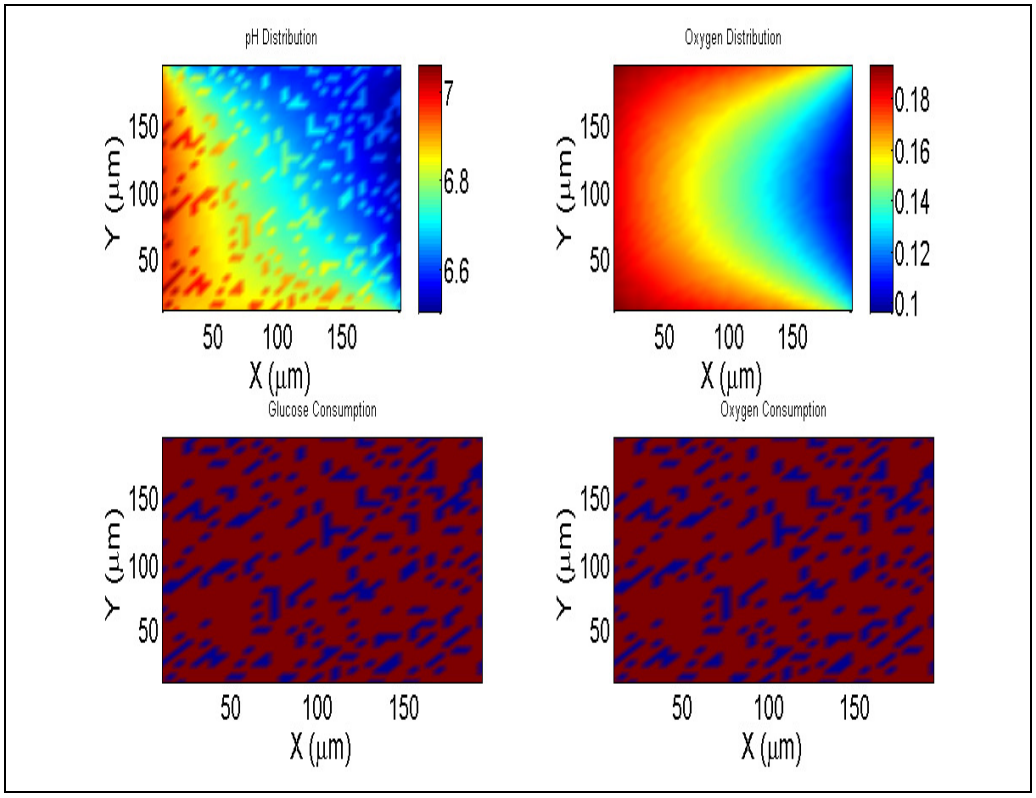

Using a color code for the tumour growth under conditions presented in Figure (18), Figure (19) highlights the tumour heterogeneities regards to the seven introduced phenotypes of cancer progenitor cells, P_1, P_2, P_3, P_4, P_5, P_6, and M cells. As demonstrated by colors in Figure (19), maturity of cancer cells is more likely in normal regions than hypoxic-acidic or acidic parts. Similar to presented results in Figure (16), the acidic region promotes the stem-like phenotype of less mature progenitors, P_1, P_2, P_3, through differentiation of cancer stem cells, while acidic-hypoxic region up regulates the self-renewal of S cell. Table (12), summarized results of previous chapter, supports the produced results.

Figure 19: Tumour heterogeneities due to the microenvironmental conditions. Presented lattice is the tumour grown under the microenvironmental conditions shown in Figure (18). Lower and left quarters of the tumour are exposed to the normal conditions while right and upper quarters are exposed to acidic-hypoxic and acidic microenvironmental conditions respectively. Values of grids that interpreted as colors show the residing cell phenotype so that value 1 associates with P_1 cells and 7 represent an M cell. As demonstrated by colors, the maturity of cancer cells is more likely in normal regions. Furthermore, The acidic region promotes the stem-like phenotype of less mature progenitors, P_1, P_2, P_3, through dedifferentiation of cancer cells, while acidic-hypoxic region up regulates the self-renewal of S cell. Longer period of realization time, allowed the tumour to grow all over the lattice.

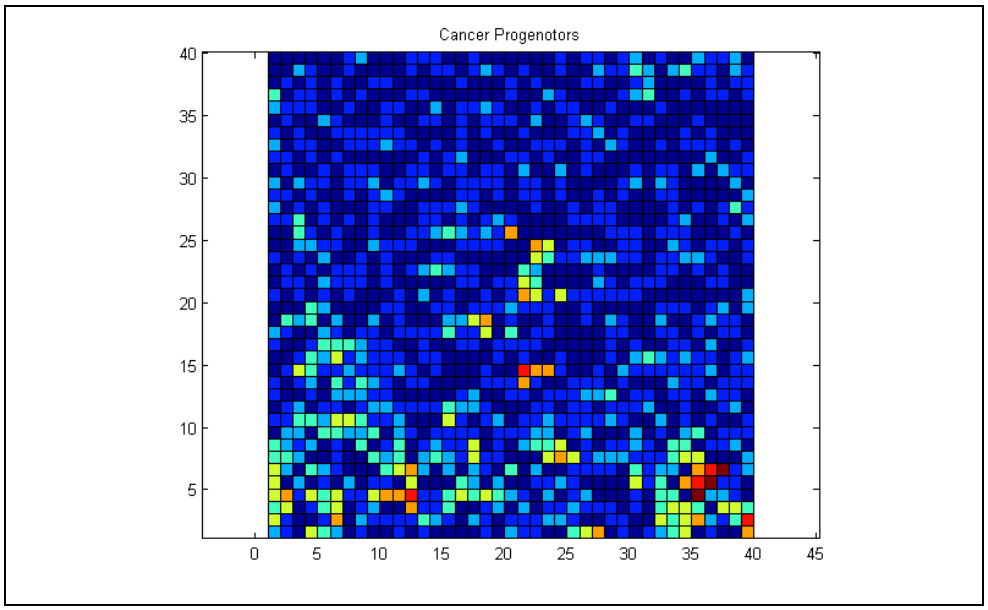

Figure (20) focuses on the S cells in cancer cell population for this realization. As demonstrated in Figure (20), normal region hosts smaller population of S cells than acidic or acidic-hypoxic regions. This figure supports the argument concluded from the results of the recent experimental observations that suggest the promotion of stem-like phenotype under acidic and hypoxic conditions of tumour microenvironment.

Figure 20: The heterogeneity in tumour exposed to microenvironmental conditions presented in Figure (18). S phenotype of cancer cells (denoted in red) is promoted in acidic and acidic-hypoxic regions.

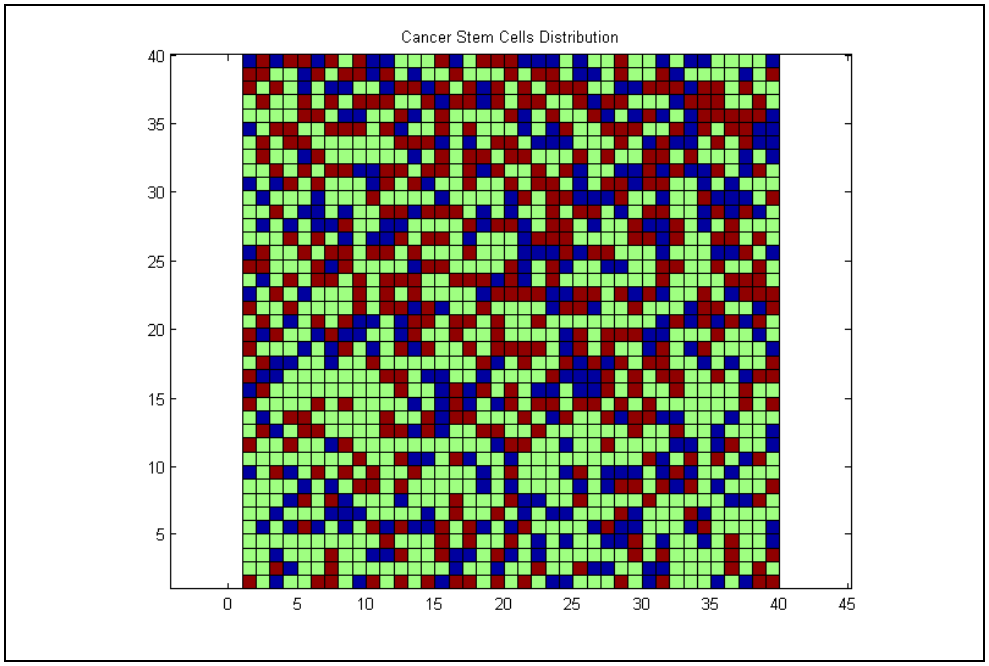

4.5. Discussion

In spite of the ever-increasing attempts to treat cancers, it's still one of the main challenges of modern medicine. Proposing the tumour heterogeneities and the dominant role of some subpopulations of tumour cells to promote the tumour progression along with the lethal damage of normal cells in tumour vicinity from the cancer therapies, suggest the importance of cell targeting to design a successful cancer treatment.

In presented model, we proposed that the tumour microenvironmental condition plays a critical role in forming tumour heterogeneities. Assuming eight distinct phenotype of cell in cancer cell population, we studied the effect of hypoxia, acidity and the coincidence of hypoxia and acidity on different division pathways of cancer cells. We built a cellular automata model equipped with a pushing mechanism under the distribution of nutrient and pH and extracellular condition. This forward model visualizes the effect of microenvironmental factors on tumour growth and heterogeneities. The results can provide a hint on which subpopulation(s) of cancer cells may be the critical group to target based on instantaneous state of the tumour.

The promotion of cancer stem cell phenotype in acidic region through the promotion of dedifferentiation of progenitors and asymmetric differentiation of S cells leads in the increased population of cancer stem cells from P_1, P_2, and P_3 phenotypes. The predicted down regulation of self-renewal of S cells results in the suppression of this phenotype in acidic regions.

Similar to acidity, hypoxia upregulates the stem-like phenotypes among cancer cell population. However, the self-renewal of S cells in hypoxic regions is more likely than acidic areas. The promotion of dedifferentiation rate of progenitors in hypoxia is relatively higher than other microenvironmental regions.

The self-renewal of S cells seems to be maximally promoted in acidic-hypoxic regions. On the other hand, the dedifferentiation rate of cancer progenitors is also upregulated n this region. Consequently, the majority of S phenotype subpopulation

is residing in acidic-hypoxic region.

Further biological experiments are needed to validate the predictions of our model about the dynamics of tumour heterogeneities. Such experiments may investigate the synergistic effect of hypoxia and acidity on cancer cells. Using an accurate cell sorting method to distinct cancer cells based on the expression of stem cell markers such as CD133+ and pluripotency potentials may be useful.

One potential direction of extension of the model is to consider different rates of transitions for cancer progenitors. The differentiation of P_3 cells, as the most mature phenotype of cancer stem cells, to P_4 cells, as the least mature phenotype of non-stem cancer cells is of special interest. Certainly, a larger scale of cellular automata modeling can obtains better prediction of reality.

In a larger scale, the model can be improved by considering the effect of cancer therapies such as anti-angiogenic therapies or treatments to normalize the vasculature inside the tumour as well as proposed therapies to lower the acidity of the tumour microenvironment by introducing a auxiliary buffering system [Molavian et al. 2009]. The effect of chemo and radiotherapy of cancer cells with an emphasis on targeting specific subpopulations of cancer cells can be added to improve the model.

References:

1. J. A. Adam, A simplified mathematical model of tumor growth. *Math. Biosci*., 81: 229-242. 1986
2. C. Aghajanian, M. W. Sill, K. M. Darcy, B. Greer, D.S. McMeekin, P.G. Rose, J. Rotmensch, M.N. Barnes, P. Hanjani, and K. K. Leslie. Phase II trial of bevacizumab in recurrent or persistent endometrial cancer: a Gynecologic Oncology Group study. *J Clin Oncol*., 1;29(16):2259-65. 2011
3. A. R. A. Anderson. A hybrid mathematical model of solid tumour invasion: the importance of cell adhesion. *Math Med Biol*., 22:163–186. 2005.
4. A. R. A. Anderson, M. A. J. Chaplain, and K. A. Rejniak. Single-Cell-Based Models in Biology and Medicine.: *Birkhauser-Verlag* Basel, Switzerland. 2007.
5. R. P. Araujo, and D. L. McElwain. A history of the study of solid tumour growth: the contribution of mathematical modelling. *Bull Math Biol.* 66(5):1039-1091. 2004.
6. S. Bao, Q. Wu, S. Sathornsumetee, Y. Hao, Z. Li, A. B. Hjelmeland, Q. Shi, R. E. McLendon, D. D. Bigner, and J. N. Rich. Stem cell-like glioma cells promote tumor angiogenesis through vascular endothelial growth factor. *Cancer Res*. 15;66(16):7843-8. 2006.
7. T. T. Batchelor, A. G. Sorensen, E. di Tomaso, W. T. Zhang, D. G. Duda, K. S. Cohen, K. R Kozak, D. P. Cahill, P. J. Chen, M. Zhu, M. Ancukiewicz, M. M. Mrugala, S. Plotkin, J. Drappatz, D. N. Louis, P. Ivy, D. T. Scadden, T. Benner, J. S. Loeffler, P. Y. Wen, and R. K. Jain. AZD2171, a pan-VEGF receptor tyrosine kinase inhibitor, normalizes tumor vasculature and alleviates edema in glioblastoma patients. *Cancer Cell*. 11, 83–95. 2007.

8. G. Bell, J. N. Davidson, and H. Scarborough. Textbook of Physiology and Biochemistry. Seventh Edition Baltimore: *The Williams and Wilkins Company*; P. 738. 1968.
9. B. C. Bernhart, and M. C. Simon. Metastasis and stem cell pathways. *Cancer Metastasis Rev*. 26(2):261-71. 2007.
10. E. Berra, E. Benizri, A. Ginouvès, V. Volmat, D. Roux, and J. Pouysségur. HIF prolyl-hydroxylase 2 is the key oxygen sensor setting low steady-state levels of HIF-1α in normoxia. *EMBO J*., 15;22(16):4082-90. 2003.
11. B. M. Boman, M. S. Wicha, J. Z. Fields, and O. A. Runquist. Symmetric division of cancer stem cells–a key mechanism in tumor growth that should be targeted in future therapeutic approaches. *Clin. Pharma- col. Ther*. 81, 893–898. 2007.
12. N. Bouck, , V. Stellmach, , and S. C. Hsu. How tumors become angiogenic. *Adv Cancer Res*. 69:135-74. 1996.
13. H. M. Byrne, and M. A. J. Chaplain. Necrosis and apoptosis: distinct cell loss mechanisms in a mathematical model of a vascular tumour growth. *J. Theor. Med*. 1, 223-235. 1998.
14. H . Byrne, D . Drasdo. Individual-based and continuum models of growing cell populations: a comparison. *J Math Biol* 58(4-5):657-687. 2009.
15. C. Calabrese , H. Poppleton, M. Kocak, T. L. Hogg, C. Fuller, B. Hamner, E. Y. Oh, M. W. Gaber, D. Finklestein, M. Allen, A. Frank, I. T. Bayazitov, S. S. Zakharenko, A. Gajjar, A. Davidoff, R. J. Gilbertson. A perivascular niche forbrain tumor stem cells. *Cancer Cell*. 11(1):69-82. 2007.
16. J. J. Casciari, S. V. Sotirchos, R. M. Sutherland. Variations in tumor cell growth rates and metabolism with oxygen concentration, glucose concentration, and extracellular pH. *J Cell Physiol*. 151(2):386-94. 1992.

17. J. J. Casciari, S. V. Sotirchos, R. M. Sutherland. Mathematical modeling of microenvironment and growth in ETM6/RO multicellular tumors spheroids. *Cell Prolif*. 25:1–22. 1992.
18. J. J. Casciari, S. V. Sotirchos, R. M. Sutherland. Glucose diffusivity in Multicellular Tumor Spheroids. *Cancer Research*. 48:3905-3909. 1998.
19. C. L. Chaffer, I. Brueckmann, C. Scheel, A. J. Kaestli, P. A. Wiggins, L. O. Rodrigues, M. Brooks, F. Reinhardt, Y. Su, K. Polyak, L. M. Arendt, C. Kuperwasser, B. Bierie, R. A. Weinberg. Normal and neoplastic nonstem cells can sontaneusly convert to a stem-like state. *Proc Natl Acad Sci U S A*. 108(19):7950-5. 2011.
20. Y. L. Chan, G. Malnic, G. Giebisch. Passive driving forces of proximal tubular fluid and bicarbonate transport: gradient dependence of H+ secretion. *Am J Physiol Renal Physiolkg*. 245:F622-F63. 1983.
21. M. A. Chaplain, J. and B. D. Sleeman. Modeling the growth of solid tumours and incorporating a method for their classification using nonlinear elasticity theory. *J. Math. Biol*. 31, 431-473. 1993.
22. R. Chen , M. C. Nishimura, S. M. Bumbaca, S. Kharbanda, W. F. Forrest, I. M. Kasman, J. M. Greve, R. H. Soriano, L. L. Gilmour, C. S. Rivers, Z. Modrusan, S. Nacu, S. Guerrero, K. A. Edgar, J. J. Wallin, K. Lamszus, M. Westphal, S. Heim, C. D. James, S. R. Vandenberg, J. F. Costello, S. Moorefield, C. J. Cowdrey, M. Prados, H. S. Phillips. A hierarchy of self-renewing tumor-initiating cell types in glioblastoma. *Cancer Cell*. 13;17(4):362-75. 2010.
23. G. Christofori, and H. Semb. The role of the cell-adhesionmolecule E-cadherin as a tumour-suppressor gene. *Trends Biochem Sci*. 24(2):73-6. 1999.

24. E. Clayton, D. P. Doup, A. M. Klein, D. J. Winton, B. D. Simons, and P. H. Jones. A Single type of progenitor cell maintains normal epidermis. *Nature*. 446:185-189. 2007.

25. C. Crone, and D. G. Levitt. Capillary permeability to small solutes. In: *Handbook of Physiology: A Critical, Comprehensive presentation of physiology knowledge and concepts, Section 2: The Cardiovascular System Vol IV: Microcirculation, part 1 (Renkin EM, and Michel CC, eds)*. Bethesda, ML: American Physiology Society. P 414 and PP. 434-437. 1963

26. G. C. Cruywagen, D. E. Woodward, P. Tracqui, G. T. Bartoo, J. D. Murray, and E. C. Alvord. The modeling of diffusive tumours. *J. Biol. Sys*. 3,937-945. 1995.

27. T. Denysenko, L. Gennero, M. A. Roos, A. Melcarne, C. Juenemann, G. Faccani, I. Morra, G. Cavallo, S. Reguzzi, G. Pescarmona, and A. Ponzetto. Glioblastoma cancer stem cell: heterogeneity, microenvironment and related therapeutic strategies. *Cell Biochem Funct*. 28(5):343-51. 2010.

28. A. Deutsch, S. Dormann. Cellular Automaton Modeling of Biological Pattern Formation. *Birkhäuser*. 2005.

29. M. W. Dewhirst, Y. Cao, B. Moeller. Cycling hypoxia and free radicals regulate angiogenesis and radiotherapy response. *Nat Rev Cancer*. 8(6):425-37. 2008.

30. J. Dings, J. Meixensberger, A. Jager, K. Roosen. Clinical experience with 118 brain tissue oxygen partial pressure catheter probes. *Neurosurgery*. 43:1082–95. 1998.

31. P. B. Dirks. Brain tumour stem cells: the undercurrents of human brain cancer and their relationship to neural stem cells. *Philos Trans R Soc Lond B Biol Sci*. 12; 363(1489): 139–152. 2008.

32. W. Duchting, and T. Vogelsaenger. Recent progress in modeling and simulation of three-dimensional tumor growth and treatment. *Biosystems*. 18, 79-91. 1985.

33. W. Duchting, and T. Vogelsaenger. Analysis, forecasting and control of three-dimensional tumor growth and treatment. *J. Med. Syst*. 8:461–475. 1984.

34. A. Eramo, L. Ricci-Vitiani, A. Zeuner, R. Pallini, F. Lotti, G. Sette, E. Pilozzi, L. M. Larocca, C. Peschle, R. De Maria, Chemotherapy resistance of glioblastoma stem cells. *Cell Death Differ*. 13(7):1238-41. 2006.

35. S. M. Evans, K. D. Judy, I. Dunphy, W. T. Jenkins, W. T. Hwang, P. T. Nelson, R. A. Lustig, K. Jenkins, D. P. Magarelli, S. M. Hahn, R. A. Collins, M. S. Grady, and C. J. Koch. Hypoxia is important in the biology and aggression of human glial brain tumors. *Clin Cancer Res.* 15;10(24):8177-84. 2004.

36. S. M. Evans, K. D. Judy, I. Dunphy, W. T. Jenkins, P. T. Nelson, R. Collins, E. P. Wileyto, K. Jenkins, S. M. Hahn, C. W. Stevens, A. R. Judkins, P. Phillips, B. Geoerger, and C. J. Koch. Comparative measurements of hypoxia in human brain tumors using needle electrodes and EF5 binding. *Cancer Res*. 64(5):1886-92. 2004.

37. I. Fatt, C. J. Giasson, and T. D. Mueller. Non-Steady-State Diffusion in a Multilayered Tissue Initiated by Manipulation of Chemical Activity at the Boundaries. *Biophysical Journal*. 74:475-486. 1998.

38. P. Fedi, S. R. Tronick, and S. A. Aaronson. Growth factors. In: *Cancer Medicine*, J.F. Holland, R.C. Bast, D.L. Morton, E. Frei, D.W. Kufe, and R.R. Weichselbaum, eds. Baltimore, MD: Williams and Wilkins. pp. 41–64. 1997.

39. S. C. Ferreira, M. L. Martins, M. J. Vilela. Reaction-diffusion model for the growth of avascular tumor. *Physical Review E*. 65:021907. 2002.

40. C. Folkins, Y. Shaked, S. Man, T. Tang, C. R. Lee, Z. Zhu, R. M. Hoffman, and R. S. Kerbel. Glioma tumor stem-like cells promote tumor angiogenesis and vasculogenesis via vascular endothelial growth factor and stromal-derived factor 1. *Cancer Res*. 15;69(18):7243-51. 2009.

41. J. Folkman. Tumor angiogenesis. In *Cancer Medicine*, J.F. Holland, R.C. Bast, D.L. Morton, E. Frei, D.W. Kufe, and R.R. Weich- selbaum, eds. Baltimore, MD: Williams and Wilkins, pp. 181–204. 1997.

42. J. A. Forsythe, B. H. Jiang, N. V. Iyer, F. Agani, S. W. Leung, R. D. Koos, and G. L. Semenza. Activation of vascular endothelial growth factor gene transcription by hypoxia-inducible factor 1. *Mol Cell Biol*. 16(9):4604-13. 1996.

43. E. Fuchs, and J. A. Segre, Stem cells: a new lease on life. *Cell*. 7;100(1):143-55. 2000.

44. D. Fukumura, L. Xu, Y. Chen, T. Gohongi, B. Seed, R. K. Jain. Hypoxia and acidosis independently up-regulate vascular endothelial growth factor transcription in brain tumors in vivo. *Cancer Res*. 15;61(16):6020-4. 2001.

45. R. Ganguly, and I. K. Puri. Mathematical model for the cancer stem cell hypothesis. *Cell Prolif*. 39, 3–14. 2006.

46. R. Ganguly, and I. K. Puri. Mathematical model for chemotherapeutic drug efficacy in arresting tumour growth based on the cancer stem cell hypothesis. *Cell Prolif*. 40, 338–354. 2007.

47. R. Gatenby, T. Vincent. Application of quantitative models from population biology and evolutionary game theory to tumor therapeutic strategies. *Mol. Cancer Ther*. 2:919–927. 2003.

48. M. A. Gates, L. B. Thomas, E. M. Howard, E. D. Laywell, B. Sajin, A. Faissner, B. Götz, J. Silver, D. A. Steindler, Cell and molecular analysis of the developing and adult mouse subventricular zone of the cerebral hemispheres. *J Comp Neurol*. 16;361(2):249-66. 1995.
49. R. J. Gilbertson, J. N. Rich. Making a tumour's bed: glioblastoma stem cells and the vascular niche. *Nat Rev Cancer*. 7(10): 733–736. 2007.
50. D. T. Gillespie. Exact stochastic simulation of coupled chemical reactions. *J. Phys. Chem.* 81 (25), pp 2340–2361. 1997.
51. D. T. Gillespie. Markov process: An introduction for Physical Scientists. *academic press*. ISBN 0122839552. 1991.
52. J. D. Gordan, M. C. Simon. Hypoxia-inducible factors: central regulators of the tumor phenotype. *Curr Opin Genet Dev*. 17:71–7. 2007.
53. N. M Grüning, M. Ralser. Cancer: Sacrifice for survival. *Nature*. 7;480(7376):190-1. 2011.
54. A. C. Guyton, and J. E. Hall. Text book of medical physiology. Philadelphia: *Elsevier Saunders*. 2006.
55. R. Jandial, U. Hoisang, M. L. Levy, E. Y. Snyder. Brain tumor stem cells and the tumor microenvironmen. *Neurosurg Focus*. 24(3–4): 27. 2008.
56. W. C. Hahn, C. M. Counter, A. S. Lundberg, R. L. Beijersbergen, M. W. Brooks, and R. A. Weinberg. Creation of human tumor cells with defined genetic elements. *Nature*. 29;400(6743):464-8. 1991.
57. D. Hanahan, R. A. Weinberg. Hallmarks of Cancer: The Next Generation. *Cell*. 144, 5, 646-674. 2011.
58. D. Hanahan, and J. Folkman. Patterns and emerging mecha- nisms of the angiogenic switch during tumorigenesis. *Cell*. 9;86(3):353-64. 1996.
59. D. Hanahan, R. A. Weinberg. The hallmarks of cancer. *Cell*. 7;100(1):57-70. 2000.

60. L. Hayflick. Mortality and immortality at the cellular level. A review. *Biochemistry (Mosc)*. 62(11):1180-90. 1997.

61. J. M. Heddleston, Z. Li, J. D. Lathia, S. Bao, A. B. Hjelmeland, and J. N. Rich. Hypoxia inducible factors in cancer stem cells. *Br J Cancer*. 2;102(5):789-95. 2010.

62. J. M. Heddleston, Z. Li, R. E. McLendon, A. B. Hjelmeland, and J. N. Rich. The hypoxic microenvironment maintains glioblastoma stem cells and promotes reprograming towards a cancer stem cell phenotype. *Cell Cycle*. 15;8(20):3274-84. 2009.

63. C. H. Heldin, K. Rubin, K. Pietras, and A. Ostman. High interstitial fluid pressure – an obstacle in cancer therapy. *Nat Rev Cancer*. 4(10):806-13. 2004.

64. G. Helmlinger, A. Sckell, M. Dellian, N. S. Forbes, R. K. Jain. Acid production in glycolysis-impaired tumors provides new insights into tumor metabolism. *Clin Cancer Res*. 8:1284–91. 2002.

65. G. Helmlinger, F. Yuan, M. Dellian, and R. K. Jain. Interstitial pH and pO2 gradients in solid tumors in vivo: high-resolution measurements reveal a lack of correlation. *Nat Med*. 3(2):177-82. 1997.

66. R. P. Hill, D. T. Marie-Egyptienne, and D. W. Hedley., Cancer stem cells, hypoxia and metastasis. *Semin Radiat Oncol*. 19(2):106-11. 2009.

67. A. B. Hjelmeland, Q. Wu, J. M. Heddleston, G. S. Choudhary, J. MacSwords, J. D. Lathia, R. McLendon, D. Lindner, A. Sloan, J. N. Rich. Acidic stress promotes a glioma stem cell phenotype. *Cell Death Differ*. 18(5):829-40. 2011.

68. S. Hockfield, and R. D. McKay. Identification of major cell classes in the developing mammalian nervous system. *J Neurosci*. 5(12):3310-28. 1985.

69. Z. Ivanovic, F. Hermitte, P. Brunet de la Grange, B. Dazey, F. Belloc, F. Lacombe, G. Vezon, and V. Praloran. Simultaneous mainte- nance of human cord blood SCID-repopulating cells and expansion of committed progenitors at low O2 concentration (3%). *Stem Cells*. 22(5):716-24. 2004.

70. R. K. Jain. Taming vessels to treat cancer, *Scientific American*. 18, 64-71. 2008.

71. R.K. Jain. Normalization of the tumour vasculature: an emerging concept in anti-angiogenic therapy. *Science*. 307(5706):58-62. 2005.

72. M. D. Johnston, C. M. Edwards, W. F. Bodmer, P. K. Maini, and S. J. Chapman. Mathematical modeling of cell population dynamics in the colonic crypt and in colorectal cancer. *Proc. Natl. Acad. Sci. USA* 104, 4008–4013. 2007.

73. Y. Kam, K. A. Rejniak, A. R. Anderson. Cellular modeling of cancer invasion: Integration of in silico and in vitro approaches. *J Cell Physiol*. 227(2):431-8. 2012.

74. A. R. Kansal, S. Torquato, G. R. Harsh IV, E. A. Chiocca, and T. S. Deisboeck. Simulated Brain Tumor Dynamics Using a Three-Dimensional Cellular Automaton. *Journal of Theoretical Biology*. 203:367–382. 2000.

75. A. R. Kansal, S. Torquato, E. A. Chiocca, and T. S. Deisboeck. Emergence of a subpopulation in a computational model of tumor growth. *Journal of Theoretical Biology*. 207:431–441. 2000.

76. B. Keith, and M. Celeste Simon. Hypoxia-inducible factors, stem cells, and cancer. *Cell*. 4; 129(3): 465–472. 2007.

77. H. Kimura, R. D. Braun, E. T. Ong, R. Hsu, T. W. Secomb, D. Papahadjopoulos, K. Hong, M. W. Dewhirst. Fluctuations in red cell flux in tumor microvessels can lead to transient hypoxia and reoxygenation in tumor parenchyma. *Cancer Res*. 1;56(23):5522-8. 1996.

78. K. W. Kinzler, and B. Vogelstein. Lessons from hereditary colorectal cancer. *Cell*. 18;87(2):159-70. 1996.

79. M. Kovacević-Filipović, M. Petakov, F. Hermitte, C. Debeissat, A. Krstić, G. Jovcić, D. Bugarski, X. Lafarge, P. Milenković, V. Praloran, and Z. Ivanović. Interleukin-6 (IL-6) and low O2 concentration (1%) synergize to improve the maintenance of hematopoietic stem cells (pre-CFC). *J Cell Physiol*. 212(1):68-75. 2007.

80. M. Lacroix. Significance, detection and markers of disseminated breast cancer cells. *Endocr Relat Cancer*. 13 1033-1067. 2006.

81. P. Laslo, C. J. Spooner, A. Warmflash, D. W. Lancki, H. J. Lee, R. Sciammas, B. N. Gantner, A. R. Dinner, and H. Singh. Multilineage transcriptional priming and determination of alternate hematopoietic cell fates. *Cell*. 25;126(4):755-66. 2006.

82. J. D. Lathia, J. Gallagher, J. M. Heddleston, J. Wang, C. E. Eyler, J. Macswords, Q. Wu, A. Vasanji, R. E. McLendon, A. B. Hjelmeland, and J. N. Rich. Integrin alpha 6 regulates glioblastoma stem cells. *Cell Stem Cell*. 7;6(5):421-32. 2010.

83. U. Lendahl, L. B. Zimmerman, and R. D. McKay. CNS stem cells express a new class of intermediate filament protein. *Cell*. 23;60(4):585-95. 1990.

84. Z. Li, and J. N. Rich. Hypoxia and hypoxia inducible factors in cancer stem cell maintenance. *Curr Top Microbiol Immunol*. 345:21-30. 2010.

85. Z. Li, S. Bao, Q. Wu, H. Wang, C. Eyler, S. Sathornsumetee, Q. Shi, Y. Cao, J. Lathia, R. E. McLendon, A. B. Hjelmeland, and J. N. Rich. Hypoxia-inducible factors regulate tumorigenic capacity of glioma stem cells. *Cancer Cell*. 2;15(6):501-13. 2009.

86. D. Liao, and R. S. Johnson. Hypoxia: a key regulator of angiogenesis in cancer. *Cancer Metastasis Rev*. 26(2):281-90. 2007.

87. D. N. Louis, H. Ohgaki, O. D. Wiestler, W. K. Cavenee, P. C. Burger, A. Jouvet, B. W. Scheithauer, and P. Kleihues. The 2007 WHO classification of tumors of the central nervous system. *Acta Neuropathol*. 114(2):97-109. 2007.

88. J. S. Lowengrub, H. B. Frieboes, F. Jin, Y. L. Chuang, X. Li, P. Macklin, S. M. Wise, and V. Cristini. Nonlinear modelling of cancer: bridging the gap between cells and tumours. *Nonlinearity* . 23(1):R1-R9. 2010.

89. Y. Mansury, M. Diggory, T. S. Deisboeck. Evolutionary game theory in an agent-based brain tumor model: exploring the 'Genotype-Phenotype' link. *J Theor Biol*. 7;238(1):146-56. 2006.

90. Y. Mansury, M. Kimura, J. Lobo, and T. S. Deisboeck. Emerging patterns in tumor systems: simulating the dynamics of multicellular clusters with an agent-based spatial agglomeration model. *J Theor Biol*. 7;219(3):343-70. 2002.

91. M. Marusic, Z. Bajzer, J. P. Freyer, and S. Vuc-Pavlovic. Analysis of growth of multicellular tumour spheroids by mathematical models. *Cell Prolif*. 27, 73-94. 1994.

92. A. M. McCord, M. Jamal, U. T. Shankavaram, F. F. Lang, K. Camphausen, and P. J. Tofilon. Physiologic oxygen concentration enhances the stem-like properties of CD133+ human glioblastoma cells in vitro. *Mol Cancer Res*. 7(4):489-97. 2009.

93. R. E. McLendon, and J. N. Rich. Glioblastoma Stem Cells: A Neuropathologist's View. *J Oncol*. 2011:397195. 2011.

94. F. Michor, T. P. Hughes, Y. Iwasa, S. Branford, N. P. Shah, C. L. Sawyers, and M. A. Nowak. Dynamics of chronic myeloid leukaemia. *Nature*. 435, 1267–1270. 2005.

95. B. J. Moeller, Y. Cao, C. Y. Li, and M. W. Dewhirst. Radiation activates HIF-1 to regulate vascular radiosensitivity in tumors: role of reoxygenation, free radicals, and stress granules. *Cancer Cell*. 5(5):429-41. 2004.

96. H. R. Molavian, M. Kohandel, M. Milosevic, and S. Sivaloganathan. Fingerprint of cell metabolism in the experimentally observed interstitial pH and pO2 in solid tumors. *Cancer Res.* 1;69(23):9141-7. 2009.

97. K. A. Moore, I. R. Lemischka. Stem cells and their niches. *Science*. 31;311(5769):1880-5. 2006.

98. M. G. Nicholas, and T. H. Foster. Oxygen diffusion and reaction kinetics in the photodynamic therapy of multicell tumor spheroid. *Phys. Mod. Biol*. 39:2161-2181. 1994.

99. A. K. Olsson, A. Dimberg, J. Kreuger, L. and Claesson-Welsh. VEGF receptor signalling - in control of vascular function. *Nat Rev Mol Cell Biol*. 7(5):359-71. 2006.

100. A. Patel, E. T. Gawlinski, S. K. Lemieux, R. A. Gatenby. A cellular automaton model of early tumor growth and invasion: The effects of native tissue vascularity and increased anaerobic tumor metabolism. *J. theor. Biol*. 213:315–331. 2001.

101. A. Perumpanani, J. A. Sherratt, J. Norbury, and H. M. Byrne. Biological inferences from a mathematical model for malignant invasion. *Invasion Metastasis*. 16, 209-221. 1996.

102. N. Platet, S. Y. Liu, M. E. Atifi, L. Oliver, F. M. Vallette, F. Berger, and D. Wion. Influence of oxygen tension on CD133 phenotype in human gliomacell cultures. *Cancer let*. 18;258(2):286-90. 2007.

103. J. Pouyssegur, F. Dayan, and N. M. Mazure. Hypoxia signalling in cancer and approaches to enforce tumour regression. *Nature*. 441:437–43. 2006.

104. L. Preziosi (ed). Cancer Modeling and Simulation. New York: *Champan & Hall*. 2003.

105. A. S. Qi, X. Zheng, C. Y. Du, and B. S. An. A cellular automaton model of cancerous growth. *J. theor. Biol*. 161, 1-12. 1993.

106. K. A. Rejniak, L. J. McCawley. Current trends in mathematical modeling of tumor- microenvironment interactions: a survey of tools and applications. *Exp Biol Med (Maywood)*. 235(4):411-423. 2010.

107. K. A. Rejniak, S. E. Wang, N. S. Bryce, H. Chang, B. Parvin, J. Jourquin, L. Estrada, J. W. Gray, C. L. Arteaga, A. M. Weaver, V. Quaranta, and A. R. Anderson. Linking changes in epithelial morphogenesis to cancer mutations using computational modeling. *PLoS Comput Biol* 6(8). 2010.

108. K. A. Rejniak, A. R. Anderson. Hybrid models of tumor growth, *Wiley Inc*. 2010.

109. T. Reya, S. J. Morrison, M. F. Clarke, and I. L. Weissman. Stem cells, cancer, and cancer stem cells. *Nature*. 1;414(6859):105-11. 2001.

110. L. Ricci-Vitiani, R. Pallini, M. Biffoni, M. Todaro, G. Invernici, T. Cenci, G. Maira, E. A. Parati, G. Stassi, L. M. Larocca, and R. De Maria. Tumour vascularization via endothelial differentiation of glioblastoma stem-like cells. *Nature*. 9;468(7325):824-8. 2010.

111. S. Seidel, B. K. Garvalov, V. Wirta, L. von Stechow, A. Schänzer, K. Meletis, M. Wolter, D. Sommerlad, A. T. Henze, M. Nistér, G. Reifenberger, J. Lundeberg, J. Frisén, and T. Acker. A hypoxic niche regulates glioblastoma stem cells through hypoxia inducible factor 2 alpha. *Brain*. 133(Pt 4):983-95. 2010.

112. G. L. Semenza., Hydroxylation of HIF-1: Oxygen sensing at the molecular level. *Physiology (Bethesda)*. 19:176-82. 2004.

113. J. A. Sherratt, and M. A. Nowak. Oncogenes, anti-oncogenes and the immune response to cancer: a mathematical model. *Proc. Roy. Soc. London [B]*. 248, 261-271. 1992.

114. R. K. Singh, M. Gutman, C. D. Bucana, R. Sanchez, N. Llansa, and I. J. Fidler. Interferons alpha and beta down-regulate the expression of basic fibroblast growth factor in human carcinomas. *PNAS*. 92,10 4562-4566. 1995.

115. S. K. Singh, I. D. Clarke, T. Hide, P. B. Dirks. Cancer stem cells in nervous system tumors. *Oncogene*. 20;23(43):7267-73. 2004.

116. S. K. Singh, I. D. Clarke, M. Terasaki, V. E. Bonn, C. Hawkins, J. Squire, P. B. Dirks. Identification of a cancer stem cell in human brain tumors. *Cancer Res*. 15;63(18):5821-8. 2003.

117. J. Smolle, and H. Stettner. Computer simulation of tumour cell invasion by a stochastic growth model. *J. theor. Biol*. 160, 63-72. 1993.

118. G. G. Steel. Growth Kinetics of Tumors. Oxford: *Clarendon Press*. 1977.

119. A. M. Stein, T. Demuth, D. Mobley, M. Berens, L. M. Sander. A mathematical model of glioblastoma tumor spheroid invasion in a three-dimensional in vitro experiment. *Biophys. J*. 92, 356–365. 2007.

120. L. Studer, M. Csete, S. H. Lee, N. Kabbani, J. Walikonis, B. Wold, R. McKay. Enhanced proliferation, survival, and dopaminergic differentiation of CNS precursors in lowered oxygen. *J Neurosci*. 1;20(19):7377-83. 2000.

121. K. R. Swanson, R. C. Rostomily, and E. C. Jr. Alvord. A mathematical modelling tool for predicting survival of individual patients following resection of glioblastoma: a proof of principle. *Br. J. Cancer*. 98, 113–119. 2008.

122. H. Symonds, L. Krall, L. Remington, M. Saenz-Robles, S. Lowe, T. Jacks, and T. Van Dyke. p53-dependent apoptosis sup- presses tumor growth and progression in vivo. *Cell*. 26;78(4):703-11. 1994.

123. J. E. Till, E. A. McCulloch, and L. Siminovitch. A Stochastic Model of Stem Cell Proliferation, Based on The Growth of Spleen Colony-Forming Cells. *Proc Natl Acad Sci U S A*. 51:29-36. 1964.

124. P. Tracqui, G. C. Cruywagen, D. E. Woodward, G. T. Bartoo, J. D. Murray, and E. C. Alvord. A mathematical model of glioma growth: the effect of chemotherapy on spatio-temporal growth. *Cell Prolif*. 28, 17-31. 1995.

125. P. Tracqui. From passive diffusion to active cellular migration in mathematical models of tumor invasion. *Acta Biotheor*. 43, 443-464. 1995.

126. C. Turner. Mathematical modeling of cancer stem cells, Master's thesis *University of Waterloo*. 2009.

127. C. Turner, A. R. Stinchcombe, M. Kohandel, S. K. Singh, and S. Sivaloganathan. Characterization of brain cancer stem cells: a mathematical approach. *Cell Prolif*. 42(4):529-40. 2009.

128. N. G. Van Kampen. Stochastic processes in physics and chemistry. Third edition. *North Holland*.. ISBN 0444529659. 2007.

129. P. Vaupel, F. Kallinowski, and P. Okunieff. Blood flow, oxygen and nutrient supply, and metabolic microenvironment of human tumors: a review. *Cancer Res*. 49: 6449–6465. 1989.

130. P. Vaupel, and A. Mayer. Hypoxia in cancer: Significance and impact on clinical outcome. *Cancer Metastasis Rev*. 26(2):225-39. 2007.

131. O. V. Volpert, K. M. Dameron, and N. Bouck. Sequential development of an angiogenic phenotype by human fibroblasts progressing to tumorigenicity. *Oncogene*. 27;14(12):1495-502.1997.

132. R. Wang, K. Chadalavada, J. Wilshire, U. Kowalik, K. E. Hovinga, A. Geber, B. Fligelman, M. Leversha, C. Brennan, and V. Tabar. Glioma stem-like cells give rise to tumour endothelium. *Nature*. 9;468(7325):829-33. 2010.

133. J. P. Ward, and J. R. King. Mathematical modeling of avascular-tumour growth. *IMA J. Math. Appl. Med. Biol*. 14, 39-69. 1997.

134. R. Wasserman, R. Acharya, C. Sibata, and K. H. Shin. A patient-specific in vivo tumor model. *Math. Bio- sci*. 136, 111-140. 1996.

135. R. A. Weinberg. The retinoblastoma protein and cell cycle control. *Cell*. 5;81(3):323-30. 1995.

136. I. L. Weissman. Stem cells: units of development, units of regeneration, and units in evolution. *Cell*. 7;100(1):157-68. 2000.

137. H. E. Wichmann, M. Loeffler. Mathematical Modeling of Cell Proliferation: Stem Cell Regulation in Hemopoiesis, Vol. I. *Boca Raton*, FL: CRC Press. 1985.

138. D. E. Woodward, J. Cook, P. Tracqui, G. C. Cruywagen, J. D. Murray, E. C. Alvord. A mathematical model of glioma growth: the effect of extent of surgical resection. *Cell Prolif*. 29, 269-328. 1996.

139. C. P. Zhang, L. L. Zhu, T. Zhao, H. Zhao, X. Huang, X. Ma, H. Wang, and M. Fan. Characteristics of neural stem cells expanded in lowered oxygen and the potential role of hypoxia-inducible factor-1α. *Neurosignals*. 15:259–65. 2006.